

**Preparation of high voluminous nanoparticle
superstructures via freezing and subsequent
lyophilization**

Von der Naturwissenschaftlichen Fakultät der
Gottfried Wilhelm Leibniz Universität Hannover

zur Erlangung des Grades

Doktor der Naturwissenschaften (Dr. rer. nat)

genehmigte Dissertation

von

Axel Freytag, M.Sc.

geboren am 09.09.1985 in Dippoldiswalde

2017

Referent: Dr. rer. nat. Nadja C. Bigall

Koreferent: Prof. Dr. rer. nat. Jürgen Caro

Tag der Promotion: 24.02.2017

„Der Kampf um den Südpol“

*Was bleibt nach dem Tode, wenn der Name nicht bleibt?
Und wie bleibt der Name? Wenn Geschichte er schreibt!
Wie schreibt er Geschichte, wenn er entdeckt, wenn er entdeckt!
Was sich unsern Blicken, bisher noch versteckt?
Was bleibt nach dem Tode, wenn nicht bleibt, wenn nicht bleibt der Ruhm?
Was bleibt nach dem Tode, große Tat, großes Menschentum.
Es ging ins 20. Jahrhundert, jedes Land, jedes war entdeckt.
Nur der kalte Pol am Süden, auf der Karte noch freies gefleckt?
Da begann der große Wettlauf, ihre Schiffe machten flott.
Zwei Kapitäne, Namenlose, später Amundsen und Scott.
Die Antarktis war bald erreicht, doch dann kam da schwerste, das schwerste Stück.
Auf Schlitten die Fahrt ins Eis begann und kein Weg vom Ziel zurück.
Und Hunger und Kälte, Einsamkeit, länger noch als ein Jahr.
Und sie fragen immerzu, wie weit schon der andere, der andere war.
Nur der erste, nur der erste, hätte wirklich erreicht sein Ziel.
Nur der zweite, nur der zweite, wär' in den Augen der Menschen nicht viel.
Und sie hetzten ihre Hunde und sich selber gnadenlos,
denn der eine würde scheitern, und der andre wär' bald groß.
Doch als Scott an den Südpol kam, da stand schon Amundsens Fahne fein.
Da brach der Frost von draußen her ihm tief in das Herz hinein.
Kein Petroleum half mehr, und kein Denken an Frau und Kind.
Und erfroren mit ihm sind vier Mann, im ewigen Eis umhüllt.
Was bleibt nach dem Tode, wenn der Name nicht bleibt?
Und wie bleibt der Name? Wenn Geschichte er schreibt!
Was bleibt nach dem Tode, wenn nicht bleibt, wenn nicht bleibt der Ruhm?
Was bleibt nach dem Tode: große Tat, großes Menschentum!
Was bleibt nach dem Tode, wenn nicht bleibt, wenn nicht bleibt der Ruhm?
Was bleibt nach dem Tode: große Tat, großes Menschentum!
Was bleibt nach dem Tode...*

„Der Kampf um den Südpol“ *Interpret*: Stern-Combo Meißen 1976

Preface

The original work presented in this thesis was conducted during my tenure in the work group of Dr. Nadja C. Bigall from December 2013 to November 2016 in the institute for physical chemistry and electrochemistry of the Gottfried Wilhelm Leibniz University of Hanover.

During this period I participated in the project “Materialien aus Überstrukturen Maßgeschneiderter Kolloidaler Nanokristallbausteine“ (MÜKoN) within the framework of the project NanoMatFutur (supporting code 03X5525) of the federal ministry of education and research (BMBF).

The thesis includes two articles and two manuscripts (submitted), which were written by myself as first author as well as four articles as first or co-author, respectively and a patent which are not included in this thesis but listed in the appendix. The following section clarifies the author contributions for each of the articles.

The first article in chapter 2.2 was written by myself with the kind support of my co-workers. I developed the fabrication method of the cryoaerogelation and tested it for noble metal and semiconducting nanoparticles. I investigated the crucial parameter for fabrication and developed immobilization techniques that allow the shaping of the resulting monoliths. I characterized the systems via optical spectroscopy and transmission as well as scanning electron microscopy (TEM and SEM). Dr. Sara Sánchez-Paradinas synthesized the CdSe/CdS quantum rods and did the fluorescence measurements on the resulting CdSe/CdS cryoaerogels. Suraj Naskar helped with additional SEM measurements. Natalja Wendt conducted nitrogen and krypton adsorption measurements to determine the surface of the cryoaerogels. Giammarino Pugliese did the TGA measurements. Under my supervision Cansunur Demirci fabricated the first hematite cryoaerogels with nanoparticles which were fabricated by Imme Kretschmer. Dr. Jan Poppe confirmed with his electrochemical active surface measurements the adsorption measurements of Natalja Wendt for the platinum cryoaerogels. Finally Dr. Massimo Colombo, Prof. Detlef W. Bahnemann, Prof. Peter

Behrens and especially Dr. Nadja C. Bigall helped with valuable discussions and corrections of the work.

The second manuscript in chapter 2.3 was again written by myself with the kind support of my co-workers. I showed the possibility of creating multicomponent aerogels via cryoaerogelation and could investigate the parameters to control the distribution of the components as well as the amount of components. I could demonstrate, that the optical properties can be influenced and that multi component cryoaerogels can be employed as photocatalyst in methanol assisted hydrogen evolution out of water. Carsten Günnemann supported me by fabricating hematite noble metal systems and characterized the systems via UV-Vis spectroscopy. Saher Hamid conducted the hydrogen evolution experiment and Suraj Naskar assisted with the SEM characterization particularly the energy dispersive x-ray measurements (EDX). Prof. Detlef W. Bahnemann and Dr. Nadja Bigall improved the work through their discussion and corrections.

The third manuscript was written by me together with Torben Kodanek and the support of our co-workers. Torben Kodanek synthesized silver nanoparticles of around 50 nm with varying shell thickness from zero to 13 nm. I employed the cryoaerogelation method to fabricate macroscopic monoliths as well as cryoaerogelfilms with thicknesses of around 10 μ m. The assemblies had defined distances to investigate plasmon coupling effects in three-dimensional systems. Torben Kodanek and I characterized the nanoparticles as well as the films and monoliths via UV-Vis spectroscopy and conducted TEM characterization of the colloidal nanoparticles and the resulting cryoaerogelfilms and –monoliths. Suraj Naskar assisted with SEM characterization and Dr. Dirk Dorfs and Dr. Nadja C. Bigall supported us with scientific discussions and corrections of our work.

The fourth article was written by myself with the kind support of Dr. Massimo Colombo and Dr. Nadja C. Bigall. I fabricated all employed nanoparticles and cryoaerogel monoliths and characterized them via UV-Vis spectroscopy, TEM and SEM. Together with Dr. Massimo Colombo we performed the catalytic measurements in the Italian Institute of Technology in

Genova. Both, Dr. Massimo Colombo and Dr. Nadja C. Bigall helped me while writing the article with constructive criticism and suggestions.

Acknowledgments

First of all, I want to thank Dr. Nadja Carola Bigall for her constant and excellent support throughout my PhD time. She introduced me in the fascinating field of nanochemistry and encouraged me every time in realizing ideas and experiments. She helped me to gain a deeper understanding in the field of aerogelation and helped me to improve my work with valuable suggestions.

Furthermore I would like to thank Prof. Jürgen Caro and PD Dr. Christian Klinke for reviewing this thesis as co-referees.

I also would like to thank all my collaboration partners, which enabled interesting experiments, investigations and publications. In particular I'd like to thank Prof. Peter Behrens, Prof. Detlef W. Bahnemann, Dr. Massimo Colombo, Dr. Sara Sánchez-Paradinas, Dr. Jan Poppe, Dr. Dirk Dorfs, Torben Kodanek, Cansunur Demirci, Carsten Günnemann, Suraj Naskar, Imme Kretschmer, Saher Hamid, Giammarino Pugliese, and Natalja Wendt.

For the introductions and support in electron microscopy I would like to thank Dr. Fritz Schulze Wischeler, Torben Kodanek, Appl. Prof. Dr. Armin Feldhoff and Frank Steinbach. Furthermore, I would like to thank all the staff that supported me with technical and organizational assistance, which are in particular: Kerstin Janze, Yvonne Gabbey-Uebbe, Kerstin Battermann, Peter Mühr, and Willi Becker.

Additionally I want to thank all the colleagues and co-workers of the work groups Bigall and Dorfs for creating a work environment with valuable advices, constructive critics and encouraging actions for each other. These colleagues are: Dominik Hinrichs, Jan F. Miethe, Franziska Lübke, Tarek Mohamed, Patrick Adel, Rasmus Himstedt, Pascal Rusch, Michael Galchenko, and Laura Altenschmidt.

Finally, I want to thank my parents André and Barbara Freytag, my Brother Toni and his family my friends Michael, Paul, Pia, Martin, Stefan, Angelika Brigitte Ilse and everybody else scattered throughout Germany, who always supported me and cheered me up when I needed it.

And I want to thank the love of my life, which I found, when I was not expecting it at all. Thank you, Tina.

Abstract

This thesis focuses on the possibilities of assembling nanoparticles into voluminous, highly porous superstructures, commonly known as aerogels. It will give an overview over the existing techniques so far as well as highlight the synthesized aerogel materials and their properties. In addition potential applications of aerogels, mentioned in literature, are spotlighted.

The main part of this work revolves around the development of a complete new assembling method for aerogels, namely the cryoaerogelation. This technique, which employs freezing nanoparticle solutions and subsequent lyophilisation, is intensively studied with electron microscopy, optical spectroscopy as well as catalytical measurements. Through this in depth characterization it is possible to understand the formation mechanism, the morphology of the cryoaerogels and in addition the properties of the resulting monolith. Furthermore this thesis demonstrates how multi component aerogels can be realized and that the monoliths can be shaped and immobilized on supports via the cryoaerogelation, which exceeds state of the art methods so far. Finally, investigations on the catalytic and photocatalytic properties reveal potential application for the synthesized materials. The work was published in two articles in international renowned journals and has two submitted manuscripts. The cryogelation procedure is patented in Germany.

Keywords: Aerogel, Nanoparticle, Freeze Drying, Fabrication Method,

Zusammenfassung

Diese Dissertation befasst sich mit den Möglichkeiten, Nanopartikel aus kolloidalen Lösungen in voluminöse und hochporöse Überstrukturen zu überführen, welche gemeinhin auch als Aerogele bekannt sind. Dabei wird ein Überblick über bestehende Herstellungsverfahren gegeben und es werden einzelne interessante Materialgruppen und deren Eigenschaften vorgestellt. Zusätzlich werden Anwendungsbeispiele aus der Literatur betrachtet.

Der Hauptteil dieser Dissertation befasst sich mit der Entwicklung eines neuartigen Herstellungsverfahrens, namentlich dem Kryoaerogeliervfahren. Bei diesem Verfahren werden Nanopartikel in kolloidaler Lösung eingefroren und anschließend gefriergetrocknet. Die daraus entstehenden Kryoaerogel werden intensiv durch Elektronenmikroskopie, Spektroskopie und katalytische Testverfahren untersucht, um anhand dieser Charakterisierungen, Rückschlüsse auf den Entstehungsmechanismus ziehen zu können. Dadurch ist es möglich, ein Verständnis für die Morphologie der resultierenden Monolithe und deren Eigenschaften zu entwickeln und die entscheidenden Einflussparameter aufzuzeigen. Weiterhin wird in dieser Arbeit die Herstellung von Multikomponentenkryoaerogelen gezeigt, denen beliebige Monolithformen vorgegeben werden und welche auf unterschiedlichen Substraten immobilisiert werden können. Abschließend zeigen Untersuchungen der katalytischen und photokatalytischen Eigenschaften vielversprechende Ergebnisse und zeigen damit mögliche Anwendungen für die hergestellten Materialien auf. Diese Dissertation wurde in Form von zwei Artikeln in international anerkannten Fachzeitschriften bereits veröffentlicht und zwei weitere Manuskripte in Fachzeitschriften eingereicht sowie das Kryoaerogeliervfahren in Deutschland bereits patentiert.

Schlagwörter: Aerogel, Nanopartikel, Gefriertrocknen, Herstellungsverfahren

Contents

| | |
|---|-----------|
| Preface..... | V |
| Acknowledgments..... | VIII |
| Abstract..... | X |
| Zusammenfassung..... | XI |
| 1. Introduction..... | 3 |
| 1.1 Motivation..... | 3 |
| 1.2 Nanoparticles..... | 5 |
| 1.2.1 Synthesis..... | 5 |
| 1.2.2 Nanoparticle Properties..... | 6 |
| 1.2.3 Nanoparticle Interactions in Assemblies..... | 10 |
| 1.3 Aerogels..... | 12 |
| 1.3.1 Fabrication Techniques..... | 12 |
| 1.3.2 Materials & Properties..... | 15 |
| 1.3.3 Metal Oxide Aerogels..... | 16 |
| 1.3.4 (Noble) Metal Aerogels..... | 17 |
| 1.3.5 Metal Chalcogenide Aerogels..... | 19 |
| 1.3.6 Organic and Carbon Aerogels..... | 21 |
| 1.3.7 Multi Component Aerogels..... | 23 |
| 1.4 Cryogels as Alternate Synthesis Route for Highly Porous Assemblies..... | 27 |
| 1.5 Applications..... | 29 |
| 1.6 References..... | 31 |
| 2. Development of a New Procedure for Aerogel Fabrication..... | 45 |
| 2.1 Summary..... | 45 |
| 2.2 Versatile Aerogel Fabrication by Freezing and Subsequent Freeze- Drying of Colloidal Nanoparticle Solutions..... | 47 |
| 2.3 Tailoring Composition and Material Distribution in Multicomponent Cryoaerogels..... | 74 |

| | | |
|-----|--|-----|
| 3. | Controlling Nanoscopic Properties within Macroscopic Objects..... | 103 |
| 3.1 | Summary..... | 103 |
| 3.2 | Macroscopic Aerogels with Controllable Nanoscopic Plasmonic Properties..... | 104 |
| 4. | From Knowledge to Application – Possibilities of Cryoaerogels in Catalysis..... | 121 |
| 4.1 | Summary..... | 121 |
| 4.2 | Catalytic Properties of Cryogelated Noble Metal Aerogels..... | 123 |
| 5. | Closing Remarks..... | 139 |
| | Appendix | 142 |

1. Introduction

1.1 Motivation

Nanoparticles (NP) are fascinating. This simple statement can be easily explained by the properties of the particle fraction between 1 nm and 100 nm. And since NP properties can significantly change from their respective bulk material, it creates high interest in science to understand the differing characteristics. It also raises the desire to exploit unique features for future applications. In the last 10 years there are more than 250.000¹ scientific publications engaging the field of NP synthesis, characterization or applications. This proves that NP research is a hot topic in science. Altered properties of NPs are for example significant increased specific surface areas. This characteristic is common for all NP independent of the material type and is caused by increasing surface to volume ratio with decreasing particle diameter. Although this fact seems trivial it has a huge impact on catalytical applications, since speed limiting steps like pore diffusion processes are shortened and saturation of catalyst surface with reactant is delayed due to the higher number of reactive sites. The employment of NP in catalysis therefore further improves reaction kinetics. Melting point depression for NP materials is another characteristic that is accompanied by a decreasing particle diameter. For example gold NPs with a size of 2.5 nm have a melting point of around 300°C compared to the melting point of bulk gold at 1064°C.[1] Other changes of properties are material dependent. For example metal particles can show a collective oscillation of their electron density. If the metal particle size is much smaller than the wavelength of the visible light, especially in the range of NPs from 1 nm to 100 nm, it is possible to create a resonance of this oscillation localized within the particle.[2] This localized surface plasmon resonance (LSPR) or commonly referred to as plasmon can be excited by light and cause colloidal gold solutions to be e.g. red depending on the particle size and shape. Additionally, the band structures of materials become more discrete resulting e.g. in the occurrence of gaps within metal band structures leading to fluorescent metals.[3, 4] Or for semiconducting materials if the NP size is in the range of its

¹ Retrieval of SciFinder Database from 21.09.2016 with articles containing the word „nanoparticle“

exciton Bohr radius, the band gap will be strongly size dependent and widen for decreasing particle sizes, since the energy levels become discrete.[5, 6] This phenomena, called quantum confinement, is already exploited and quantum dots are e.g. employed in modern display techniques.[7]

The synthesis of NPs with the above mentioned fascinating and unique properties are well studied and demonstrated for the wet chemical bottom up approaches. Referring to top down methods such as laser ablation or grinding will lead to broad particle size distribution and therefore a blurring of the properties instead of sharp characteristics.[8-11] However, employing wet chemical approaches gives colloidal NPs solutions with limited applications. As a result a lot of scientists are trying to transfer NP out of their solutions into macroscopic structures, while keeping the NP properties. Different methods have been developed each with certain advantages or disadvantages. For example co-sputtering or depositions techniques can already retain the properties of e.g. plasmonic NPs but are limited to thin films, lacking specific surface area when coming to applications such as plasmon enhanced catalysis[12-14] or sensing.[9, 15-17] One of the most promising methods is the gelation of NPs into hydrogels and subsequent supercritical drying, the so called aerogelation.[18, 19] The big advantage of this procedure is the fabrication of highly voluminous and ultra light macroscopic superstructures of NP, which still have a huge specific surface area, quantum confinement or LSPR. Yet, the aerogelation also comes with a drawback, namely being a complex procedure due to chemically adjusting the surface of the NP to obtain gels and a high energy effort to supercritical dry the gels, mostly with carbon dioxide (CO₂).

At the time of starting this thesis it can be asserted, that there is a need for optimizing techniques for the transfer of NP from their synthesis solution into superstructures. This need is reasoned on the one hand by the desire to exploit the unique properties of NP to improve catalytical, optical or sensing devices. On the other hand existing techniques can be improved by the means of simplicity, scaling for industrial application and economical factors. This thesis dedicates its focus to optimise the synthesis of aerogels to improve drawbacks of the technique, while keeping the advantages.

1.2 Nanoparticles

1.2.1 Synthesis

To assemble nanoparticles into aerogels they have to be synthesized first. In general there are two approaches to fabricate the necessary building blocks. One way is the decrease of the particle size by breaking, grinding or etching solid material.[20, 21] These procedures, which are called top down methods, have the disadvantages of a poor control over the size distribution, material composition and shape of the resulting nanoparticles. The other synthesis route is the wet chemical approach, which starts from a precursor solution and is called bottom up method. The method offers high control over particle size distribution, material composition and shape but is in return more complex compared to the top down routes. However, bottom up methods can be considered as the state of the art synthesis routes in nanochemistry, when producing quantum dots, complex heterogeneous structures or narrow particle distributions. In principal the wet chemical approach employs a precursor solution which is precipitated in a precisely controlled way. For the precipitation diverse reducing agents and ligands for stabilization as well as different precursor concentrations and varying temperatures to influence the seed growth and nucleation kinetics are applied. As example two particle syntheses shall be highlighted due to their importance for this thesis. The citrate reduction method from Enustun et al.[22] enables to reduce dissolved noble metal salt with citrate as reducing agent during boiling the precursor solutions. The resulting nanoparticles are already stabilized through the very same citrate. If a stronger reducing agent is employed, such as sodium borohydride, the reduction of the gold metal salt can be realized already at room temperature and can be transferred for silver, palladium and platinum as well. However, the synthesis in organic solvents will allow even higher control over the nanoparticles such as narrow size distributions. More sophisticated syntheses are necessary to synthesize heterostructures. For example CdSe/CdS quantum rods are fabricated by the seed mediated growth approach of Carbone et al.[23] First seeds of CdSe are synthesized by decomposing CdO in a mixture of high boiling long chained organic solvents (e.g. tri-n-octylphosphine oxide,

hexylphosphonic acid, and octadecylphosphonic acid) and subsequently adding a second precursor (e.g. tri-n-octylphosphine-selenium) in the hot precursor solution. By adjusting the time at which the solution boils at 380°C the CdSe seed size can be controlled precisely. In a second step CdS crown will be grown on the seeds, employing the very same system but with a different precursor (e.g. tri-n-octylphosphine-sulfur) and the previously synthesized CdSe seeds. Applying different ligands lead to different shapes of the nanoparticle, because of their affinity to different facets of the seed.

1.2.2 Nanoparticle Properties

Depending on the type of material and the particle size different physical properties can be observed. To understand the effects that might occur during synthesis and the assembly of the nanoparticles they shall be explained shortly. However, this work will not provide an in-depth explanation, since it is beyond the scope of this work and further reading is recommended on plasmonic and electronic properties of semiconductors.[5, 24, 25]

Three types of materials are distinguished within solid state physics, namely metals, semiconductors and insulators. In metals electrons can move freely through the crystal lattice due to overlapping atomic orbitals. Under specific conditions, the electrons on the surface can be excited by e.g. light in the visible range into collective oscillations. These oscillations (or energy) dissipate very fast due to the propagation of the oscillations over the whole bulk. However, when the crystallite size decreases into nanometer scale the induced oscillations can't propagate freely, but are restricted to the nanoparticle. This localized charge carrier density oscillations induce high scattering and absorption phenomena. Depending on the excitation energy the oscillation can be brought into resonance, and absorption and scattering increase significantly. This effect is known as localized surface plasmon resonance (also LSPR or plasmon in short) and is illustrated in figure 1.

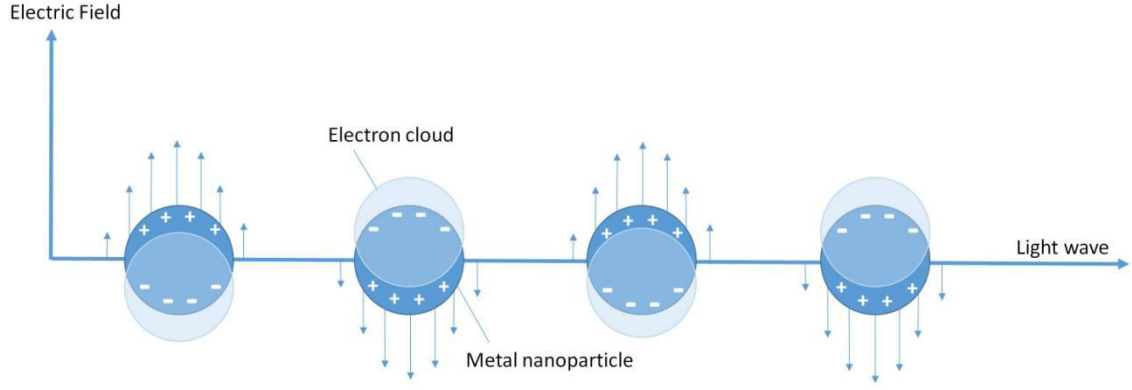


Figure 1. Illustration of the charge carrier density oscillation in metal nanoparticle induced by light. Note that the charge carrier are restricted to the nanoparticle and that the electric field is considered to be homogeneous over the whole particle (electrostatic approximation is valid)

To describe the phenomena in a quantitatively way some simplifications are necessary. If for example the particle size is much smaller than the wavelength of the light, and therefore the penetration depth of the light is bigger than the particle, the electric field over the particle can be considered as homogenous (for bigger particles the electric field will decrease exponentially with the penetration depth). With this condition, also called the electrostatic approximation, the cross section for scattering and absorption of a spherical particle can be calculated as follows:

$$\sigma_{sca}(\omega) = k^4 \cdot \frac{8}{3} \pi R^6 \left[\frac{\varepsilon(\omega) - \varepsilon_m}{\varepsilon(\omega) + 2\varepsilon_m} \right]^2 \quad (1)$$

$$\sigma_{abs}(\omega) = k \cdot 4\pi R^3 \text{Im} \left[\frac{\varepsilon(\omega) - \varepsilon_m}{\varepsilon(\omega) + 2\varepsilon_m} \right] \quad (2)$$

σ is the cross section for scattering (sca) or absorption (abs), ω is the frequency, k is the wave number, R is the radius of the sphere and ε is the dielectric function of the material of the nanoparticle and ε_m is the dielectric function of the surrounding medium (for the derivation refer to [26]). The extinction of a nanoparticle will be the sum of absorption and scattering. From the equations (1) and (2) we can derive the optical behavior of the nanoparticles. With increasing particle volume the absorption will increase linear, while the scattering increases quadratic. In other words, scattering becomes more dominant as the particle size increases. Another important finding

is, that the scattering or absorption has a maximum if the denominator becomes 0. For $\varepsilon(\omega) = -2\varepsilon_m$ the LSPR will occur and is only dependent on the dielectric functions of the material and its surroundings. However, this approximation is not completely accurate. As already mentioned for bigger particles the electrostatic approximation is not valid and the approximation was performed for spheres. Other shapes like nanorods, can have multiple LSPRs (e.g. in longitudinal and transversal direction). In addition the dielectric function for very small particles is not a constant but depends on the size. The parameters which define the energetic position of the LSPRs are particle size, shape and material.

When investigating semiconductors, the electronic structure differs from metals. Derived from the molecular orbital theory semiconductors consist of a finite but high number of overlapped atomic orbitals forming so called bands.[27] In semiconductors there are the valence band and the conduction band, which is separated from the valence band through the band gap. For bulk materials this band gap is considered to be a constant. However, when the particle size decreases, it also decreases the number of atoms and therefore the number of atomic orbitals (as illustrated in figure 2). For example, nanoparticles of the size of 3 nm will have roughly estimated around 1000 atoms (depending on the material). Thus, the “bands” become more discrete and the band gap will increase. Yet, calculation of the band gap is very extensive due to the high number of atoms for bigger particles (e.g. 10 nm range between 25.000 and 35.000 atoms depending on the material). Therefore a more adaptive approach is the concept of the effective mass of the charge carriers.[28] This concept derives from solid state theory and investigates the interaction of semiconductors when excited. An electron from the valence band will be excited into the conduction band, if a photon of the corresponding energy is absorbed. As result a positive charge, referred as hole h^+ , will be created in the valence band. Due to the dimensions of the nanoparticle, the electron and hole are restricted in their mobility, forming a bound pair also described as exciton. The average distance of these two particles is referred to as exciton bohr radius.

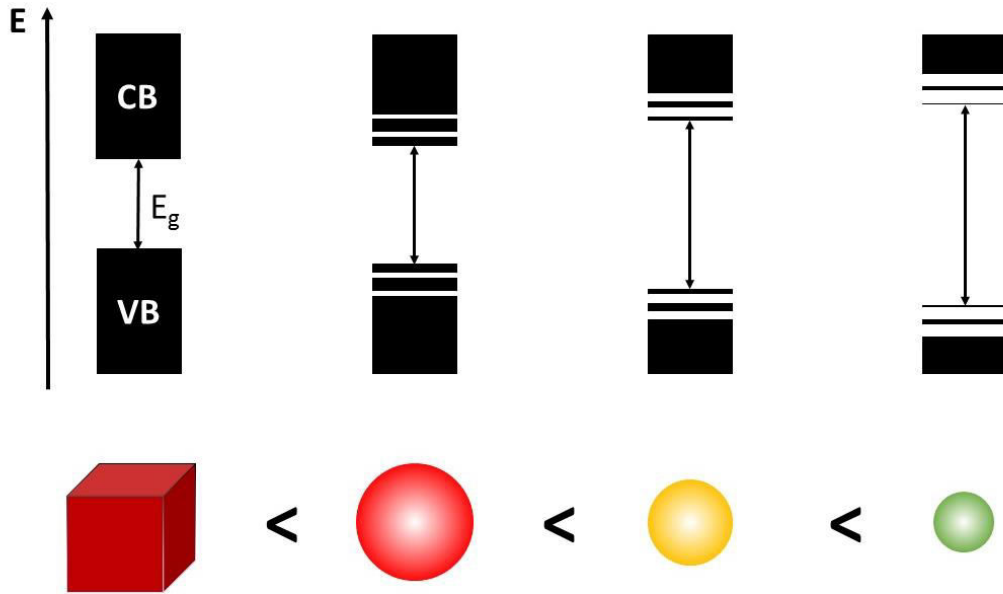


Figure 2. The quantum confinement effect illustrated on the example of CdSe. VB and CB are abbreviations for valence band and conductive band, respectively. The energy of the band gap increases with decreasing particle size and VB and CB become more discrete. The cube refers to the solid bulk material, while the spheres corresponds to CdSe seeds of the size of around 6 nm (red), around 4 nm (yellow) and around 2 nm (green).

Decreasing the particle size will further decrease the mobility and increase the energy needed to “activate” the exciton and results in a broadening of the band gap. If the exciton bohr radius is small enough, namely in the range of the particle size, these phenomena can be mathematically described with the particle in the box model. Brus[29] then combined the particle in a box model with the effective mass approach and derived the following equation to estimate the band gap in dependence of the crystallite size:

$$E_{NP} = E_{bulk} + \frac{h^2\pi^2}{2R^2} \left(\frac{1}{m_e^*} + \frac{1}{m_h^*} \right) - \frac{1.8e^2}{\epsilon R} \quad (3)$$

E is the energy of the band gap of the nanoparticle (NP) or the solid bulk material (bulk), h is the planck constant, R is the radius of the nanoparticle, m_e^* is the effective mass of the excited electron, m_h^* is the effective mass of the excited hole, e is the elementary charge and ϵ the permittivity.

1.2.3 Nanoparticle Interactions in Assemblies

The above mentioned nanoparticle properties will effect each other in assemblies and influence the physical behavior of the resulting superstructures significantly. Therefore it is crucial to understand the possible interactions between the nanoparticles, which are expected. In general possible interactions in assemblies are: plasmon-plasmon and semiconductor-semiconductor. Plasmon-semiconductor interactions are investigated recently and very complex. They can occur as e.g. near field enhancement[30] for separated nanoparticles or quenching of the exciton (also referred to as hot electron injection)[31] for nanoparticles in contact. However the plasmon-semiconductor interactions are not part of this work.

Plasmon-plasmon interactions may occur when two or more plasmonic particles are brought into defined distances to each other or even have direct contact. In the previous sections we reported already about propagating oscillations in bulk materials. If several plasmonic nanoparticles are in direct contact to each other within an assembly, the charge carrier oscillations can also propagate between the particles. Despite being restricted to the assembly, the energy of the oscillation will vary, depending on the number of particles, broadening the absorption signals.[32] This behavior can also be observed for agglomerates. However, broadening optical signals are not only related to propagating plasmons. The scattering through nanoparticles increases quadratic with increasing particle volume, as already demonstrated in equation (1). When assembling plasmonic nanoparticles the scattering will dominate the extinction spectra, resulting in high extinction especially at higher wavelength. Yet, when plasmonic properties can be brought into defined distances to each other the resonances can couple and further increase the absorption.[33, 34] A detailed investigation and explanation of such superstructure is part of this thesis and will be given in section 3.2.

Semiconductor-semiconductor interactions are also of high interest for researcher. These interactions are not necessarily restricted to superstructures but can be employed also in heterostructure synthesis or better known as band gap engineering. The structure of nanoparticles (or assemblies) is modified to influence the mobility of the exciton within the structure. For

example, by combining a semiconductor A with a specific band gap with a semiconductor B (which possess a wider band gap with an energy level of the valence band below the valence band of semiconductor A – type I structure) as illustrated in Figure 3.

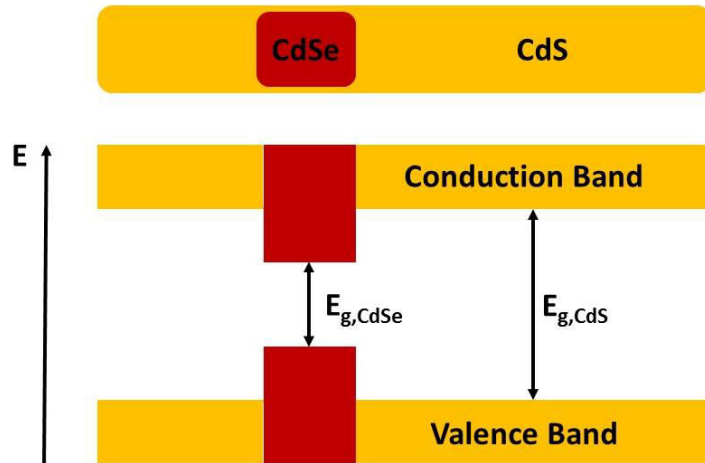


Figure 3. Band gap engineering on the example of a CdSe core CdS quantum rod. The energy gap of CdS is much bigger than CdSe and therefore excitons excited in CdS will transfer to CdSe.

As result an electron hole pair created in semiconductor B will be transferred to semiconductor A because of the lower energy of the band gap. Subsequent, the average distance of the electron hole pair and the non-irradiative recombinations decrease (because lower energy band gaps enable less non-irradiative processes). The specific combination of semiconductor materials is often reported as band gap engineering and can be of type I materials, such as the example or type II. Such heterostructures possess high quantum efficiency and are realized as core-shell quantum dots[35, 36] or quantum rods[23] and even more sophisticated structures like double quantum well quantum dots.[37] Tailoring nanoparticle heterostructures is an extensively studied field within the nanochemistry and further explanations would be out of scope of this thesis. Observations of influencing the exciton mobility could be also made in assembled nanoparticle superstructures. Sánchez-Paradinas et al.[38] demonstrated delocalized excitons in quantum rod aerogels proofing the influence of nanoparticle assemblies on their physical properties.

1.3 Aerogels

1.3.1 Fabrication Techniques

Following the IUPAC Definition, aerogels are “gels comprised of a microporous solid in which the dispersed phase is a gas”.[39] Since this definition is somewhat abstract, it shall be explained in more detail. The main volume fraction of an aerogel is pore volume which is usually filled with air. The solid material forms a filigree and well interconnected network building the macroscopic object. Consequently aerogels have properties such as low density, high specific surface areas as well as low thermal conductivity due to air as main component. Aerogels can have further properties such as transparency (see figure 1) or catalytic activity depending on the material of the filigree network.[40-42]

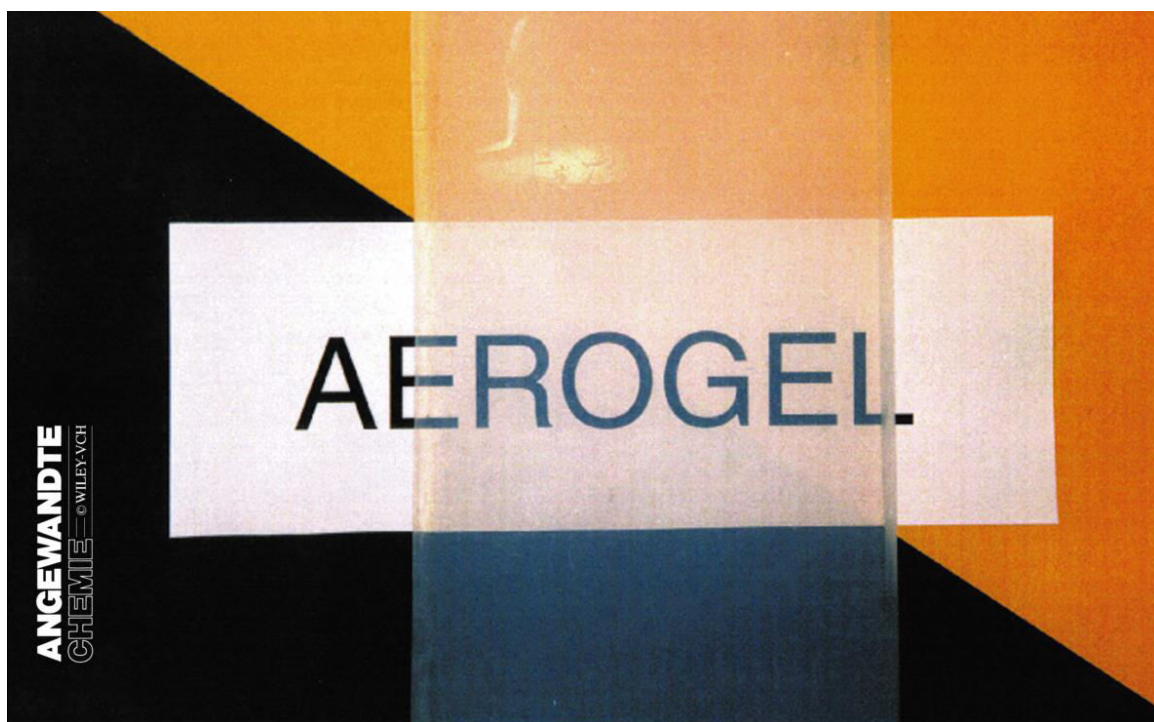


Figure 4. Transparent silica aerogel from[40]. Reprinted with permission of Wiley-VCH.

While different materials and properties of aerogels will be discussed in later sections, this first section will show the general possibilities to fabricate aerogels. The very first aerogel was fabricated by Kistler in 1931.[18] He postulated that it would be possible to replace the liquid

within jellies with a gas without the jelly suffering from shrinkage. For this hypothesis he utilized the sol-gel process to fabricate jellies e.g. of silica, alumina, etc. This first step is already important as a filigree network of solid material will only be obtained if the gel formation out of the precursor occurs slow. To be more specific the growth rate of the nanoscaled particles which are formed within the solution has to be at the same speed or slower as the crosslinking between the NPs. If the growth rate is faster, dense precipitates instead of voluminous jellies will be fabricated. This step is very time consuming and Kistler took more than one week to prepare one gel.[43, 44] He then exchanged the liquids of the jellies to suitable ones with a low critical point like ethanol or ether and dried them supercritical in an autoclave. Due to the raise of temperature and pressure over the critical point the fluid is “converted directly into a permanent gas without discontinuity”.[18] Capillary forces, which usually occur at evaporation of liquids, can be prevented because of the supercritical drying, thus enabling the exchange liquid to gas in jellies or gels without shrinkage. The process is also illustrated in figure 2. If the drying of the jelly or “wet gel” is performed under standard conditions the resulting monolith would be a xerogel, which has significant lower porosity and specific surface area compared to aerogels. The difference to aerogels is the strong shrinkage during the drying process because of the capillary forces while the liquid evaporates.[40]

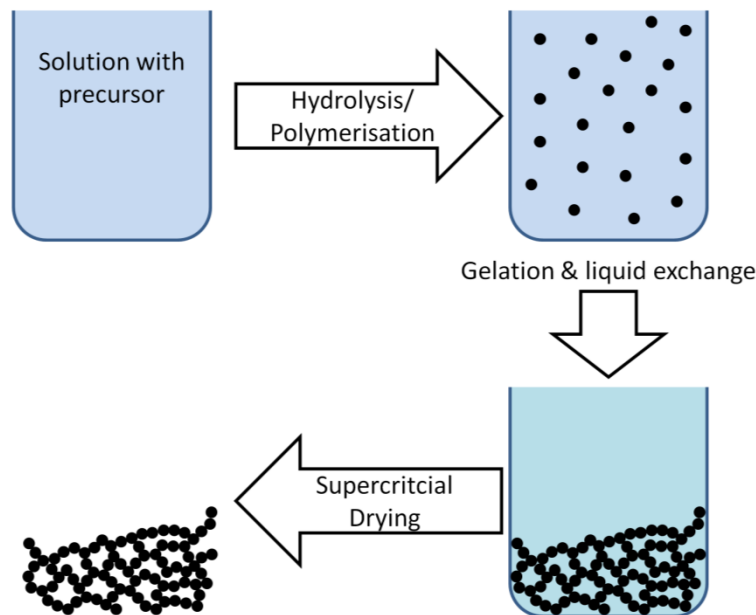


Figure 5. Illustration of the sol-gel process with subsequent aerogel formation. A precursor solution (e.g. of a metal alkoxide) is hydrolyzed resulting first in the formation of small particles and later on in the formation of gels. The liquid is exchanged and the gel supercritical dried to obtain the aerogel.

Kistler fabricated inorganic aerogels of silica, alumina and tungstic oxide as well as organic aerogels of agar, gelatine and cellulose.[18] While the process fits perfect for the synthesis of metal oxide aerogels such as the oxides of silicon and aluminium, it is difficult to transfer this process to other inorganic materials. Yet NPs of noble metals or semiconducting materials show far more interesting properties due to the occurrence of plasmons or fluorescence. Therefore adjusted fabrication procedures were necessary. However, since the sol gel process utilises hydrolysis and polymerisation it was only logical that further organic aerogels were synthesized. In 1989 the work group around Pekala published the first resin-based aerogels by the polycondensation of resorcinol with formaldehyde (RF aerogels).[45] A subsequent treatment of these RF aerogels at high temperatures under inert atmosphere lead to the first carbon aerogels. And soon silica and RF aerogels were modified to improve their mechanical properties by e.g. crosslinking through the group of Leventis.[46, 47] Starting from 2004 until 2007 the group around Brock developed and published a new procedure, which allowed the aerogel formation for NP out of stable colloidal solutions.[19, 48-50] The mechanism of this method was intensely studied and aroused wide

interest in the community of NP research. They first synthesized metal chalcogenide NPs and capped them with thiol ligands. In this way they obtained stable colloids, which they subsequently destabilized. By a controlled ligand removal they induced the gelation process. The ligand removal could be achieved via chemical oxidation or photochemical oxidation of the capping agents. Afterwards the solution of the gel is exchanged to remove oxidation agents and to employ a liquid with a low supercritical point. In literature different gel types can be found like e.g. hydrogel or acetogel. It refers to the liquid in which the gel is kept and gels which are kept in water or acetone will be described as hydrogels or acetogels, respectively. In principle this procedure can be applied to all colloidal systems and can be considered as state of the art preparation technique for aerogels built from NPs. It also enables the synthesis of aerogels that partly retain the properties of the employed NP building blocks (see next section). However, for each system the surface chemistry has to be adjusted. Each employed ligand requires a proper removal technique and in addition the controlled destabilisation needs time. Up to now, many groups are searching for new ways to start and control the gelation. There are reports on the gelation start through centrifugation,[51] heating,[52, 53] irradiation with light in the visible or UV range.[49] Liquid exchanges are performed multiple times in order to remove liquids with high critical points completely, since they could interfere in the drying process. Also all fabrication steps demand a certain level of handling to not destroy the very fragile hydrogel. Closing on fabrication techniques it should be stated that there are methods to obtain aerogels from sols or colloidal NP solution. Yet, they are complex multi step processes and time consuming which makes a scale up for industrial application difficult and expensive.

1.3.2 Materials & Properties

All aerogels have some common properties as previously mentioned. They are in detail: low density, high specific surface area as well as low thermal conductivity. They can be directly derived from the principal nature of aerogels consisting of a filigree network of matter and mostly pores filled with air. However since there are many materials that can be employed in aerogels, there are also many aerogels and properties can vary enormously between each other. Especially

when coming to NP based aerogels, and the NPs itself show unique properties like e.g. localized surface Plasmon resonances[54, 55], photoluminescence[56] or phonon scattering.[57] However, this section won't give a complete overview over all employed aerogel materials, since there are more than 10.000² publications in the last 10 years alone. Its aim is to give a brief introduction which material types are synthesized and which properties can be expected of such aerogels. In general literature divides between single component aerogels and multicomponent aerogels. Yet this separation is not distinct since alloyed NP of CdSe/CdS or Pt/Ag are to be found in the single component section. It refers more to the employed starting material if there was one component (e.g. CdSe/CdS quantum dots) applied for aerogel fabrication or multiple components (e.g. quantum dots with noble metal NP). Within this classification there are also different materials employed ranging from (noble) metals, metal oxides, metal chalcogenides, organic particles to carbon.

1.3.3 Metal Oxide Aerogels

Metal oxide aerogels are the longest known types of aerogels and also the probably most applied ones too. Starting in 1931 Kistler demonstrated the possibility for silica and alumina aerogels as well as others. Beside, being unique in appearance and properties there was no direct application and therefore interest in his findings were low. Maybe this was reasoned by the high time consumption for the gel preparation. Faster reactions only lead to non voluminous precipitates. In 1960s the work group around Teichner expanded the idea from Kistler by using alkoxy silanes (e.g. tetraethoxysilane (TEOS)) as precursor in the sol-gel process and performing the reaction in methanol as solvent. This allowed a faster synthesis of the gels and avoided additional solvent exchanges. They were able to synthesize also titania, zirconia as well as other metal oxide aerogels by employing metal alkoxides as precursors .[58] Brinker et al. then introduced a two step synthesis in which the precursors were prehydrolyzed and in the second step a defined amount of aqueous acid or base was added to start gelation.[59] This enabled the group of Hrubesh et al. to fabricate aerogels with a broader density range.[60] The properties of metal oxide aerogels are

² SciFinder request from 18.10.2016 with the keyword „aerogel“ gives 10.195 article in the past 10 years

fascinating and soon industry started fabrication on a technical scale. Since alkoxy silanes are very expensive BASF, Henkel or Hoechst developed adjusted synthesis routes by replacing the alkoxy silanes with sodium silicates.[61-64] Many of the materials i.e. silica aerogels have a high transparency as it is shown in figure 1. The density of these materials are in the range between 0.003 and 1 g cm^{-3} while the specific surface area can be up to $1600 \text{ m}^2 \text{ g}^{-1}$ depending on the synthesis route and of course the employed metal oxide.[40, 42, 60, 65, 66] The thermal conductivity for silica aerogels was determined in the range of 0.017 to $0.021 \text{ W m}^{-1} \text{ K}^{-1}$ (bulk silica would be $1.38 \text{ W m}^{-1} \text{ K}^{-1}$).[40, 67] It is extremely low and is visualized in figure 3. Summarizing metal oxide aerogels are well investigated, can be synthesized with a high level of control, and silica aerogels already found their way into industrial application.

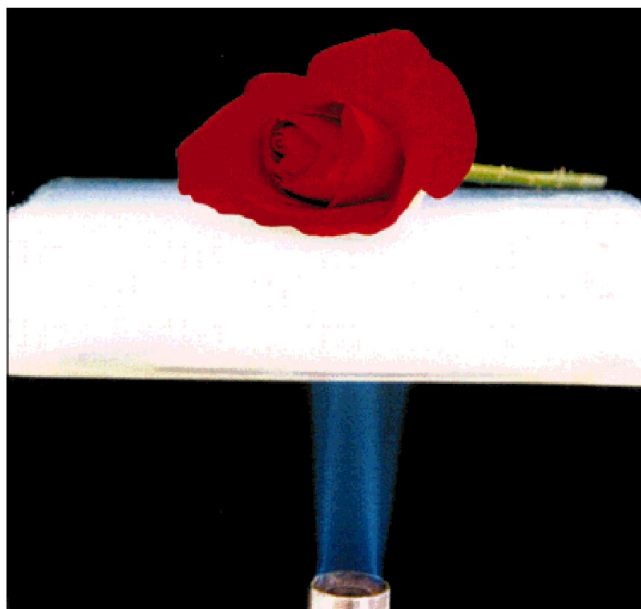


Figure 6. Silica aerogel with extremely low thermal conductivity from[40]. Reprinted with permission of Wiley-VCH.

1.3.4 (Noble) Metal Aerogels

Although there were different attempts to fabricate metal aerogels it was not achieved until 2009. Literature reported so far of metal doped oxides or carbon based aerogels.[65, 68, 69] The first reported pure (noble) metal aerogels were synthesized in 2009 by the workgroup of Eychmüller.[70] They were able to produce aerogels from gold, silver and platinum NP. NPs were

obtained by a modified citrate reduction method and subsequent destabilizing the colloidal solution in a controlled way with hydrogen peroxide lead to voluminous hydrogels. Supercritical drying of the obtained hydrogels leads to voluminous monoliths. The obtained monoliths with densities of 0.016 g cm^{-3} and specific surface areas of around $48 \text{ m}^2 \text{ g}^{-1}$ (see figure 4).[70] This surface area seems low, but when concerning metal and noble metal aerogels one has to consider the significantly high atomic weights of the corresponding elements, that result in low specific surface areas.

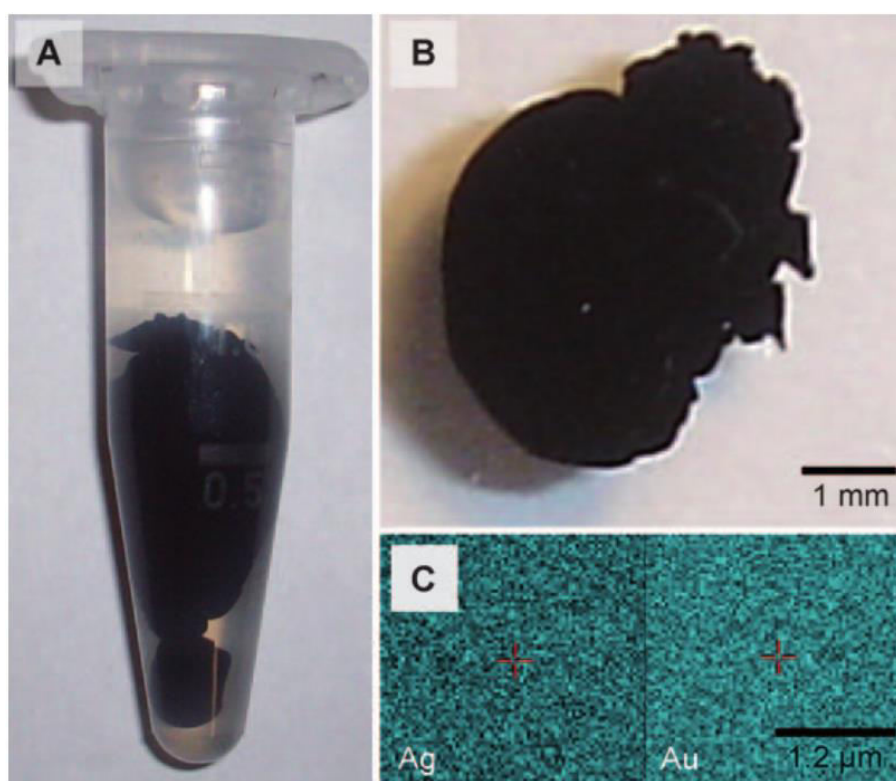


Figure 7. First noble metal (A) hydrogels and (B) aerogels made of gold and silver and (C) the elemental distribution from[70] Reprinted with permission of Wiley-VCH.

However unique properties of the (noble) metal NPs, such as localized surface plasmon resonance (LSPR) could not be retained in the final superstructure. Around the same time the workgroup of Leventis et al. synthesized metal aerogels by the approach of nanosmelting.[71] For this technique metal oxides were gelled and subsequently pyrolyzed to reduce the metal oxides to their respective metal. Aerogels made of Co, Ni, Sn, Cu and Fe were fabricated and it could be shown that such

aerogel had huge specific surfaces up to $163 \text{ m}^2 \text{ g}^{-1}$.^[71] However the technique is limited to materials that can be reduced at high temperatures and through the need of carbon the aerogels are mixed materials in the end. Furthermore Eychmüller and his coworkers reported on the attempt of in-situ reduction of noble metal precursor for direct gel formation similar to the original sol-gel method from Kistler. They fabricated β -cyclodextrin modified Pd aerogels with specific surface area up to $92 \text{ m}^2 \text{ g}^{-1}$ which are up to date the highest reported surfaces for pure noble metal aerogels.^[72-74] Yet some problems remain. The existing techniques won't enable the desired degree of control over metal aerogels e.g. controlling plasmon-plasmon interactions. When coming to the accessibility of particle surfaces and retaining the NP properties, such as LSPR, within the aerogel it needs to be improved by the means of employing less ligands or prevent the occurrence of interparticle interactions.

1.3.5 Metal Chalcogenide Aerogels

Already in 1997 first attempts were made by the group of Gacion et al. to synthesize metal chalcogenide aerogels.^[75] They employed CdS NPs and created wet gels using the sol-gel process. Yet they did not dry the gels supercritically but under ambient conditions and therefore obtained xerogels of CdS. The first aerogels consisting of metal chalcogenides were reported in 2005 by the workgroup of Brock et al.^[19] Here, stable colloids of CdS, CdSe, ZnS NPs were synthesized and subsequently capped the NPs with thiol groups. The capping of the NPs was then slowly removed by chemical oxidation (for CdSe photochemical oxidation) to induce the gelation process (see figure 5).

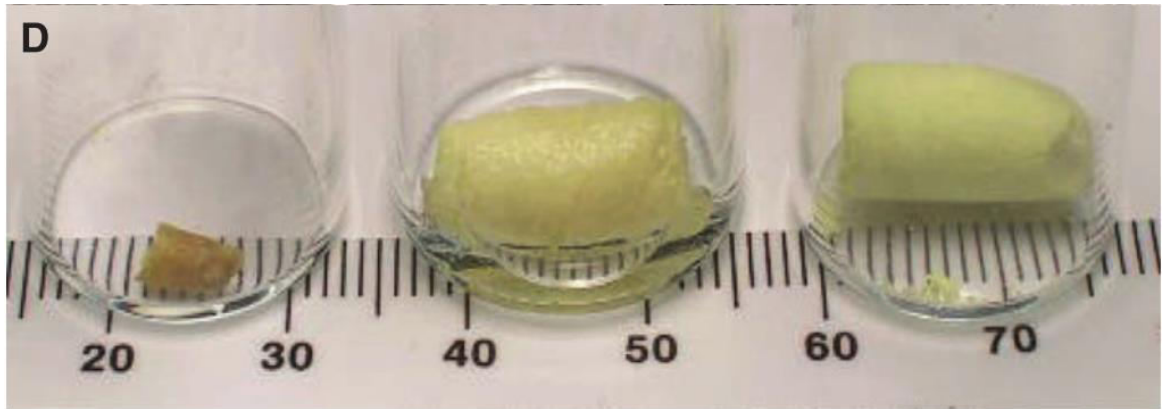


Figure 8. Comparison between a xerogel (right), a wet hydrogel (middle) and a supercritically dried aerogel of CdS from [19]. Reprinted with permission of the American Association for the Advancement of Science.

However it is not the only way to produce metal chalcogenide aerogels. The very same group employed the thiolysis of metal precursor to obtain GeS aerogels[76] and another route would be the crosslinking between small metal chalcogenide clusters as reported by Bag et al.[77] Finally all gels were supercritically dried with CO₂. All these synthesis routes lead to a wide variety of metal chalcogenide materials such as PbS,[78] CdTe,[79] ZnS,[19] GeS[49] etc. with interesting properties. The fabricated CdS and ZnS aerogels of Brock had densities of 0.07 and 0.34 g cm⁻³ and specific surface areas ranging from 120 up to 250 m² g⁻¹ and the other metal chalcogenides are in the same range.[19] Yet the most fascinating property were strongly emitting aerogels of e.g. CdSe/ZnS[80] or CdTe[79]. Just recently it could be shown that the radiative lifetimes within CdSe/CdS quantumrod aerogels were extremely prolonged compared to their colloidal solution (see figure 6).[81] This might be a hint that the pathways of electrons and holes in assembled superstructure can be modified with direct effects on the lifetime of electron/hole pairs and the quantum efficiency of the radiative processes.[81]

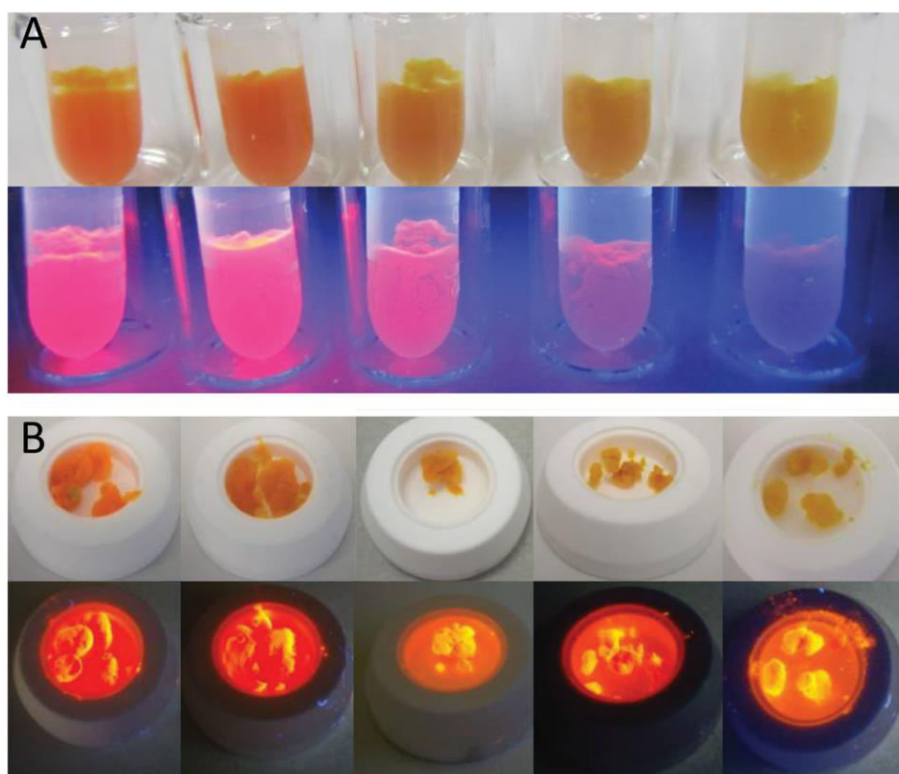


Figure 9. Photographs of highly luminescent CdSe/CdS (A) hydrogels and (B) corresponding aerogels under daylight (top) and uv-light (bottom) from [60]. The effect of increasing oxidizing agent (H_2O_2) can be observed from left to right. Reprinted with permission of Wiley-VCH.

Naskar et al. reported on CdSe platelets with a CdS crown, so called quantum wells, which exceeds >10% quantum yield in the final aerogel.[82] Closing on metal chalcogenide aerogels the techniques allows a proper transfer of the colloidal NP into assembled superstructures while retaining most of the properties of the single building blocks to certain extend. Yet they are still complex multi step procedures which are time consuming.

1.3.6 Organic and Carbon Aerogels

Reporting on organic and carbon aerogels is an especially wide research area with outstanding properties such as density, surface area as well as adsorption behavior. Or to express the properties in a more popular way: It is the world record section. Since the formation of organic and carbon aerogels is very close related to each other they shall be discussed together in this section. In principal there are two strategies for the fabrication. The first approach would be the cellulose

based aerogel. It was developed by Kistler around the same time as the silica aerogels.[43] It exploits the dissolution and the coagulation of cellulose in different liquids. The second approach would be the resin based aerogels, in this case a resin precursor is crosslinked in a catalyzed polycondensation reaction. The first resin-based aerogel was reported by the group of Pekala et al. by starting a polycondensation reaction of resorcinol with formaldehyde (RF aerogel).[45] Short after that report the first carbon aerogels were synthesized by the same group. They treated the synthesized RF aerogel at high temperature (between 800 and 1200°C) under an inert atmosphere to carbonize the RF aerogel.[83] A complete different synthesis for carbon aerogels are hard templating methods. Here a highly porous inorganic (mostly silica or zeolites) template is infiltrated with a carbon precursor (e.g. furfuryl alcohol) and after carbonization the template is dissolved.[84, 85] Carbon aerogels synthesized via hard templating are characteristic for their regular mesoporosity. In general, organic and carbon aerogels show densities below 0.1 g cm^{-3} and specific surface areas up to $720 \text{ m}^2 \text{ g}^{-1}$. [45] Close related to the group of carbon aerogels are the aerographenes. These materials consist of carbon nanotubes that were crosslinked with graphene oxide sheets. Densities of below 0.16 mg cm^{-3} were achieved, being the least dense solid material known at this moment (see figure 7).[86]



Figure 10. The currently least dense solid material known: “Ultra Flyweight Carbon Aerogel” from[86]. Reprinted with permission of Wiley-VCH.

The specific surface area of this material is compared to its density with around $270 \text{ m}^2 \text{ g}^{-1}$ rather low. To obtain higher specific surface areas carbonized RF aerogels were further activated with CO_2 . [87] However the highest reported specific surface areas were carbon aerogels after the hard templating method employing zeolites as templates. So far surfaces up to $3800 \text{ m}^2 \text{ g}^{-1}$ were reported surpassing even the highest surfaces of silica aerogels. [88] The employment of preformed structures not only allows huge surface areas but also generates a hierarchical pore system which can be optimized for transport behavior within the aerogel and separation processes. In addition these materials show high absorption capacities at high absorption rates. For example aerographene shows 68.8 to $720 \text{ g g}^{-1} \text{ s}^{-1}$ absorption rates depending on the absorbed liquid or material. [86] At the same time carbon and organic aerogels are mechanically strong unlike the pure metal or metal chalcogenide aerogels. [86] Like the metal oxide aerogels the organic and carbon aerogels are known for a long time now and well investigated. Properties of resulting aerogels can be controlled very well.

1.3.7 Multi Component Aerogels

As shown in the previous sections, there are already a wide range of properties that the corresponding aerogels possess. However through combining multiple components further interactions and therefore new properties can occur. The right combination of components can also eliminate drawbacks from aerogel properties i.e. mechanical stability. Yet it is far from easy to combine different components in one aerogel especially since the crucial crosslinking or gelation step needs to be adjusted very carefully. This section will present the most investigated or promising concepts for multi component aerogels namely inorganic-organic hybrid materials, metal-metal oxide and metal-semiconducting (i.e. metal chalcogenides) NPs.

The term inorganic-organic hybrid aerogels is unspecific. When talking about these materials, in literature inorganic is often related, but not limited to ceramic components such as silica, alumina, etc. [40] Especially since silica is the oldest and best investigated component for aerogels. [18, 40] The main reasons for synthesizing hybrid materials are, beside broadening the spectrum of possible

aerogels and their properties, to adjust specifically properties such as hydrophobicity or elasticity by functionalizing surface groups of silica (see figure 8).[46, 89-92]

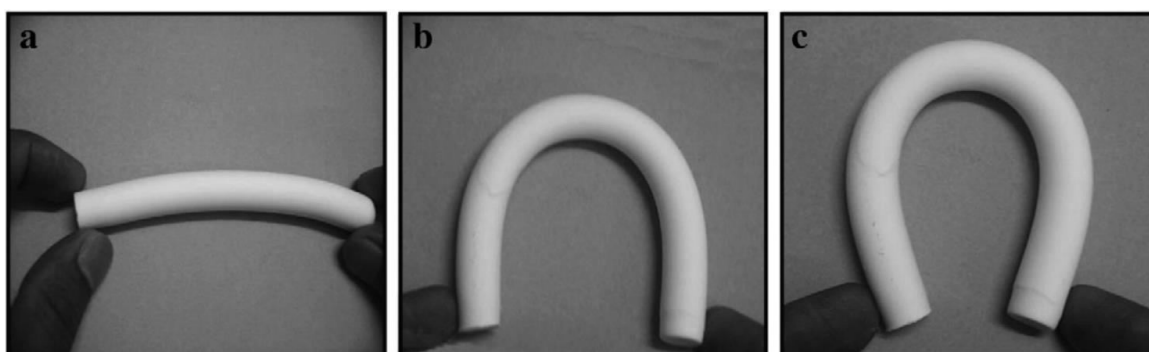


Figure 11. Increasing the elasticity of silica aerogels by employing mixtures of alkoxysilanes and organosilanes as precursor from[91] Reprinted with permission of Elsevier.

It also improves the mechanical stability. Additionally the basic properties such as low density or high specific surface are retained. A general synthesis route is the addition of organic linker molecules such as dyes, enzymes etc. in the sol before the gelation. Depending on chemical interactions between inorganic precursor and organic molecule the aerogel network can be a matrix embedding the inorganic part, an interpenetrating network of both components or a modified inorganic network with functionalized groups. Reported organic components for silica aerogels are poly(2-vinylpyridine) as polymer matrix and N,N-dimethylacrylamide for interpenetrated networks.[93, 94] The modification of surface groups is reported several times and can be performed with alkoxysilanes in which one or more groups are replaced by for example alkyl or aryl groups.[46, 89, 95] There are also approaches which are very similar to metal organic frameworks. Here, organic spacer are brought in between small silica cluster and depending on the employed spacer the specific surface can be increased.[96] Density and specific surface in general depend on the composition of components but are in the similar range as the single component aerogels.[97-100]

Metal-metal oxide materials have a very high potential for application. Combining the advantages of the high specific surfaces and often an “inert” nature against chemical reactions of metal oxide

(i.e. silica) with the catalytic properties of metal NPs promises a new generation of catalysts, filter material or in medical applications. The fabrication can be performed in different ways. The already synthesized metal oxide aerogel can be impregnated with metal salt precursors and subsequently treated under reducing conditions in H₂ atmosphere.[69, 101] Since the conditions at the supercritical drying can be already reducing, especially if hydrogen is mixed in the autoclave, another option would be to incorporate metal salts already in the sol-gel process.[102-105] Already in 1937 Foster and Keyes synthesized with Pt/SiO₂ and Ni/SiO₂ the first metal-metal oxide aerogels in that way.[68] Currently these mixed aerogels are also fabricated by employing colloidal solution of different components and co-gelate them.[106-108] Properties of the combined materials are often very similar. For example silica aerogels with metals (Pt, Mg, Ti or Cu) have reported specific surfaces in the range of 70 to 700 m² g⁻¹ based on the total aerogel mass.[69, 101-103] Close related to the metal-metal oxide aerogels are the mixed metal oxides. They are easily fabricated over the sol-gel process as long as the condensation rates are similar. If the reaction rates differ too much, phase segregation may occur.[109, 110] There was also the effect of “core-shell” structure observed, when the slower reacting component forms a shell around the sol particles of the faster reacting component.[111]

The group of metal-metal chalcogenide aerogels is the most recent field of aerogels and up to now there are barely reports on mixed metal-semiconductor aerogels. However, from a physical point this concept is the most interesting one. The idea is to employ semiconducting NPs with a high efficiency of creating electron-hole pairs with long lifetimes and combine them with metal particles (e.g. platinum). Through the higher Fermi level of the metal, the excited electron of the semiconductor is more likely to transfer to the metal instead of going back to its ground state via irradiative or non-irradiative processes. With this excited electron (sometimes also referred as hot electron) chemical reactions could be catalyzed on the surface of the metal. For that concept short pathways between metal and semiconductor material are absolutely necessary and aerogelation is one possible method of obtaining macroscopic objects which fulfill these requirements. So far, there are reports on the cogelation of a metal and a semiconducting NP for the system Ag with

CdTe by the Eychmüller group[112] (see figure 9) and Ag with CdSe by the Arachchige group.[113]

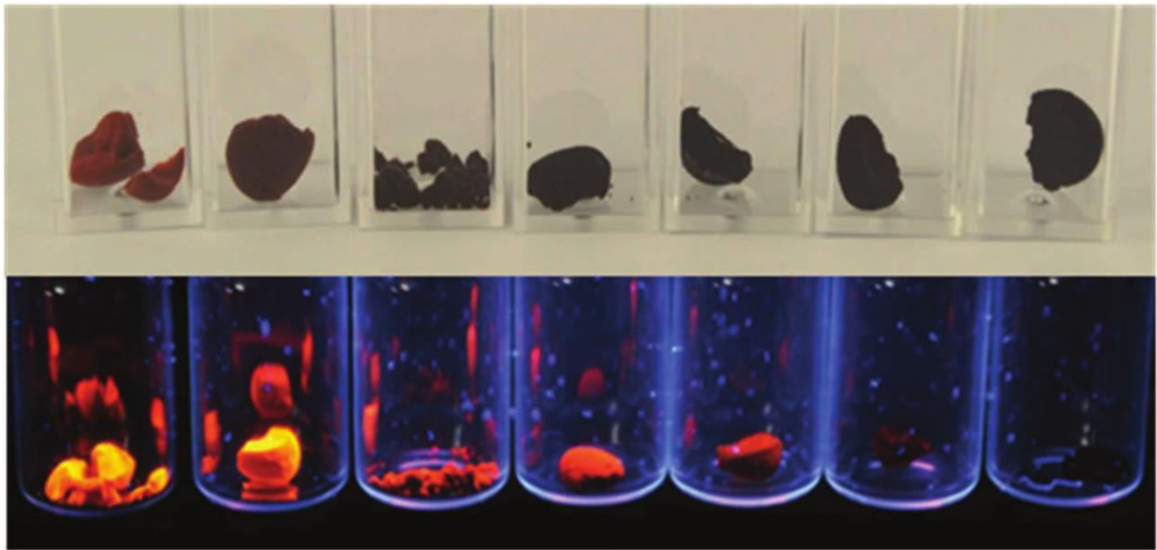


Figure 12. Mixed aerogels from Au and CdTe under daylight (top) and UV-light (bottom) with increasing Au ratio (from left to right) from [112]. Reprinted with permission of Wiley-VCH.

1.4 Cryogels as Alternate Synthesis Route for Highly Porous Assemblies

The most crucial part in fabricating aerogels is the transfer of the voluminous network out of its solution to obtain a dry gel. When the solution evaporates, usually capillary forces destroy the filigree network leading to strong shrinkage of the gel. Kistler solved the problem by supercritically dry his gels and therefore avoid capillary forces due to evaporation. However, this is not the only possibility to avoid the evaporation of a liquid. When water is frozen (ice temperature below 0°C) and the ambient pressure is decreased below 6mbar, a liquid phase of water won't exist anymore. Instead if energy is applied and the temperature rises again, the ice crystal will sublime. This method is already known as freeze drying and is widely applied in life science. Freeze drying should be able to dry gels without shrinkage. However, reports on freeze dried materials always presented powders and no voluminous structures.[40, 114] This is most likely due to one big problem. Ice crystals expand during freezing and when a hydrogel is completely frozen, the filigree network will eventually be destroyed through the ice itself. Moor et al.[115] revealed that the ice crystallite size depends strongly on the freezing velocity. However even with their highest freezing rates living tissues still suffered damage from the freezing process. Therefore a preformed structure will always suffer damages when frozen over. Yet, there is another possibility which exploits the ice crystal formation. Zhang et al. [116] extensively investigated the interactions between nanoparticles and freezing aqueous solutions and came up with a model which describes the particle behaviour. Depending on the size nanoparticles are pushed away from the growing ice crystal or immobilized within the ice crystal (see figure 10).

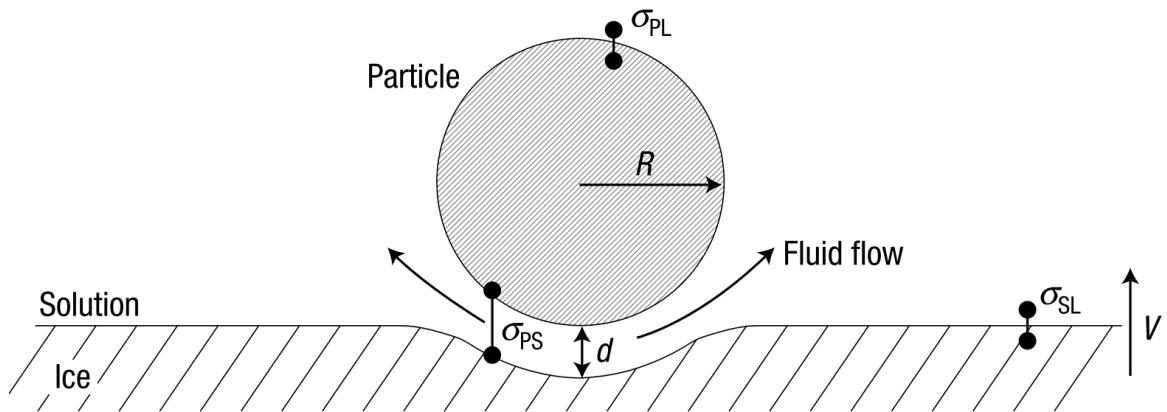


Figure 13. Qualitative theoretical framework for the inclusion of particles in ice. σ_{SL} is the interfacial free energy between the solid and the liquid phase, and σ_{PS} and σ_{PL} are the surface free energies between the particle and the solid phase and the particle and the liquid phase, respectively. Reprinted with permission of Nature Publishing group.

Thanks to this model a critical ice growth velocity can be derived. At this velocity nanoparticles become overgrown by the ice crystal and can be expressed as:

$$v_c = \frac{\Delta\sigma a_0}{3\eta R} \quad (4)$$

v_c is the critical ice growth velocity, $\Delta\sigma$ is the balance of the surface forces at the ice/solution/particle boundaries, a_0 is the average intermolecular distance, η is the dynamic viscosity of the fluid and R is the radius of the nanoparticle. If the freezing velocity and the nanoparticle size are adjusted accordingly the nanoparticles can be assembled by the ice itself whereas the ice crystals act as a template. Zhang et al.[117] even discovered the possibility of aligning assemblies if the freezing gradient is directed. However he could only show such behaviour for polymers but in principal this techniques should also apply for any other nanoparticles.

1.5 Applications

The properties of aerogels excel their respective bulk material properties often by more than a magnitude. The specific surface area is a good example by increasing several magnitudes between aerogel and bulk material. This can be exploited for various applications especially in catalysis. There are many reports on catalytic properties of aerogels. For example for noble metal aerogels as electrocatalysts,[118] nitrogen doped carbon aerogels for oxygen reduction reaction[119] or mixed metal oxides as catalyst for hydrogenation[120] or car exhaust catalyst.[41] There are plenty of reviews which list possible application of aerogels in (electro)catalysis.[40, 118, 121, 122] The porosity and surface makes aerogels also suitable filter and absorbens material. Espacially carbon[121, 123] and silica aerogels.[124, 125] The most popular application of a silica aerogel by the means of public perception was for stardust collection (see figure 11).[126] In this stardust collector silica aerogels acted as filter material, which could resist the high velocity of the space dust, slowing it down and captivate it. Due to the low weight it was better suited than any other material.

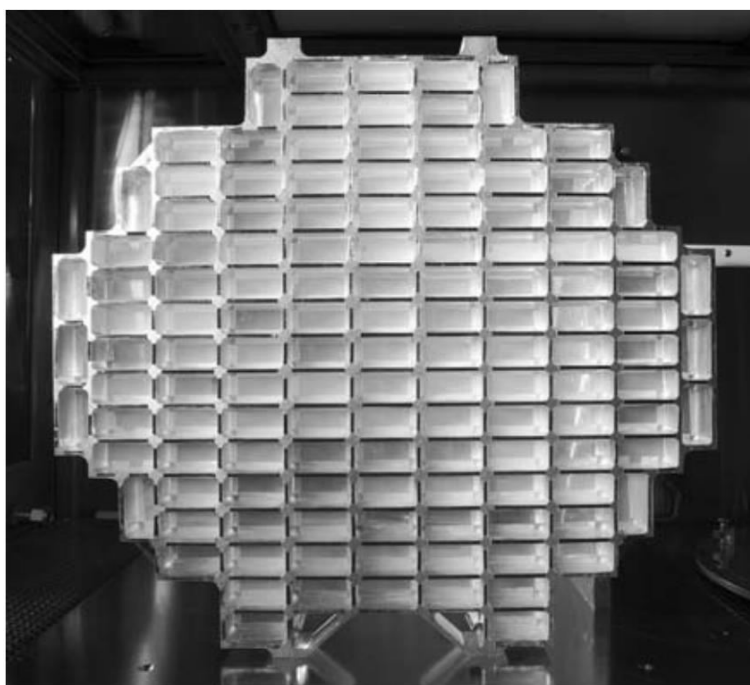


Figure 14. Image of stardust cometary particle collector made of silica aerogels from [127]. Reprinted with permission from Springer Science + Business Media, LLC 2006.

For carbon aerogels there are also reports for the application as battery electrodes or even supercapacitors.[121, 128] Silica aerogels with their low thermal conductivity and high optical transparency are employed as air-glass or thermal insulation material (see figure 12).[129, 130]



Figure 15. Super-insulating aerogel glass developed within an European project (ENK6-CT-2002-00648) for energy efficiency from[130] Reprinted with permission from Springer Science + Business Media, LLC 2006.

Aerogels can be even applied for noise cancellation in acoustics.[40, 131] Although nearly every report on aerogels lists possible application, they are not often found in the everyday life or within industrial technology. The main reason for that is that aerogel fabrication is complex, time consuming and therefore expensive. However, taking into account that the intensive research of aerogels started around 20 years ago, there surely will be optimized methods or even development of new procedures which overcome current existing problems.

1.6 References

- [1] Buffat, P.; Borel, J. P., Size effect on the melting temperature of gold particles. *Physical Review A* **1976**, 13, (6), 2287-2298.
- [2] Rycenga, M.; Cobley, C. M.; Zeng, J.; Li, W.; Moran, C. H.; Zhang, Q.; Qin, D.; Xia, Y., Controlling the synthesis and assembly of silver nanostructures for plasmonic applications. *Chem. Rev. (Washington, DC, U. S.)* **2011**, 111, (6), 3669-3712.
- [3] Shang, L.; Dong, S.; Nienhaus, G. U., Ultra-small fluorescent metal nanoclusters: Synthesis and biological applications. *Nano Today* **2011**, 6, (4), 401-418.
- [4] Huang, C.-C.; Yang, Z.; Lee, K.-H.; Chang, H.-T., Synthesis of Highly Fluorescent Gold Nanoparticles for Sensing Mercury(II). *Angewandte Chemie International Edition* **2007**, 46, (36), 6824-6828.
- [5] Haug, H.; Koch, S. W., *Quantum Theory of the Optical and Electronic Properties of Semiconductors*. World Scientific: 1994.
- [6] Norris, D. J.; Bawendi, M. G., Measurement and assignment of the size-dependent optical spectrum in CdSe quantum dots. *Physical Review B* **1996**, 53, (24), 16338-16346.
- [7] Bullis, K., Quantum Dots Produce More Colorful Sony TVs. *MIT Technology Review* **2013**.
- [8] Feng, X.; Hu, M. Z. In *Ceramic nanoparticle synthesis*, 2004; American Scientific Publishers: 2004; pp 687-726.
- [9] Murphy, C. J.; Sau, T. K.; Gole, A. M.; Orendorff, C. J.; Gao, J.; Gou, L.; Hunyadi, S. E.; Li, T., Anisotropic metal nanoparticles: synthesis, assembly, and optical applications. *J. Phys. Chem. B* **2005**, 109, (29), 13857-13870.
- [10] Sakamoto, M.; Fujistuka, M.; Majima, T., Light as a construction tool of metal nanoparticles: Synthesis and mechanism. *J. Photochem. Photobiol., C* **2009**, 10, (1), 33-56.

- [11] Dahl, J. A.; Maddux, B. L. S.; Hutchison, J. E., Toward Greener Nanosynthesis. *Chem. Rev. (Washington, DC, U. S.)* **2007**, 107, (6), 2228-2269.
- [12] Wadell, C.; Antosiewicz, T. J.; Langhammer, C., Optical Absorption Engineering in Stacked Plasmonic Au-SiO₂-Pd Nanoantennas. *Nano Lett.* **2012**, 12, (9), 4784-4790.
- [13] Amendola, V.; Scaramuzza, S.; Agnoli, S.; Polizzi, S.; Meneghetti, M., Strong dependence of surface plasmon resonance and surface enhanced Raman scattering on the composition of Au-Fe nanoalloys. *Nanoscale* **2014**, 6, (3), 1423-1433.
- [14] Wang, J.; Xu, W.; Wu, J.; Yu, G.; Zhou, X.; Xu, S., Plasmon-enhanced catalysis of photo-induced charge transfer from TCNQF₄⁻ to TCNQF₄²⁻. *J. Mater. Chem. C* **2014**, 2, (11), 2010-2018.
- [15] Wang, C.; Liu, R.; Zhang, W.; Wang, Y.; Xu, K.; Yue, Z.; Liu, G., Multichannel scan surface plasmon resonance biochip with stationary optics and baseline updating capability. *J. Biomed. Opt.* **2013**, 18, (11), 115002/1-115002/4.
- [16] Jain, P. K.; Huang, X.; El-Sayed, I. H.; El-Sayed, M. A., Noble Metals on the Nanoscale: Optical and Photothermal Properties and Some Applications in Imaging, Sensing, Biology, and Medicine. *Acc. Chem. Res.* **2008**, 41, (12), 1578-1586.
- [17] Homola, J.; Yee, S. S.; Gauglitz, G., Surface plasmon resonance sensors: review. *Sens. Actuators, B* **1999**, 54, (1-2), 3-15.
- [18] Kistler, S. S., Coherent expanded aerogels and jellies. *Nature (London, U. K.)* **1931**, 127, 741.
- [19] Mohanan, J. L.; Arachchige, I. U.; Brock, S. L., Porous Semiconductor Chalcogenide Aerogels. *Science (Washington, DC, U. S.)* **2005**, 307, (5708), 397-400.
- [20] Denes, F. S.; Manolache, S., Macromolecular plasma-chemistry: an emerging field of polymer science. *Prog. Polym. Sci.* **2004**, 29, (8), 815-885.

- [21] Sommer, M.; Stenger, F.; Peukert, W.; Wagner, N. J., Agglomeration and breakage of nanoparticles in stirred media mills-a comparison of different methods and models. *Chem. Eng. Sci.* **2005**, 61, (1), 135-148.
- [22] Enustun, B. V.; Turkevich, J., Coagulation of colloidal gold. *J. Am. Chem. Soc.* **1963**, 85, (21), 3317-28.
- [23] Carbone, L.; Nobile, C.; De Giorgi, M.; Sala, F. D.; Morello, G.; Pompa, P.; Hytch, M.; Snoeck, E.; Fiore, A.; Franchini, I. R.; Nadasan, M.; Silvestre, A. F.; Chiodo, L.; Kudera, S.; Cingolani, R.; Krahne, R.; Manna, L., Synthesis and Micrometer-Scale Assembly of Colloidal CdSe/CdS Nanorods Prepared by a Seeded Growth Approach. *Nano Letters* **2007**, 7, (10), 2942-2950.
- [24] Holland, W. R.; Hall, D. G., Surface-Plasmon Dispersion-Relation - Shifts Induced by the Interaction with Localized Plasma Resonances. *Physical Review B* **1983**, 27, (12), 7765-7768.
- [25] Zeng, S.; Baillargeat, D.; Ho, H.-P.; Yong, K.-T., Nanomaterials enhanced surface plasmon resonance for biological and chemical sensing applications. *Chemical Society Reviews* **2014**, 43, (10), 3426-3452.
- [26] Kreibig, U.; Vollmer, M., *Optical properties of metal clusters*. Springer-Verlag Berlin Heidelberg: 1995.
- [27] Lippens, P. E.; Lannoo, M., Calculation of the band gap for small CdS and ZnS crystallites. *Physical Review B* **1989**, 39, (15), 10935-10942.
- [28] Brus, L. E., A simple model for the ionization potential, electron affinity, and aqueous redox potentials of small semiconductor crystallites. *The Journal of Chemical Physics* **1983**, 79, (11), 5566-5571.
- [29] Brus, L., Electronic wave functions in semiconductor clusters: experiment and theory. *J. Phys. Chem.* **1986**, 90, (12), 2555-60.

- [30] Xiao, S.; Zou, Y.; Wu, J.; Zhou, Y.; Yi, T.; Li, F.; Huang, C., Hydrogen bonding assisted switchable fluorescence in self-assembled complexes containing diarylethene: controllable fluorescent emission in the solid state. *J. Mater. Chem.* **2007**, 17, (24), 2483-2489.
- [31] Kamat, P. V., Quantum Dot Solar Cells. The Next Big Thing in Photovoltaics. *J. Phys. Chem. Lett.* **2013**, 4, (6), 908-918.
- [32] Zhang, H.; Fung, K.-H.; Hartmann, J.; Chan, C. T.; Wang, D., Controlled Chainlike Agglomeration of Charged Gold Nanoparticles via a Deliberate Interaction Balance. *J. Phys. Chem. C* **2008**, 112, (43), 16830-16839.
- [33] Sonnichsen, C.; Reinhard, B. M.; Liphardt, J.; Alivisatos, A. P., A molecular ruler based on plasmon coupling of single gold and silver nanoparticles. *Nat Biotechnol* **2005**, 23, (6), 741-5.
- [34] Halas, N. J.; Lal, S.; Chang, W.-S.; Link, S.; Nordlander, P., Plasmons in Strongly Coupled Metallic Nanostructures. *Chemical Reviews* **2011**, 111, (6), 3913-3961.
- [35] Dabbousi, B. O.; Rodriguez-Viejo, J.; Mikulec, F. V.; Heine, J. R.; Mattoussi, H.; Ober, R.; Jensen, K. F.; Bawendi, M. G., (CdSe)ZnS Core–Shell Quantum Dots: Synthesis and Characterization of a Size Series of Highly Luminescent Nanocrystallites. *The Journal of Physical Chemistry B* **1997**, 101, (46), 9463-9475.
- [36] Peng, X.; Schlamp, M. C.; Kadavanich, A. V.; Alivisatos, A. P., Epitaxial Growth of Highly Luminescent CdSe/CdS Core/Shell Nanocrystals with Photostability and Electronic Accessibility. *Journal of the American Chemical Society* **1997**, 119, (30), 7019-7029.
- [37] Dorfs, D.; Eychmueller, A., A Series of Double Well Semiconductor Quantum Dots. *Nano Lett.* **2001**, 1, (11), 663-665.

- [38] Sánchez-Paradinas, S.; Dorfs, D.; Friebe, S.; Freytag, A.; Wolf, A.; Bigall, N. C., Aerogels from CdSe/CdS Nanorods with Ultra-long Exciton Lifetimes and High Fluorescence Quantum Yields. *Advanced Materials* **2015**, 6152-6156.
- [39] McNaught, A. D.; Wilkinson, A., *Compendium of Chemical Terminology*. 2nd Edition ed.; Blackwell Scientific Publications: Oxford, 1997.
- [40] Huesing, N.; Schubert, U., Aerogels - airy materials: chemistry, structure, and properties. *Angew. Chem., Int. Ed.* **1998**, 37, (1/2), 22-45.
- [41] Armor, J. N.; Carlson, E. J.; Zambri, P. M., Aerogels as hydrogenation catalysts. *Applied Catalysis* **1985**, 19, (2), 339-348.
- [42] Gesser, H. D.; Goswami, P. C., Aerogels and related porous materials. *Chem. Rev.* **1989**, 89, (4), 765-88.
- [43] Kistler, S. S., Coherent expanded aerogels. *J. Phys. Chem.* **1932**, 36, 52-64.
- [44] Kistler, S. S., The nature of coagulation, viscosity and thixotropy in colloidal systems. *J. Phys. Chem.* **1932**, 36, 2948-66.
- [45] Pekala, R. W., Organic aerogels from the polycondensation of resorcinol with formaldehyde. *J. Mater. Sci.* **1989**, 24, (9), 3221-7.
- [46] Leventis, N.; Sotiriou-Leventis, C.; Zhang, G.; Rawashdeh, A.-M. M., Nanoengineering Strong Silica Aerogels. *Nano Lett.* **2002**, 2, (9), 957-960.
- [47] Leventis, N., Three-Dimensional Core-Shell Superstructures: Mechanically Strong Aerogels. *Acc. Chem. Res.* **2007**, 40, (9), 874-884.
- [48] Brock, S. L., Filling a Void. *Science (Washington, DC, U. S.)* **2007**, 317, (5837), 460-461.
- [49] Brock, S. L.; Arachchige, I. U.; Kalebaila, K. K., Metal chalcogenide gels, xerogels and aerogels. *Comments Inorg. Chem.* **2006**, 27, (5-6), 103-126.

- [50] Arachchige, I. U.; Brock, S. L., Sol-Gel Methods for the Assembly of Metal Chalcogenide Quantum Dots. *Acc. Chem. Res.* **2007**, 40, (9), 801-809.
- [51] Cheng, W.; Rechberger, F.; Niederberger, M., From 1D to 3D - macroscopic nanowire aerogel monoliths. *Nanoscale* **2016**, 8, (29), 14074-14077.
- [52] Gauthier, B. M.; Bakrania, S. D.; Anderson, A. M.; Carroll, M. K., A fast supercritical extraction technique for aerogel fabrication. *J. Non-Cryst. Solids* **2004**, 350, 238-243.
- [53] Stengl, V.; Bakardjieva, S.; Subrt, J.; Szatmary, L., Titania aerogel prepared by low temperature supercritical drying. *Microporous Mesoporous Mater.* **2006**, 91, (1-3), 1-6.
- [54] Bigall, N. C.; Haertling, T.; Klose, M.; Simon, P.; Eng, L. M.; Eychmuller, A., Monodisperse Platinum Nanospheres with Adjustable Diameters from 10 to 100 nm: Synthesis and Distinct Optical Properties. *Nano Lett.* **2008**, 8, (12), 4588-4592.
- [55] Lal, S.; Link, S.; Halas, N. J., Nano-optics from sensing to waveguiding. *Nat. Photonics* **2007**, 1, (11), 641-648.
- [56] Dorfs, D.; Hickey, S.; Eychmuller, A. In *Type-I and type-II core-shell quantum dots: synthesis and characterization*, 2010; Wiley-VCH Verlag GmbH & Co. KGaA: 2010; pp 331-366.
- [57] Courtens, E.; Pelous, J.; Phalippou, J.; Vacher, R.; Woignier, T., Brillouin-scattering measurements of phonon-fracton crossover in silica aerogels. *Phys. Rev. Lett.* **1987**, 58, (2), 128-31.
- [58] Nicolaon, G. A.; Teichner, S. J., New preparation process for silica xerogels and aerogels, and their textural properties. *Bull. Soc. Chim. Fr.* **1968**, (5), 1900-6.
- [59] Brinker, C. J.; Keefer, K. D.; Schaefer, D. W.; Ashley, C. S., Sol-gel transition in simple silicates. *J. Non-Cryst. Solids* **1982**, 48, (1), 47-64.
- [60] Tillotson, T. M.; Hrubesh, L. W., Transparent ultralow-density silica aerogels prepared by a two-step sol-gel process. *J. Non-Cryst. Solids* **1992**, 145, (1-3), 44-50.

- [61] Herrmann, G.; Iden, R.; Mielke, M.; Teich, F.; Ziegler, B., On the way to commercial production of silica aerogel. *Journal of Non-Crystalline Solids* **1995**, 186, 380-387.
- [62] Jansen, R.-M.; B.Kessler; Wonner, J.; Zimmermann, A. DE-A 431 6540 A1, **1993**.
- [63] Jansen, R.-M.; Zimmermann, A. EP-A 690 023 A2, **1993**.
- [64] Dolhaine, H.; Wolf-Leistekow, J. EP-B 409 083 A1, **1991**.
- [65] Pajonk, G. M.; Repellin-Lacroix, M.; Abouarnadasse, S.; Chaouki, J.; Klvana, D., From sol-gel to aerogels and cryogels. *J. Non-Cryst. Solids* **1990**, 121, (1-3), 66-7.
- [66] Fricke, J.; Emmerling, A., Aerogels - recent progress in production techniques and novel applications. *J. Sol-Gel Sci. Technol.* **1998**, 13, (1/2/3), 299-303.
- [67] Kistler, S. S.; Caldwell, A. G., Thermal conductivity of silica aërogeel. *Ind. Eng. Chem.* **1934**, 26, 658-62.
- [68] Foster, H. D.; Keyes, D. B., Catalysts for the vapor-phase oxidation of acetaldehyde. *Ind. Eng. Chem.* **1937**, 29, 1254-60.
- [69] Taghavi, M. B.; Pajonk, G. M.; Teichner, S. J., On the structure-sensitive and structure-insensitive catalytic reactions and their new characteristics, demonstrated with copper-supported catalysts. *Journal of Colloid and Interface Science* **1979**, 71, (3), 451-465.
- [70] Bigall, N. C.; Herrmann, A.-K.; Vogel, M.; Rose, M.; Simon, P.; Carrillo-Cabrera, W.; Dorfs, D.; Kaskel, S.; Gaponik, N.; Eychmueller, A., Hydrogels and Aerogels from Noble Metal Nanoparticles. *Angew. Chem., Int. Ed.* **2009**, 48, (51), 9731-9734, S9731/1-S9731/10.
- [71] Leventis, N.; Chandrasekaran, N.; Sotiriou-Leventis, C.; Mumtaz, A., Smelting in the age of nano: iron aerogels. *Journal of Materials Chemistry* **2009**, 19, (1), 63-65.

- [72] Herrmann, A.-K.; Formanek, P.; Borchardt, L.; Klose, M.; Giebeler, L.; Eckert, J.; Kaskel, S.; Gaponik, N.; Eychmueller, A., Multimetallic Aerogels by Template-Free Self-Assembly of Au, Ag, Pt, and Pd Nanoparticles. *Chem. Mater.* **2014**, 26, (2), 1074-1083.
- [73] Herrmann, A.-K.; Bigall, N. C.; Lu, L.; Eychmueller, A. In *Ordered and nonordered porous superstructures from metal nanoparticles*, 2012; Wiley-VCH Verlag GmbH & Co. KGaA: 2012; pp 339-359.
- [74] Herrmann, A.-K.; Liu, W.; Gaponik, N.; Bigall, N.-C.; Eychmueller, A., Metal nanoparticle aerogels and their applications. *ECS Trans.* **2013**, 45, (20, Fullerenes, Nanotubes, and Carbon Nanostructures--221st ECS Meeting, 2012), 149-154, 6 pp.
- [75] Gacoin, T.; Malier, L.; Boilot, J.-P., New Transparent Chalcogenide Materials Using a Sol-Gel Process. *Chem. Mater.* **1997**, 9, (7), 1502-1504.
- [76] Kalebaila, K. K.; Georgiev, D. G.; Brock, S. L., Synthesis and characterization of germanium sulfide aerogels. *J. Non-Cryst. Solids* **2006**, 352, (3), 232-240.
- [77] Bag, S.; Trikalitis, P. N.; Chupas, P. J.; Armatas, G. S.; Kanatzidis, M. G., Porous Semiconducting Gels and Aerogels from Chalcogenide Clusters. *Science (Washington, DC, U. S.)* **2007**, 317, (5837), 490-493.
- [78] Arachchige, I. U.; Mohanan, J. L.; Brock, S. L., Sol-Gel Processing of Semiconducting Metal Chalcogenide Xerogels: Influence of Dimensionality on Quantum Confinement Effects in a Nanoparticle Network. *Chem. Mater.* **2005**, 17, (26), 6644-6650.
- [79] Gaponik, N.; Wolf, A.; Marx, R.; Lesnyak, V.; Schilling, K.; Eychmueller, A., Three-dimensional self-assembly of thiol-capped CdTe nanocrystals: gels and aerogels as building blocks for nanotechnology. *Adv. Mater. (Weinheim, Ger.)* **2008**, 20, (22), 4257-4262.
- [80] Arachchige, I. U.; Brock, S. L., Highly Luminescent Quantum-Dot Monoliths. *J. Am. Chem. Soc.* **2007**, 129, (7), 1840-1841.

- [81] Sanchez-Paradinas, S.; Dorfs, D.; Friebe, S.; Freytag, A.; Wolf, A.; Bigall, N. C., Aerogels from CdSe/CdS Nanorods with Ultra-long Exciton Lifetimes and High Fluorescence Quantum Yields. *Adv. Mater. (Weinheim, Ger.)* **2015**, *27*, (40), 6152-6156.
- [82] Naskar, S.; Miethe, J. F.; Sanchez-Paradinas, S.; Schmidt, N.; Kanthasamy, K.; Behrens, P.; Pfner, H.; Bigall, N. C., Photoluminescent Aerogels from Quantum Wells. *Chem. Mater.* **2016**, *28*, (7), 2089-2099.
- [83] Pekala, R. W.; Alviso, C. T.; Lemay, J. D. In *Organic aerogels: a new type of ultrastructured polymer*, 1992; Wiley: 1992; pp 671-83.
- [84] Ryoo, R.; Joo, S. H.; Jun, S., Synthesis of Highly Ordered Carbon Molecular Sieves via Template-Mediated Structural Transformation. *The Journal of Physical Chemistry B* **1999**, *103*, (37), 7743-7746.
- [85] Jun, S.; Joo, S. H.; Ryoo, R.; Kruk, M.; Jaroniec, M.; Liu, Z.; Ohsuna, T.; Terasaki, O., Synthesis of New, Nanoporous Carbon with Hexagonally Ordered Mesostructure. *Journal of the American Chemical Society* **2000**, *122*, (43), 10712-10713.
- [86] Sun, H.; Xu, Z.; Gao, C., Multifunctional, Ultra-Flyweight, Synergistically Assembled Carbon Aerogels. *Advanced Materials* **2013**, *25*, (18), 2554-2560.
- [87] Hanzawa, Y.; Kaneko, K.; Pekala, R. W.; Dresselhaus, M. S., Activated Carbon Aerogels. *Langmuir* **1996**, *12*, (26), 6167-6169.
- [88] Wang, L.; Yang, R. T., Molecular hydrogen and spillover hydrogen storage on high surface area carbon sorbents. *Carbon* **2012**, *50*, (9), 3134-3140.
- [89] Schwertfeger, F.; Glaubitt, W.; Schubert, U., Hydrophobic aerogels from Si(OMe)₄/MeSi(OMe)₃ mixtures. *Journal of Non-Crystalline Solids* **1992**, *145*, 85-89.
- [90] Wäsche, R., Better ceramics through chemistry VI. Hrsg. von A. K. Cheetham, C. J. Brinker, M. L. Mecartney und C. Sanchez. Materials Research Society Proceedings Vol. 346, 1048 Seiten, MRS Pittsburgh, Pennsylvania 1994, \$ 52.00 (MRS Member), \$ 60.00

(US List), \$69.00 (Foreign List), \$ 69.00 (Foreign List), ISBN 1-55899-246-4. *Materials and Corrosion* **1995**, 46, (5), 334-335.

[91] Nadargi, D. Y.; Latthe, S. S.; Hirashima, H.; Rao, A. V., Studies on rheological properties of methyltriethoxysilane (MTES) based flexible superhydrophobic silica aerogels. *Microporous Mesoporous Mater.* **2008**, 117, (3), 617-626.

[92] Maleki, H.; Duraes, L.; Portugal, A., An overview on silica aerogels synthesis and different mechanical reinforcing strategies. *J. Non-Cryst. Solids* **2014**, 385, 55-74.

[93] Novak, B. M.; Auerbach, D.; Verrier, C., Low-Density, Mutually Interpenetrating Organic-Inorganic Composite Materials via Supercritical Drying Techniques. *Chemistry of Materials* **1994**, 6, (3), 282-286.

[94] Mulik, S.; Sotiriou-Leventis, C.; Leventis, N., Time-Efficient Acid-Catalyzed Synthesis of Resorcinol-Formaldehyde Aerogels. *Chem. Mater.* **2007**, 19, (25), 6138-6144.

[95] Zhang, G.; Dass, A.; Rawashdeh, A.-M. M.; Thomas, J.; Council, J. A.; Sotiriou-Leventis, C.; Fabrizio, E. F.; Ilhan, F.; Vassilaras, P.; Scheiman, D. A.; McCorkle, L.; Palczer, A.; Johnston, J. C.; Meador, M. A.; Leventis, N., Isocyanate-crosslinked silica aerogel monoliths: preparation and characterization. *J. Non-Cryst. Solids* **2004**, 350, 152-164.

[96] Loy, D. A.; Jamison, G. M.; Baugher, B. M.; Russick, E. M.; Assink, R. A.; Prabakar, S.; Shea, K. J., Alkylene-bridged polysilsesquioxane aerogels: highly porous hybrid organic-inorganic materials. *Journal of Non-Crystalline Solids* **1995**, 186, 44-53.

[97] Pajonk, G. M.; Elaloui, E.; Achard, P.; Chevalier, B.; Chevalier, J.-L.; Durant, M., Physical properties of silica gels and aerogels prepared with new polymeric precursors. *Journal of Non-Crystalline Solids* **1995**, 186, 1-8.

[98] Pajonk, G. M., Transparent silica aerogels. *J. Non-Cryst. Solids* **1998**, 225, 307-314.

- [99] Hüsing, N.; Schwertfeger, F.; Tappert, W.; Schubert, U., Influence of supercritical drying fluid on structure and properties of organically modified silica aerogels. *Journal of Non-Crystalline Solids* **1995**, 186, 37-43.
- [100] Hüsing, N.; Schubert, U., Organofunctional Silica Aerogels. *Journal of Sol-Gel Science and Technology* **1997**, 8, (1), 807-812.
- [101] Astier, M.; Bertrand, A.; Teichner, S. J., *Bull. Soc. Chim. Fr.* **1980**, 218.
- [102] Heinrichs, B.; Pirard, J. P.; Pirard, R. Transition metal-aerogel support catalyst. EP629442A1, 1994.
- [103] Feinle, A.; Huesing, N., Mixed metal oxide aerogels from tailor-made precursors. *J. Supercrit. Fluids* **2015**, 106, 2-8.
- [104] Fang, G.; Zhou, J.; Liang, C.; Cai, Y.; Pan, A.; Tan, X.; Tang, Y.; Liang, S., General synthesis of three-dimensional alkali metal vanadate aerogels with superior lithium storage properties. *J. Mater. Chem. A* **2016**, 4, (37), 14408-14415.
- [105] UaCearnaigh, D. C.; Baghi, R.; Hope-Weeks, L. J., Sol-gel synthesis of a series of first row d-block ferrites via the epoxide addition method. *RSC Adv.* **2016**, 6, (53), 48212-48221.
- [106] Liu, Z.; Xu, K.; She, P.; Yin, S.; Zhu, X.; Sun, H., Self-assembly of 2D MnO₂ nanosheets into high-purity aerogels with ultralow density. *Chem. Sci.* **2016**, 7, (3), 1926-1932.
- [107] Shukla, N.; Saxena, A.; Gupta, V.; Rawat, A. S.; Kumar, V.; Rai, P. K.; Shrivastava, S., Removal of lead from water using low density metal oxide nanoparticles. *Adv. Sci., Eng. Med.* **2015**, 7, (5), 398-405.
- [108] Bechu, A. M.; Tobin, Z. M.; Carroll, M. K.; Anderson, A. M. In *Copper-alumina aerogels: Fabrication, characterization, and catalytic application*, 2015; American Chemical Society: 2015; pp NERM-145.

- [109] Hirashima, H.; Gengyo, M.; Kojima, C.; Imai, H., Effects of aging and drying on structure of V₂O₅ gels. *Journal of Non-Crystalline Solids* **1995**, 186, 54-58.
- [110] Fricke, J.; Emmerling, A., Aerogels. *Journal of the American Ceramic Society* **1992**, 75, (8), 2027-2035.
- [111] Yoldas, B. E., Formation of titania-silica glasses by low temperature chemical polymerization. *Journal of Non-Crystalline Solids* **1980**, 38-39, Part 1, 81-86.
- [112] Hendel, T.; Lesnyak, V.; Kuehn, L.; Herrmann, A.-K.; Bigall, N. C.; Borchardt, L.; Kaskel, S.; Gaponik, N.; Eychmueller, A., Mixed Aerogels from Au and CdTe Nanoparticles. *Adv. Funct. Mater.* **2013**, 23, (15), 1903-1911.
- [113] Nahar, L.; Esteves, R. J. A.; Hafiz, S.; Ozgur, U.; Arachchige, I. U., Metal-Semiconductor Hybrid Aerogels: Evolution of Optoelectronic Properties in a Low-Dimensional CdSe/Ag Nanoparticle Assembly. *ACS Nano* **2015**, Ahead of Print.
- [114] Pajonk, G. M., Drying methods preserving the textural properties of gels. *J. Phys., Colloq.* **1989**, (C4, Proc. Int. Symp. Aerogels--ISA 2, 2nd, 1988), C4-13/C4-22.
- [115] Moor, H., Freeze fixation of living cells and its application to electron microscopy. *Z. Zellforsch. Mikrosk. Anat.* **1964**, 62, (4), 546-80.
- [116] Zhang, H.; Hussain, I.; Brust, M.; Butler, M. F.; Rannard, S. P.; Cooper, A. I., Aligned two- and three-dimensional structures by directional freezing of polymers and nanoparticles. *Nat. Mater.* **2005**, 4, (10), 787-793.
- [117] Zhang, H.; Cooper, A. I., Aligned porous structures by directional freezing. *Adv. Mater. (Weinheim, Ger.)* **2007**, 19, (11), 1529-1533.
- [118] Liu, W.; Herrmann, A.-K.; Geiger, D.; Borchardt, L.; Simon, F.; Kaskel, S.; Gaponik, N.; Eychmueller, A., High-Performance Electrocatalysis on Palladium Aerogels. *Angew. Chem. Int. Ed.* **2012**, 51, (23), 5743-5747.

- [119] Gong, K.; Du, F.; Xia, Z.; Durstock, M.; Dai, L., Nitrogen-Doped Carbon Nanotube Arrays with High Electrocatalytic Activity for Oxygen Reduction. *Science (Washington, DC, U. S.)* **2009**, 323, (5915), 760-764.
- [120] Schneider, M.; Duff, D. G.; Mallat, T.; Wildberger, M.; Baiker, A., High Surface Area Platinum-Titania Aerogels: Preparation, Structural Properties, and Hydrogenation Activity. *Journal of Catalysis* **1994**, 147, (2), 500-514.
- [121] Antonietti, M.; Fechler, N.; Fellingner, T.-P., Carbon Aerogels and Monoliths: Control of Porosity and Nanoarchitecture via Sol-Gel routes. *Chem. Mater.* **2014**, 26, (1), 196-210.
- [122] Du, A.; Zhou, B.; Zhang, Z.; Shen, J., A special material or a new state of matter: a review and reconsideration of the aerogel. *Materials* **2013**, 6, 941-968.
- [123] Nardecchia, S.; Carriazo, D.; Ferrer, M. L.; Gutierrez, M. C.; del Monte, F., Three dimensional macroporous architectures and aerogels built of carbon nanotubes and/or graphene: synthesis and applications. *Chem. Soc. Rev.* **2013**, 42, (2), 794-830.
- [124] Soleimani Dorcheh, A.; Abbasi, M. H., Silica aerogel; synthesis, properties and characterization. *J. Mater. Process. Technol* **2008**, 199, (1-3), 10-26.
- [125] Gurav, J. L.; Jung, I.-K.; Park, H.-H.; Kang, E. S.; Nadargi, D. Y., Silica aerogel: synthesis and applications. *J. Nanomater.* **2010**, No pp. given.
- [126] Elsila, J. E.; Glavin, D. P.; Dworkin, J. P., Cometary glycine detected in samples returned by Stardust. *Meteoritics & Planetary Science* **2009**, 44, (9), 1323-1330.
- [127] Jones, S. M., Aerogel: Space exploration applications. *J. Sol-Gel Sci. Technol.* **2006**, 40, (2/3), 351-357.
- [128] An, H.; Wang, Y.; Wang, X.; Zheng, L.; Wang, X.; Yi, L.; Bai, L.; Zhang, X., Polypyrrole/carbon aerogel composite materials for supercapacitor. *J. Power Sources* **2010**, 195, (19), 6964-6969.

- [129] Pajonk, G. M., Some applications of silica aerogels. *Colloid Polym. Sci.* **2003**, 281, (7), 637-651.
- [130] Koebel, M.; Rigacci, A.; Achard, P., Aerogel-based thermal superinsulation: an overview. *Journal of Sol-Gel Science and Technology* **2012**, 63, (3), 315-339.
- [131] Gerlach, R.; Kraus, O.; Fricke, J.; Eccardt, P. C.; Kroemer, N.; Magori, V., Modified silica aerogels as acoustic impedance matching layers in ultrasonic devices. *J. Non-Cryst. Solids* **1992**, 145, (1-3), 227-32.

2. Development of a New Procedure for Aerogel Fabrication

2.1 Summary

As described earlier in the section of the aerogel materials and applications, current fabrication techniques are complicated and time consuming while being not able to fully retain colloidal properties. The following two papers report on the development of a complete new fabrication procedure namely cryoaerogelation and demonstrate how the resulting superstructure can be influenced and controlled. The method focuses on the assembling of colloidal NPs by freezing them in liquid nitrogen and subsequent freeze drying. With this, it is possible to avoid evaporation of the liquid phase which usually leads to the destruction of gel structures due to capillary forces. Instead the cryoaerogelation, as shown in section 2.2, exploits the sublimation of water at pressures below 6.1 mbar. With the whole process being completely physical, it allows to assemble every colloidal NP in an aqueous solution. The versatility could be demonstrated by synthesizing cryoaerogels from Au, Ag, Pd and Pt. In addition cryogels were made from metal oxides (hematite) as well as metal chalcogenides. The shape and properties of the employed NPs could be retained to some extent. Adjusting the surface chemistry was not necessary and therefore the employment of oxidizing agents could be disclaimed. The resulting cryoaerogel structures also differ from hydrogelated aerogels. While the last mentioned usually shows a well interconnected wire like network, cryoaerogels possess sheets made of few NP layers in thickness and with a lateral dimension in the size of micrometer. These sheets form well interconnected network building up the macroscopic monolith. For the first time noble metal aerogels could be shown that still possess plasmonic properties. If the volume fraction of NPs exceeds 0.1 vol% the cryoaerogelation shows no shrinkage during the fabrication process. With this it is possible to shape the resulting aerogel monolith. We were able to produce tube-like and more sophisticated structures like e.g. a smiley by employing silicon molds. The cryoaerogelation enables also the immobilization of aerogel

structures on various employed substrates. Furthermore, if a temperature gradient is applied like in e.g. oriented freezing, the whole aerogel film on the substrate gets a preferred orientation along the temperature gradient. Section 2.2 demonstrates the mostly perpendicular orientation of aerogel-sheets on a substrate and while focusing on the structures and the procedure of the cryoaerogelation itself, section 2.3 demonstrates the possibility of fabricating tailored multi-component cryoaerogels. Several metal-metal oxide aerogels were fabricated such as noble metal-titania aerogels, noble metal-hematite aerogels as well as platinum-metal oxide hydroxides (of Ni, Co, Mn). It is shown that the amount and number of materials can be freely varied. In addition, investigations of the component distribution revealed the influence of the surface charge of the employed NP. The surface charge can be switched via ligand exchange and subsequently influence a homogeneous or heterogeneous distribution of NPs on a micrometer scale. The resulting optical properties were found to be a mixture of the single components and occurring particle interactions. Furthermore section 2.3 demonstrates the application of such multi component cryoaerogels in photocatalytic hydrogen evolution reaction as a proof of principle measurement. It could be shown that comparable values for hydrogen evolution in aerogels were achieved, but with a much faster and less complex synthesis route. Furthermore the comparison of colloidal solution and the cryoaerogels revealed a significant increase in performance through the cryoaerogelation making it a valuable strategy to optimize materials.

2.2 Versatile Aerogel Fabrication by Freezing and Subsequent Freeze-Drying of Colloidal Nanoparticle Solutions

Axel Freytag, Sara Sánchez-Paradinas, Suraj Naskar, Natalia Wendt, Massimo Colombo, Giammarino Pugliese, Jan Poppe, Cansunur Demirci, Imme Kretschmer, Detlef W. Bahnemann, Peter Behrens and Nadja C. Bigall

Angewandte Chemie International Ed. **2016**, 55, 1200-1203

DOI:[10.1002/anie.201508972](https://doi.org/10.1002/anie.201508972)

Reprinted with permission from *Angewandte Chemie International Edition*.
Copyright (2016) Wiley VCH

Nanoparticle Aerogels

International Edition: DOI: 10.1002/anie.201508972
German Edition: DOI: 10.1002/ange.201508972

Versatile Aerogel Fabrication by Freezing and Subsequent Freeze-Drying of Colloidal Nanoparticle Solutions

Axel Freytag, Sara Sánchez-Paradinas, Suraj Naskar, Natalja Wendt, Massimo Colombo, Giammarino Pugliese, Jan Poppe, Cansunur Demirci, Imme Kretschmer, Detlef W. Bahnemann, Peter Behrens, and Nadja C. Bigall*

Abstract: A versatile method to fabricate self-supported aerogels of nanoparticle (NP) building blocks is presented. This approach is based on freezing colloidal NPs and subsequent freeze drying. This means that the colloidal NPs are directly transferred into dry aerogel-like monolithic superstructures without previous lyogelation as would be the case for conventional aerogel and cryogel fabrication methods. The assembly process, based on a physical concept, is highly versatile: cryogelation is applicable for noble metal, metal oxide, and semiconductor NPs, and no impact of the surface chemistry or NP shape on the resulting morphology is observed. Under optimized conditions the shape and volume of the liquid equal those of the resulting aerogels. Also, we show that thin and homogeneous films of the material can be obtained. Furthermore, the physical properties of the aerogels are discussed.

Ever since the first synthesis of aerogel structures from colloidal NP building blocks in 2005,^[1] there has been much interest in these self-supporting superstructures. This is mostly because of the large surface-to-volume ratio of these monoliths, being close to that of their building blocks, in combination with them being assembled into a self-supported and macroscopic monolith.^[2] For the development of macroscopic materials with nanoscopic properties, the formation of this kind of aerogel superstructure is widely recognized to have been a quantum leap, since the macroscopic monoliths exhibit many of the nanoscopic properties, such as size quantization for many different quantum dot building blocks, or plasmon–exciton interactions in mixed aerogels.^[3,4] To date, when fabricating aerogels and aerogel-like structures (that is, nanosponges, metal foams),^[5,6] chemical gelation

(sol–gel), dealloying, or deposition methods are employed to create self-supported structures, followed by subsequent drying or template removal.^[2,5,7–9] One major drawback of the conventional aerogel synthesis is that the synthetic route is a multistep procedure,^[2,10,11] because the colloidal NPs first need to be destabilized in a controlled way in order to form hydro- or alcogels,^[12] and only once these superstructures have formed they can be transformed to aerogels by supercritical drying.^[1,2,12] The nano- and microscopic morphologies of the superstructure are strongly dependent on the destabilization step which means that solvents, surfactants, zeta potential, and especially the type of destabilizing procedure/agent are critical parameters for the nanoscopic morphology of the resulting gels, so that the chemical gelation procedure needs to be adjusted for each system.^[13–17] The synthesis of aerogels can be time consuming, complex, and expensive. Furthermore, conventional lyogelation methods are frequently accompanied by syneresis effects, so that it is very difficult to synthesize special external shapes, which in turn would be of interest for possible applications. Herein, we propose an alternative assembly method (see Figure 1) based on a physical process. By freezing aqueous NP colloids in situ and subsequent freeze-drying, monolithic aerogels are obtained that consist of a self-supported network of thin platelets building up the gel network, the platelets being mostly 2D assemblies of the NP building blocks. The advantage of our strategy is the suitability for many different NP systems, since there is no chemical selectivity. Under optimum conditions, the volume and shape of the liquid equal the volume and shape of the resulting aerogel. Additionally we show that thin and homogeneous films of the monolith can be obtained.

[*] A. Freytag, Dr. S. Sánchez-Paradinas, S. Naskar, J. Poppe, C. Demirci, Dr. N. C. Bigall
Institut für Physikalische Chemie und Elektrochemie
Leibniz Universität Hannover
Callinstrasse 3A, 30167 Hannover (Deutschland)
E-mail: nadja.bigall@pci.uni-hannover.de
A. Freytag, Dr. S. Sánchez-Paradinas, S. Naskar, N. Wendt, J. Poppe, C. Demirci, I. Kretschmer, Prof. Dr. D. W. Bahnemann, Prof. Dr. P. Behrens, Dr. N. C. Bigall
Laboratorium für Nano- und Quantenengineering (LNQE)
Leibniz Universität Hannover
Schneiderberg 39, 30167 Hannover (Deutschland)
Dr. M. Colombo
Nanochemistry Department, Istituto Italiano di Tecnologia
Via Morego, 30, 16163 Genova (Italien)

G. Pugliese
Istituto Italiano di Tecnologia
Via Morego, 30, 16163 Genova (Italien)
N. Wendt, Prof. Dr. P. Behrens
Institut für Anorganische Chemie, Leibniz Universität Hannover
Callinstrasse 9, 30167 Hannover (Deutschland)
I. Kretschmer, Prof. Dr. D. W. Bahnemann
Institut für Technische Chemie, Leibniz Universität Hannover
Callinstrasse 3, 30167 Hannover (Deutschland)
Prof. Dr. D. W. Bahnemann
Laboratory for Nanocomposite Materials, Department of Photonics,
Faculty of Physics, Saint-Petersburg State University, Ulianovskaia
street 3, Peterhof, 198504 Saint Petersburg (Russland)

Supporting information and ORCID(s) from the author(s) for this article are available on the WWW under <http://dx.doi.org/10.1002/anie.201508972>.

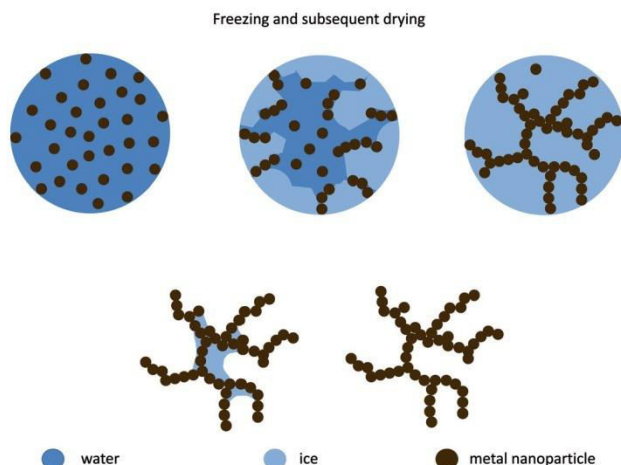


Figure 1. Freezing mechanism (top line) of a droplet of metal nanoparticle colloid in liquid nitrogen from colloidal solution (left) to frozen system (right) and subsequent removal of the ice template (bottom) by lyophilization.

By fast freezing aqueous colloidal NP solutions, which were as droplets injected directly into liquid nitrogen, and by subsequent freeze drying the frozen objects, we obtained highly porous and voluminous monolithic aerogels consisting solely of the respective material. These self-supporting aerogels have densities ranging from 20 to 60 mg cm⁻³, representing around 0.2% of the density of the corresponding bulk materials, which is similar to other reported NP aerogels.^[18] It should be noted that this equals approximately the volume fraction of the particles in the original colloidal

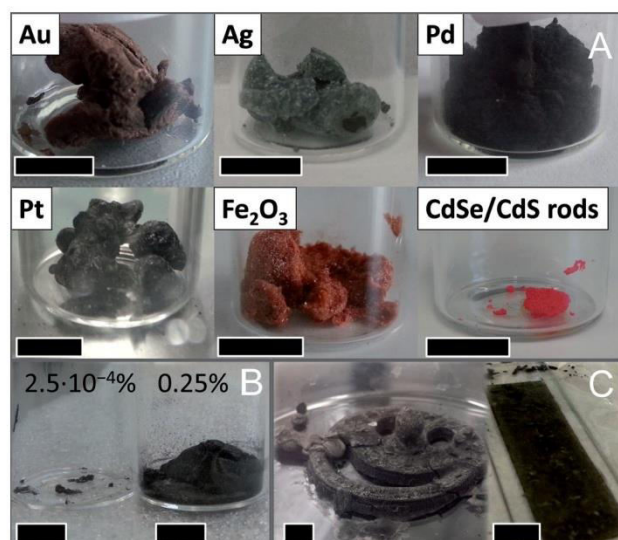


Figure 2. A) Photographs of aerogels of Au, Ag, Pd, Pt, Fe₂O₃, and CdSe/CdS rod-like NPs (scale bar: 1 cm). B) Influence of NP volume fraction of the colloidal solution on the final volume of the monolith, both resulting from 1 mL Pd-colloid (volume fractions of $2.5 \times 10^{-4}\%$ and 0.25% from left to right, respectively). C) Examples for a variety of shapes possible by cryogelation route: smiley in a Petri dish or thin film on glass slide.

solution. With this method, we were able to synthesize aerogel materials of noble metal NPs, as well as metal oxide and semiconductor NPs. For example, in Figure 2 A, photographs of aerogels are shown, consisting of Au, Ag, Pd, and Pt, as well as of hematite NPs (Fe₂O₃) and of quantum rods (CdS rods grown around CdSe seeds, which are known to exhibit high fluorescence quantum yields and large Stokes shifts).^[19,20] This shows a major strength of this method, namely being versatile towards many different NP materials from aqueous solution. Furthermore, this method is also applicable for different ligand molecules. Citrate, thioglycolic acid, and mercaptosuccinic acid covered nanoparticles were for example successfully tested for synthesizing Pt aerogels by means of this cryogelation method (Supporting Information, Section S3). However, it should be noted that when employing fluorescent NPs such as the CdSe/CdS seeded nanorods (Supporting Information, Section S2), the ligand concentration should be low enough to yield a morphology similar to those of other nanoparticles. At the same time the ligand concentration must be high enough to ensure that the resulting monoliths are still fluorescent.

The aerogel monoliths show no shrinkage in comparison to the frozen colloid droplets, if the NP concentration (NP volume fraction) is at least 0.1% before freezing (Figure 2 B). Instead, a clear shrinkage or collapse of the macroscopic structure was observed, when the volume fraction of the NC concentration was below 0.1%. Interestingly, for the higher NP concentrations, the shape of the frozen colloid resembles the shape of the resulting aerogel (Figure 2 C). For example, films on glass substrates could be fabricated by the doctor blade method, and other shapes (see “smoking smiley” in Figure 2 C left and Supporting Information) were synthesized. Therefore, our new cryogelation method is advantageous in comparison to conventional aerogels (and xerogels) resulting from lyogelated gels, which are frequently accompanied by syneresis^[2,4,7,11,21,22] (i.e. the gels are usually smaller than the colloid liquid). This fact opens the opportunity to create more sophisticated macroscopic shapes. That is, for possible industrial applications the desired shapes can be realized.

In Figure 3, scanning electron (SEM) micrographs and transmission electron (TEM) micrographs of a Pd aerogel are shown in four different magnifications. In general, the microscopic structure of our aerogels consists of highly porous, non-ordered, and well-interconnected networks of 10 nm to 100 nm thin sheets of several μm lengths and widths, (see inset in Figure 3 B) and of wires, which again consist of rolled-up sheets (see Supporting Information, Section S4). Most of the sheets, which build up the free-standing gel network, appear bent, and they exhibit a surface roughness on the nanometer scale. As can be derived from TEM images (Figure 3 C, D), the surface roughness is caused by NPs which are assembled mostly laterally to build up the mesoporous sheets.

In the microscopic regime, the morphologies of the aerogels of different nanomaterials investigated were similar, always consisting of networks of sheet-like assemblies of the NPs and enrolled sheets. The microscopic morphologies were found to be similar for different sizes of the employed nanoparticles (investigated from 3.5 nm to 120 nm diameters)

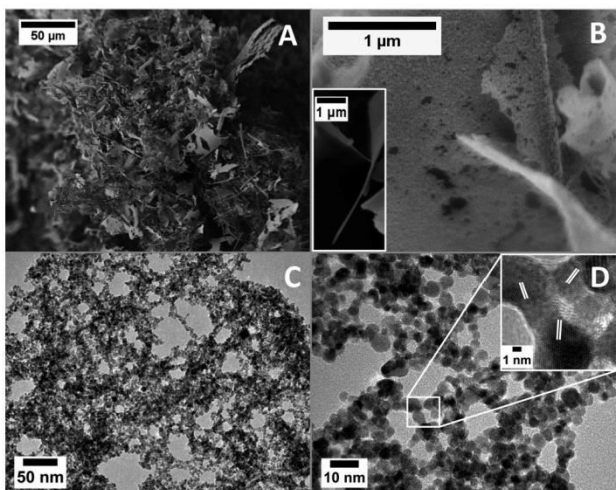


Figure 3. Electron microscope images of a Pd aerogel. SEM images show the interconnected network (A) with a closer look onto the thin sheets (B) and their thickness (inset in B). TEM images reveal mesopores within sheets (C) build of randomly oriented quasi-spherical NPs (D). The inset shows direct contact of the NPs and white bars the (111) face of Pd (lattice distance was measured to be 2.2 Å; previously reported value: 2.246 Å).^[23]

and shapes (spheres and rods; Supporting Information, Sections S4–S6) of NPs, materials (Au, Ag, Pt, Pd, hematite, CdSe/CdS), and also for different surface ligands (for example, citrate, mercaptopropionic acid, thioglycolic acid, and chloride ions/hydroxides) as long as the ligand concentrations are low (1 to 2 weight percent; Supporting Information, Section S7) in comparison to the inorganic NP concentration.

For samples such as Pd, Pt, and hematite NPs, as well as CdSe/CdS nanorods, the shapes and sizes of the building blocks are retained, and they assemble randomly oriented to get in contact with each other hence forming the sheet-like structures with free interstitial spaces resulting in high porosity (see Figure 3C, D). We observed an increasing thickness of the nanosheets with higher concentrations (volume fraction) of the colloids employed.

It should be noted that in most but not in all cases the sizes and shapes of the NP building blocks were retained: exceptions were Au and Ag, for which deviations in the crystallite sizes were observed (Supporting Information, Section S4).

Based on our observations from electron microscopy and macroscopic appearances, we postulate the following gelation mechanism for our cryogelation method (see Figure 1): during the fast freezing, the NPs are excluded from the ice crystallites and assemble in the space between them. This effect is supported by the observations and derived model of Zhang et al.,^[24] who observed that when freezing NP solutions with high-enough freezing speed, the NPs are not built into the ice crystallites (which in turn only takes place for low freezing speed). This effect has also already been exploited in techniques such as directional freezing.^[24,25] In our system, by fast freezing (according to Moor),^[26] many small ice crystallites are rapidly formed. Therefore, the NPs are pushed to the

crystallite boundaries. A continuous network of the crystallite boundaries filled with NPs is built, which is responsible for the self-supporting nature of the aerogel after ice template removal. A critical NP concentration is needed to form a sheet network with sufficient mechanical stability for providing a self-supported monolith. The observed strong shrinkage at lower NP concentrations is attributed to a poor interconnection of NPs and NP sheets with each other. The higher the NP concentration before freezing, the more NPs are driven in the space between the ice crystals, resulting in thicker assemblies and hence thicker sheets in the aerogel network (see also the Supporting Information, Section S6). The ice removal in the cryogelation process has to be performed by freeze drying to circumvent capillary forces, which appear at the liquid phase and which would lead to destruction of the filigree network.

To date, the highest specific surface area measured by nitrogen adsorption measurements and also by electrochemical methods is in the order of $33 \text{ m}^2 \text{ g}^{-1}$ ($6.4 \times 10^3 \text{ m}^2 \text{ mol}^{-1}$), which was measured for a Pt NP aerogel from a 0.025 vol% concentrated solution. This is in the same order of magnitude as the maximum specific surface geometrically estimated for the same NP size (3.5 nm quasi-spherical particles) of $74 \text{ m}^2 \text{ g}^{-1}$. The specific surface area of these aerogels is hence comparable to other metal foams (9 to $81 \text{ m}^2 \text{ g}^{-1}$)^[6,27] and (bi)metallic aerogels (46 to $92 \text{ m}^2 \text{ g}^{-1}$).^[28–30] The nitrogen adsorption measurements also confirmed the presence of macro- and mesopores (for detailed discussion of nitrogen adsorption and electrochemical measurements, see the Supporting Information, Section S8). From the external dimensions of our aerogels and their total mass, the porosity was estimated to be 99.4% for Pd and 99.7% for Pt, Ag and Au aerogels.

In Figure 4, some of the specific properties obtained of the different NP aerogels are highlighted (for a detailed discussion of the various aerogels, see the Supporting Information, Section S9). The aerogels as synthesized from CdSe/CdS

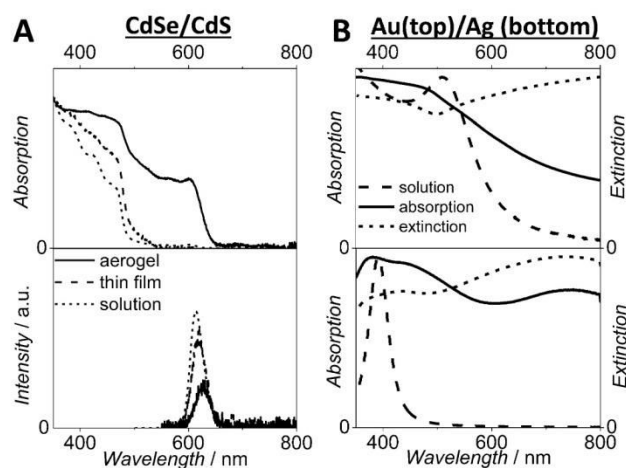


Figure 4. A) Spectroscopic investigation of the CdSe/CdS aerogels (top: absorption, bottom: emission spectra) determined by means of an integrating sphere. B) absorption (solid line) and extinction (long dashed line) spectra of the aerogels from Au (top) and Ag NPs (bottom).

nanorods (Figure 4A) exhibit fluorescence, and the band edges of CdSe and CdS are still recognizable in their absorption spectra. We observe a shift to longer wavelengths for both emission and absorption spectra, which we attribute to the interparticle interactions caused by the close proximity. A decrease in luminescence quantum yield in comparison to the aqueous NP solution is observed (from 24% to 14% for thin aerogel films and 4.8% for aerogel monoliths).

The absorption and extinction spectra of both Au and Ag aerogels (Figure 4B) show a drastic change in comparison to the pristine NP solutions (see the Supporting Information). However, most notably, the aerogels exhibit extinction and absorption maxima, which we attribute to localized surface plasmon resonances and interplasmon coupling.^[31]

In conclusion, in the recent work we have shown the fabrication of aerogels of pure noble metal, metal oxide, and semiconductor NPs by freezing and subsequent freeze-drying. These aerogels are self-supporting, non-ordered, and highly voluminous structures, with a particle density similar to the respective colloidal solution, without any chemical gelation agent or difficult solvent exchange and removal step. If fabricated on substrates, oriented thin films can be achieved, and the cryogelation method also allows different desirable shaping of the monoliths. The resulting aerogels exhibit high specific surface areas with accessible NCs. The assembly method can partially retain the nanoscopic properties of suitable building blocks such as size quantization (including photoluminescence) and plasmonic behavior. The developed procedure is easy, fast and extremely versatile towards different materials, NP shapes, and surface ligands, and is likely expandable to many more aqueous colloidal NP systems.

Acknowledgements

N.C.B., A.F., S.S.-P., S.N., and J.P. are grateful for financial support from the German Federal Ministry of Education and Research (BMBF) within the framework of NanoMatFutur, support code 03X5525. I.K. and D.W.B. gratefully acknowledge financial support from the Deutsche Forschungsgemeinschaft (DFG, SPP1613). We also would like to thank Dr. Dirk Dorfs and Dominik Hinrichs for scientific discussions.

Keywords: aerogels · cryogels · noble metal nanoparticles · voluminous superstructures

How to cite: *Angew. Chem. Int. Ed.* **2016**, *55*, 1200–1203
Angew. Chem. **2016**, *128*, 1217–1221

- [1] J. L. Mohanan, I. U. Arachchige, S. L. Brock, *Science* **2005**, *307*, 397–400.
- [2] N. Hüsing, U. Schubert, *Angew. Chem. Int. Ed.* **1998**, *37*, 22–45; *Angew. Chem.* **1998**, *110*, 22–47.
- [3] T. Hendel, V. Lesnyak, L. Kühn, A.-K. Herrmann, N. C. Bigall, L. Borchardt, S. Kaskel, N. Gaponik, A. Eychmüller, *Adv. Funct. Mater.* **2013**, *23*, 1903–1911.
- [4] S. Sánchez-Paradinas, D. Dorfs, S. Friebe, A. Freytag, A. Wolf, N. C. Bigall, *Adv. Mater.* **2015**, *27*, 6152–6156.
- [5] B. C. Tappan, S. A. Steiner III, E. P. Luther, *Angew. Chem. Int. Ed.* **2010**, *49*, 4544–4565; *Angew. Chem.* **2010**, *122*, 4648–4669.
- [6] K. S. Krishna, C. S. S. Sandeep, R. Philip, M. Eswaremoorthy, *ACS Nano* **2010**, *4*, 2681–2688.
- [7] S. Brock, H. Yu in *Aerogels Handbook* (Eds.: M. A. Aegerter, N. Leventis, M. M. Koebel), Springer, New York, **2011**, pp. 367–384.
- [8] N. Leventis, *Acc. Chem. Res.* **2007**, *40*, 874–884.
- [9] W. Liu, A.-K. Herrmann, N. C. Bigall, P. Rodriguez, D. Wen, M. Oezaslan, T. J. Schmidt, N. Gaponik, A. Eychmüller, *Acc. Chem. Res.* **2015**, *48*, 154–162.
- [10] H. D. Gesser, P. C. Goswami, *Chem. Rev.* **1989**, *89*, 765–788.
- [11] S. L. Brock, *Angew. Chem. Int. Ed.* **2009**, *48*, 7484–7486; *Angew. Chem.* **2009**, *121*, 7620–7622.
- [12] S. S. Kistler, *Nature* **1931**, *127*, 741.
- [13] S. L. Brock, I. U. Arachchige, K. K. Kalebaila, *Comments Inorg. Chem.* **2006**, *27*, 103–126.
- [14] J. L. Mohanan, S. L. Brock, *J. Sol-Gel Sci. Technol.* **2006**, *40*, 341–350.
- [15] H. Yu, R. Bellair, R. M. Kannan, S. L. Brock, *J. Am. Chem. Soc.* **2008**, *130*, 5054–5055.
- [16] H. Yu, S. L. Brock, *ACS Nano* **2008**, *2*, 1563–1570.
- [17] Q. Yao, S. L. Brock, *Inorg. Chem.* **2011**, *50*, 9985–9992.
- [18] A.-K. Herrmann, P. Formanek, L. Borchardt, M. Klose, L. Giebeler, J. Eckert, S. Kaskel, N. Gaponik, A. Eychmüller, *Chem. Mater.* **2014**, *26*, 1074–1083.
- [19] D. V. Talapin, R. Koeppel, S. Götzinger, A. Kornowski, J. M. Lupton, A. L. Rogach, O. Benson, J. Feldmann, H. Weller, *Nano Lett.* **2003**, *3*, 1677–1681.
- [20] L. Carbone, C. Nobile, M. De Giorgi, F. D. Sala, G. Morello, P. Pompa, M. Hytch, E. Snoeck, A. Fiore, I. R. Franchini, M. Nadasan, A. F. Silvestre, L. Chiodo, S. Kudara, R. Cingolani, R. Krahn, L. Manna, *Nano Lett.* **2007**, *7*, 2942–2950.
- [21] N. Leventis, C. Chidambareswarapattar, A. Bang, C. Sotiriou-Leventis, *ACS Appl. Mater. Interfaces* **2014**, *6*, 6872–6882.
- [22] A. Eychmüller, *Angew. Chem. Int. Ed.* **2005**, *44*, 4839–4841; *Angew. Chem.* **2005**, *117*, 4917–4919.
- [23] A. Kern, W. Eysel, Mineralogisch-Petrograph. Inst., Univ. Heidelberg, Germany **1993**.
- [24] H. Zhang, I. Hussain, M. Brust, M. F. Butler, S. P. Rannard, A. I. Cooper, *Nat. Mater.* **2005**, *4*, 787–793.
- [25] L. Qian, H. Zhang, *J. Chem. Technol. Biotechnol.* **2011**, *86*, 172–184.
- [26] H. Moor, *Z. Zellforsch. Mikrosk. Anat.* **1964**, *62*, 546–580.
- [27] D. Walsh, L. Arcelli, T. Ikoma, J. Tanaka, S. Mann, *Nat. Mater.* **2003**, *2*, 386–390.
- [28] W. Liu, A.-K. Herrmann, D. Geiger, L. Borchardt, F. Simon, S. Kaskel, N. Gaponik, A. Eychmüller, *Angew. Chem. Int. Ed.* **2012**, *51*, 5743–5747; *Angew. Chem.* **2012**, *124*, 5841–5846.
- [29] N. C. Bigall, A.-K. Herrmann, M. Vogel, M. Rose, P. Simon, W. Carrillo-Cabrera, D. Dorfs, S. Kaskel, N. Gaponik, A. Eychmüller, *Angew. Chem. Int. Ed.* **2009**, *48*, 9731–9734; *Angew. Chem.* **2009**, *121*, 9911–9915.
- [30] A.-K. Herrmann, P. Formanek, L. Borchardt, M. Klose, L. Giebeler, J. Eckert, S. Kaskel, N. Gaponik, A. Eychmüller, *Chem. Mater.* **2014**, *26*, 1074–1083.
- [31] W. R. Holland, D. G. Hall, *Phys. Rev. B* **1983**, *27*, 7765–7768.

Received: September 24, 2015

Revised: October 26, 2015

Published online: December 7, 2015

Supporting Information

Versatile Aerogel Fabrication by Freezing and Subsequent Freeze-Drying of Colloidal Nanoparticle Solutions

*Axel Freytag, Sara Sánchez-Paradinas, Suraj Naskar, Natalja Wendt, Massimo Colombo, Giammarino Pugliese, Jan Poppe, Cansunur Demirci, Imme Kretschmer, Detlef W. Bahnemann, Peter Behrens, and Nadja C. Bigall**

anie_201508972_sm_miscellaneous_information.pdf

Table of contents:

1. Experimental section
2. Nanoparticle characterization
3. Ligand exchange experiments
4. Electron microscopic imaging of the aerogels
5. Shaping of the aerogels
6. Size/volume fraction dependency
7. TGA & XRD measurements
8. Specific surface area measurements
9. Optical characterization
10. References

1. Experimental Section

Solutions of the noble metal nanoparticles were synthesized following slightly modified previously reported methods for gold, silver, palladium and platinum.^[1-2] All solutions were filled with distilled water (18 M Ω cm) to reach a total volume of 500 mL including the noble metal precursor and reducing agent solutions and were stirred vigorously throughout the whole reaction to ensure complete mixing of the liquids. For the synthesis of **gold** nanoparticles, we used 29 mL of a 0.2 wt% tetrachloroaurate (III) trihydrate solution (ABCR, 99.99%) at room temperature. A total amount of 11.6 mL of a 1 wt% trisodium citrate dihydrate (ABCR, 99.0%) were added to the gold precursor solution and after 30 seconds 5.8 mL of a 0.17 wt%, ice-cold sodium borohydride (Fluka, \geq 99%) were quickly injected. The yellow solution turned to red immediately.

For the synthesis of **silver** nanoparticles we used 12 mL of a 0.2 wt% silver nitrate (Alfa Aesar, 99.9%) solution which was heated to 100 °C. Subsequently, we added 11.6 mL of a 1 wt% trisodium citrate dihydrate solution, and after 30 seconds, 5.5 mL of a 0.076 wt% ice-cold sodium borohydride solution was quickly injected. The color of the solution turned to yellow immediately.

For the synthesis of **platinum** nanoparticles 36.2 mL of a 0.2 wt% platinum(IV)chloride (acros, 99%) in water solution were boiled for 1 min at 100 °C and a total amount of 11.6 mL of a 1 wt% trisodium citrate dihydrate solution was added. After 30 seconds, 5.5 mL of a 0.076 wt% ice-cold sodium borohydride solution were quickly injected in the above mixture and the color changed from yellow to a dark brown.

For the synthesis of **palladium** nanoparticles 0.0513 g palladium(II)chloride (Sigma Aldrich, 99.999%) were dissolved in 37 wt% hydrochloric acid (Sigma Aldrich, reagent grade) with a molar ratio equal to 1:2 and filled up to 100 mL with distilled water. The temperature of the solution was raised to 80 °C, and then 11.6 mL of a 1 wt% trisodium citrate dihydrate solution was added. After 30 seconds, 5.5 mL of a 0.076 wt% ice-cold sodium borohydride solution were quickly injected, and stirred for 10 minutes at 80 °C. The color of the solution changed from yellow to black.

A **ligand exchange** was carried out with the platinum colloid by exchanging citrate against thioglycolic acid (TGA, Sigma Aldrich >99%) and mercaptosuccinic acid (MSA, Sigma Aldrich >99%) as described in literature.^[3] High concentration of ligands were used to ensure complete exchange. For 1 L of Pt-colloid (2.8×10^{-4} M) an aqueous solutions of MSA (2.6 g, 10 mL) or TGA (50 mL, 70 mM) solution was added dropwise under stirring, adjusting the pH to 12 for TGA or 7 for MSA with NaOH (0.1 M) and stir for 24h in the dark.

Synthesis of CdSe/CdS nanorods. The nanocrystals are synthesized following a seeded growth approach^[4] which is based on the anisotropic growth of CdS over previously prepared spherical CdSe seeds. In a first stage the CdSe seeds are prepared by mixing Tri-n-octylphosphine oxide (TOPO, ABCR 99 %) (3.0 g), Octadecylphosphonic acid (ODPA, PCI Synthesis 99 %) (0.280 g) and CdO (Alfa Aesar, 99.99 %) (0.060 g) in a 50 mL flask. The reaction mixture was heated to 150 °C and degassed under vacuum for 1 hour. In order to dissolve the CdO and to obtain a clear and colorless solution, the temperature was raised to 300 °C under nitrogen flow. At this point, 1.8 mL of Tri-n-octylphosphine (TOP, ABCR 97 %) was injected into the flask, and the temperature was allowed to rise up to 380 °C. Once the temperature had reached 380 °C, a 1:1 Se (Alfa Aesar, 99.99%): TOP solution (0.058 g Se + 1.8 mL TOP) was quickly injected. For obtaining red fluorescent CdSe seeds the temperature was allowed to recover before cooling the solution to room temperature. The synthesized seeds were washed by repeated precipitation with methanol and redissolution in toluene, and were finally dissolved in toluene. The synthesis of the CdSe/CdS nanorods was based on the above-mentioned work. Briefly, CdO (0.240 g) was mixed in a flask with TOPO (12.0 g), ODPA (1.12 g) and hexylphosphonic acid (HPA, PCI Synthesis 99 %, 0.32 g). The flask was first degassed under vacuum for about 1 hour at 150 °C and then heated up to 300 °C under nitrogen. Once the temperature had reached 300 °C, 7.2 mL of TOP was injected and the resulting solution was heated to 380 °C under nitrogen. At this point, a TOP solution containing sulfur precursor (0.52 g S + 7.2 mL TOP) in which the seeds in toluene (the concentration of dots in

the toluene solution was always 400 μM) are dissolved was quickly injected. After injection, the temperature was allowed to recover to the pre-injection temperature before removing the heating mantle. The nanorods obtained were washed several times and finally stored in 8 mL toluene. The CdSe/CdS nanorods were phase transferred from organic to aqueous solution by exchanging the ligands of the as-prepared nanoparticles (TOP/TOPO) with 3-mercaptopropionic acid (MPA, Sigma Aldrich $\geq 99\%$).^[6] Briefly, two batches of 750 μL of the as-prepared nanoparticles from toluene solution were precipitated with methanol and re-dissolved in 10 mL hexane. This solution was mixed with 10 mL of a solution consisting of 10 mL methanol, potassium hydroxide (3.56 mmol) and the corresponding ligand MPA, (2.78 mmol). After shaking for one hour, the organic phase was discarded by a separation funnel and the aqueous part containing the nanoparticles with the thiol ligands was centrifuged. Finally, the solid from the two batches was redissolved in a total volume of 900 μL of aqueous 0.1 M potassium hydroxide solution. Before the preparation of the gels, the solution was washed once up to three times with water in a centrifuge filter tube (Amicon Ultra-15 Centrifugal Filter form Merck Millipore). This cleaning step eliminates the excess ligand used in the phase transfer.

Synthesis of hematite nanoparticles. The hematite nanoparticles were synthesized following the hydrolysis method of Faust et al.^[6] First, 150 mL of a 0.1 M iron-III-chloride hexahydrate (Sigma Aldrich, $>99\%$) were injected dropwise into 600 mL boiling distilled water. The solution was additionally boiled for 5 min under reflux and then cooled down with an ice bath. The resulting clear solution was then dialyzed against distilled water to increase the pH and remove ionic species.

Cryogelation. All colloids (noble metals, hematite, CdSe seeded CdS rods) were used at room temperature. In a solvent resistant ultrafiltration cell (Merck Millipore), by means of a 10 kDa polyethersulfon membrane (Sartorius Stedim) and at a pressure of 5-6 bar, the volume of the colloids was reduced from 500 mL to 50 mL. These 50 mL were then filled into a centrifuge tube with an inbuilt filter (Vivaspin 20, 30kDa, Sartorius or Amicon Ultra-15, 10kDa, Merck Millipore), and the volume of the solution was further reduced to 5 mL or even 0.5 mL depending on the intended volume fraction (at 3800 rcf for 3 to 10 min). Then the solutions were washed three times with 15 mL deionized water. Subsequently, the colloids were immediately frozen via direct injection in liquid nitrogen. In the liquid nitrogen, the samples were kept for additional 5 minutes. Finally, the samples were placed into a freeze dryer (Christ) at <0.05 mbar for 24 to 48 h, and the resulting aerogels were stored under ambient conditions.

Thin films. Thin aerogel films were prepared by doctoral bladeing of NC colloids on NaOH treated glass slides and subsequent immersion in a liquid nitrogen bath. NaOH treatment was done by dipping glass slides (microscope slides, Roth) for 2h in a 5M NaOH solution at room temperature, rinse them with distilled water and subsequent drying at 80°C for 15h. Finally the thin films were dried for 2h in a freeze dryer (Christ) at <0.05 mbar for 24 to 48 h.

Thermogravimetric analyses (TGA). TGA were carried out using a TA Instruments TGA Q500. Samples were heated at $5^\circ\text{C}/\text{min}$ in N_2 flow (50 mL min^{-1}).

Scanning electron microscopy (SEM). SEM was performed using a JEOL JFM 6700F electron microscope operated at 2 kV. The samples were prepared by placing small aerogel pieces onto an adhesive carbon polymer pad.

Transmission electron microscopy (TEM). TEM was performed by a FEI Tecnai G2 F20 electron microscope, operated at 200 kV. The samples were prepared by ultrasonating the aerogel in water for 30 seconds followed by drop casting onto a copper mesh (Quantifoil) covered with a carbon film and drying under vacuum. Alternatively, the TEM grids were prepared by slightly pressing the carbon coated copper grids on the aerogel samples.

X-ray diffraction (XRD). XRD was carried out using a Bruker D8 Advance in reflection mode.

Nitrogen sorption measurements were carried out on a Quantachrome Autosorb 3. From the adsorption isotherms, specific surface areas were determined using the Brunauer–Emmett–Teller (BET) method. The pore size distributions were calculated by the density functional theory from the desorption branch of the isotherm. Both analyses were performed with the help of the software ASIqwin 2.0 from Quantachrome.

Optical spectroscopic measurements UV/Vis absorption spectra of the noble metal colloids were recorded using a 3 mL quartz cuvette and the spectrophotometer Cary 5000 (Agilent Technologies) equipped with an integrating sphere (Labsphere). Fluorescence measurements were performed with a Fluoromax-4 spectrofluorometer (HORIBA Jobin Yvon Inc.). Absorbance and photoluminescence (PL) spectra of the films and monoliths were acquired in a Dual-FL (HORIBA Jobin Yvon Inc.) equipped with a Quanta- ϕ integrating sphere (HORIBA). Time-correlated single photon counting (fluorescence lifetime) measurements were performed on a Fluoromax-4 combined with the Fluorohub TCSPC unit, using two pulsed diodes (operating at 368 nm and 454 nm, respectively) with a pulse fwhm of less than 1.6 ns and a repetition rate of 500 kHz. All spectra were measured at room temperature.

Electrochemical characterizations. The Pt cryogels were dispersed in water by sonication for about 15 min to yield a platinum concentration of 1 mg mL^{-1} . Subsequently, 4 μL of this cryogel dispersion were dropcasted onto glassy carbon disc electrodes (CH Instruments, 3 mm diameter) and the solvent was evaporated by drying at 85°C for 10 min. Cyclic voltammetry experiments were conducted in a five-necked electrochemical cell using a conventional three-electrode setup and a PARSTAT 4000 electrochemical workstation (Princeton Applied Research). The Pt-modified glassy carbon electrode, an Ag/AgCl (3 M NaCl) and a Pt wire were used as working, reference and counter electrode, respectively. A Haber-Luggin capillary was used to minimize the uncompensated solution resistance and to avoid contamination by chloride ions. All experiments were carried out in 0.5 M sulfuric acid, which was deaerated by purging the cell with nitrogen for about 15 min prior to the measurements. The electrochemical surface area (ECSA) was determined from the charge associated with the underpotential deposition of hydrogen by integrating the peaks in the range between 0 and 0.4 V vs RHE and subtraction of the capacitive contribution. For Pt a specific charge of $210\text{ }\mu\text{F cm}^{-2}$ was assumed.

2. Nanoparticle characterization

Quasi-spherical noble metal nanoparticle (gold, silver, palladium, platinum)

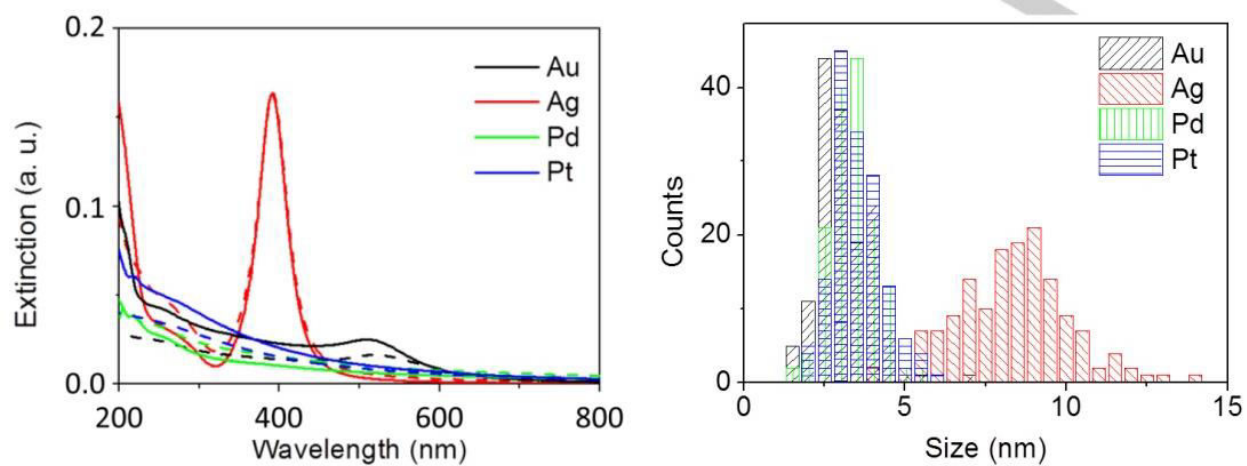


Figure SI-2.1. Extinction spectra (left diagram) of the synthesized aqueous noble metal nanoparticle solutions (solid lines) and the 100 times concentrated solution (re-diluted for comparison). Particle size distribution (right) of the synthesized noble metal nanoparticles. The diameters were $3.3 \text{ nm} \pm 0.4 \text{ nm}$ (Au), $8.6 \text{ nm} \pm 2.3 \text{ nm}$ (Ag), $3.6 \text{ nm} \pm 0.6 \text{ nm}$ (Pd), and $3.8 \text{ nm} \pm 0.7 \text{ nm}$ (Pt).

CdSe/CdS quantum rods

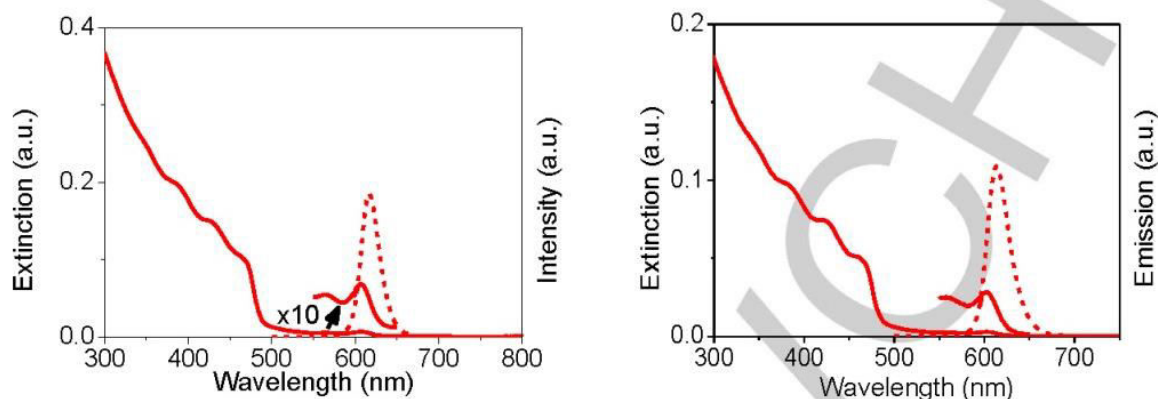


Figure SI-2.2. Extinction spectra (left) of the CdSe/CdS quantum rods (solid lines) and their emission spectra (dashed line). The PLQY was determined to be 51% (with a lifetime of 19.8 ns) in the organic solution and 23.6% (with a lifetime of 18 ns) in aqueous solution after the phase transfer (right). Particle size distribution (not shown) gives 36.4 nm \pm 2.9 nm rod length and 5.7 nm \pm 0.8 nm rod thickness.

Iron oxide

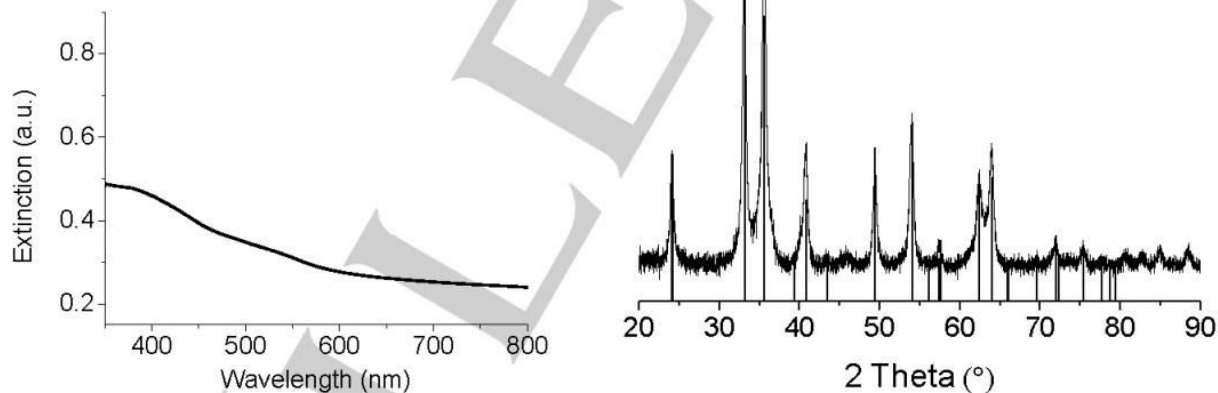


Figure SI-2.3. Extinction spectra of the hematite nanoparticles (left) and x-ray diffraction pattern to confirm hematite modification (right). Sample preparation modified particle size and therefore allows no crystallite size determination via Debye-Scherrer equation. Black solid bars represent reflexes for bulk hematite semiconductor.^[7] Particle size distribution (not shown) gives a particle diameter of 8.5 nm \pm 1.9 nm.

3. Ligand exchange experiments

Ligand exchange experiments have been conducted on 3.5 nm Pt particles to check the influence on the structure and the stability of the resulting monoliths. We observed that the mechanical stability of the aerogel monoliths has increased after ligand exchange. We did not observe any change in the nanoscopic structure (meaning interparticle distances or shape - see SI-3. 1). However there might be a slight influence on the microscopic structure. We observe a slightly different ratio of sheets to wires when changing the surface ligands from citrate to MSA and TGA.

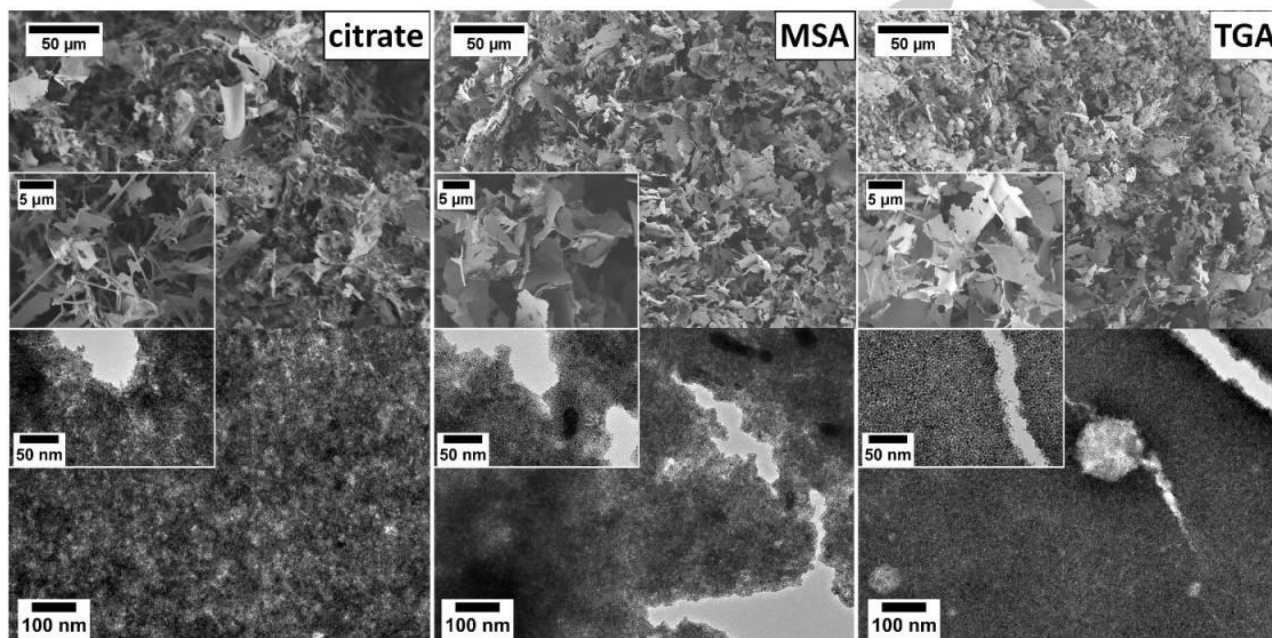


Figure SI-3.1: SEM micrographs show the morphology of Pt aerogels fabricated from different ligands. The ratio of sheets to wires seem to increase slightly but no other changes could be observed. In the TEM images/micrographs we cannot observe any influence of the ligands on the nanoscopic assembling or on the size or the shape of the Pt nanoparticles. There is no difference in interparticle distances visible.

4. Electron microscopic imaging of the aerogels

The following pictures show aerogels of gold (SI-4.1), silver (SI-4.2), palladium (SI-4.3), platinum (SI-4.4), CdSe/CdS quantum rods (SI-4.5), and hematite (SI-4.6) in different magnifications from SEM and TEM and in addition TEM images after the catalytic experiments for the noble metals.

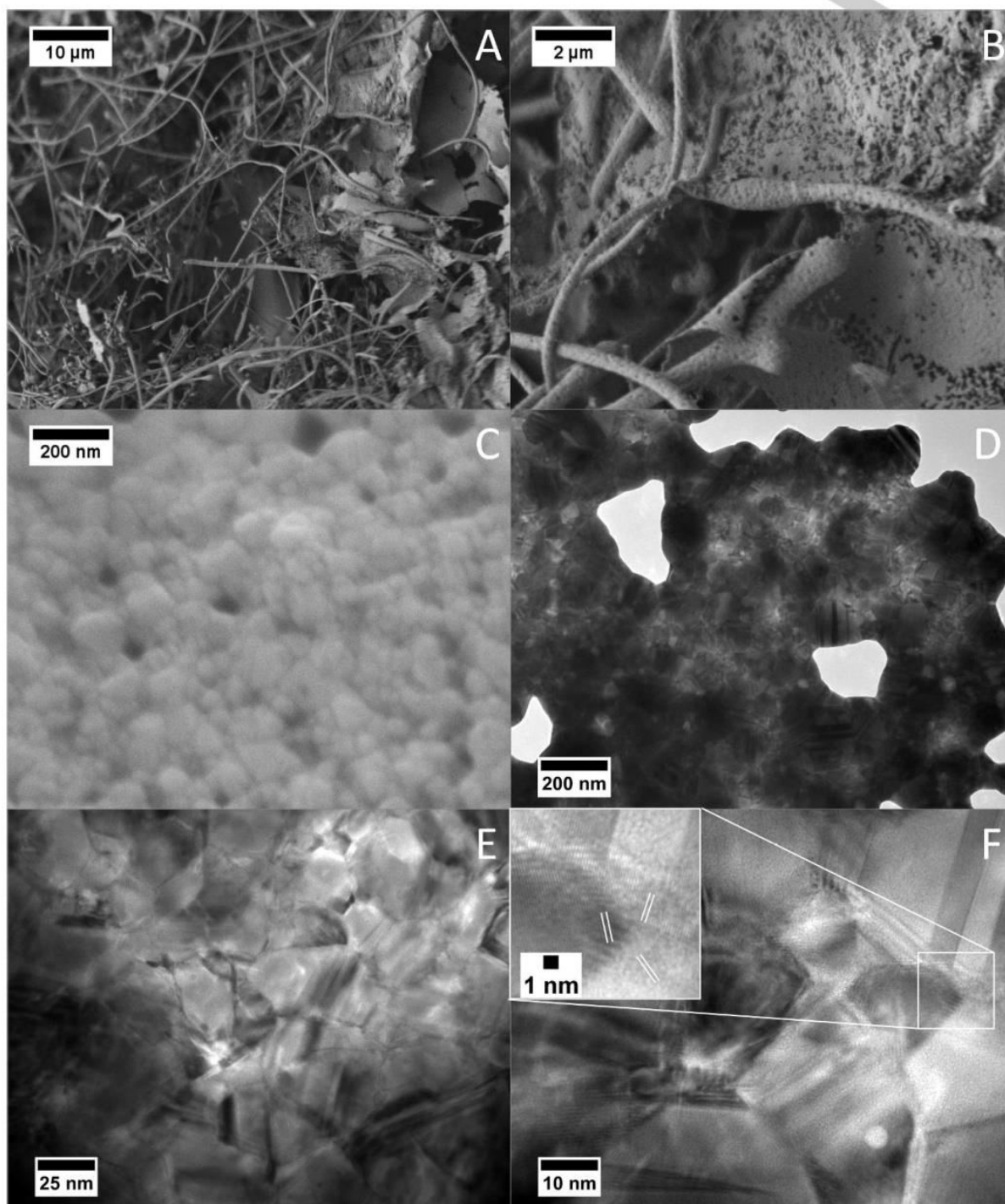
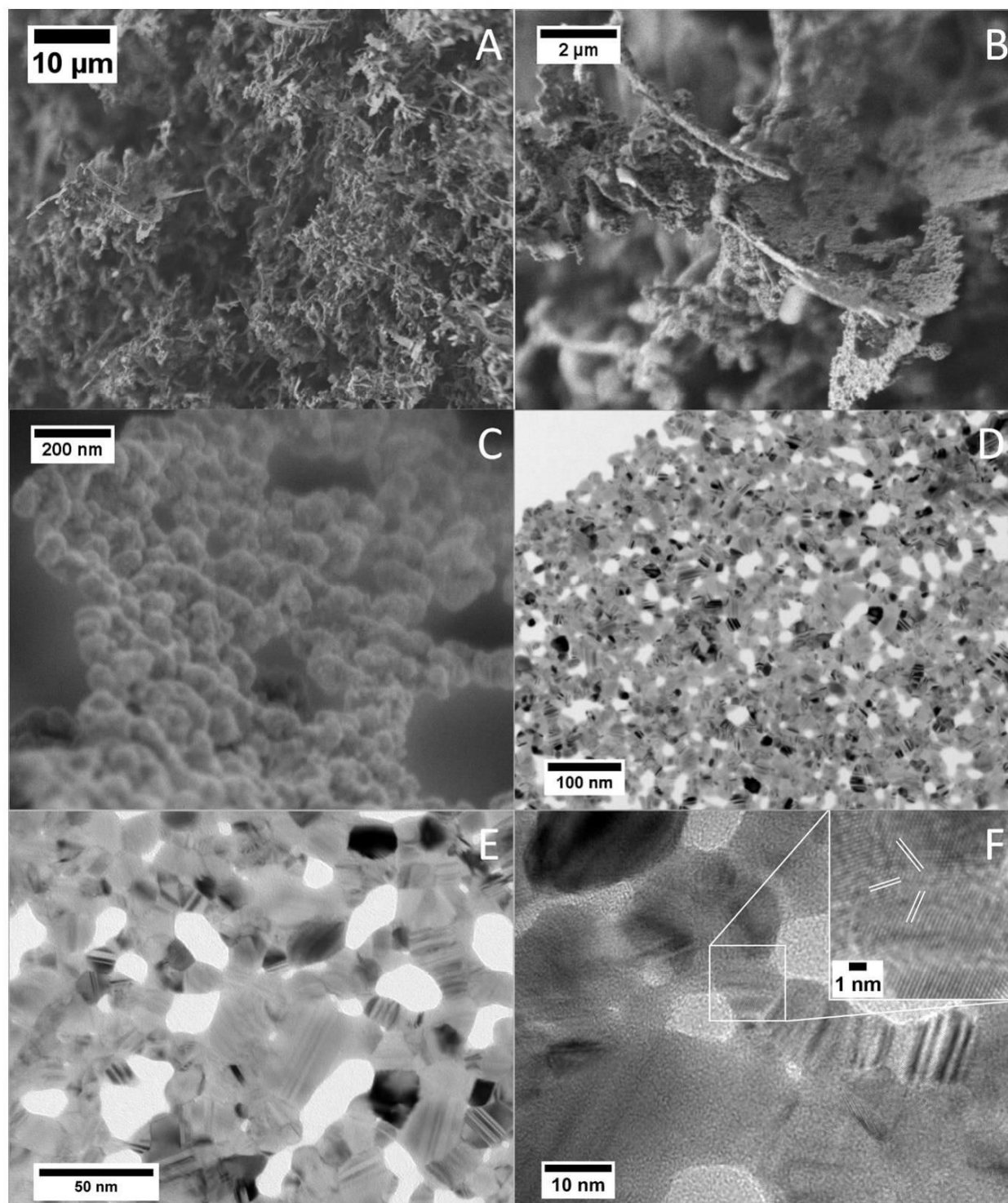
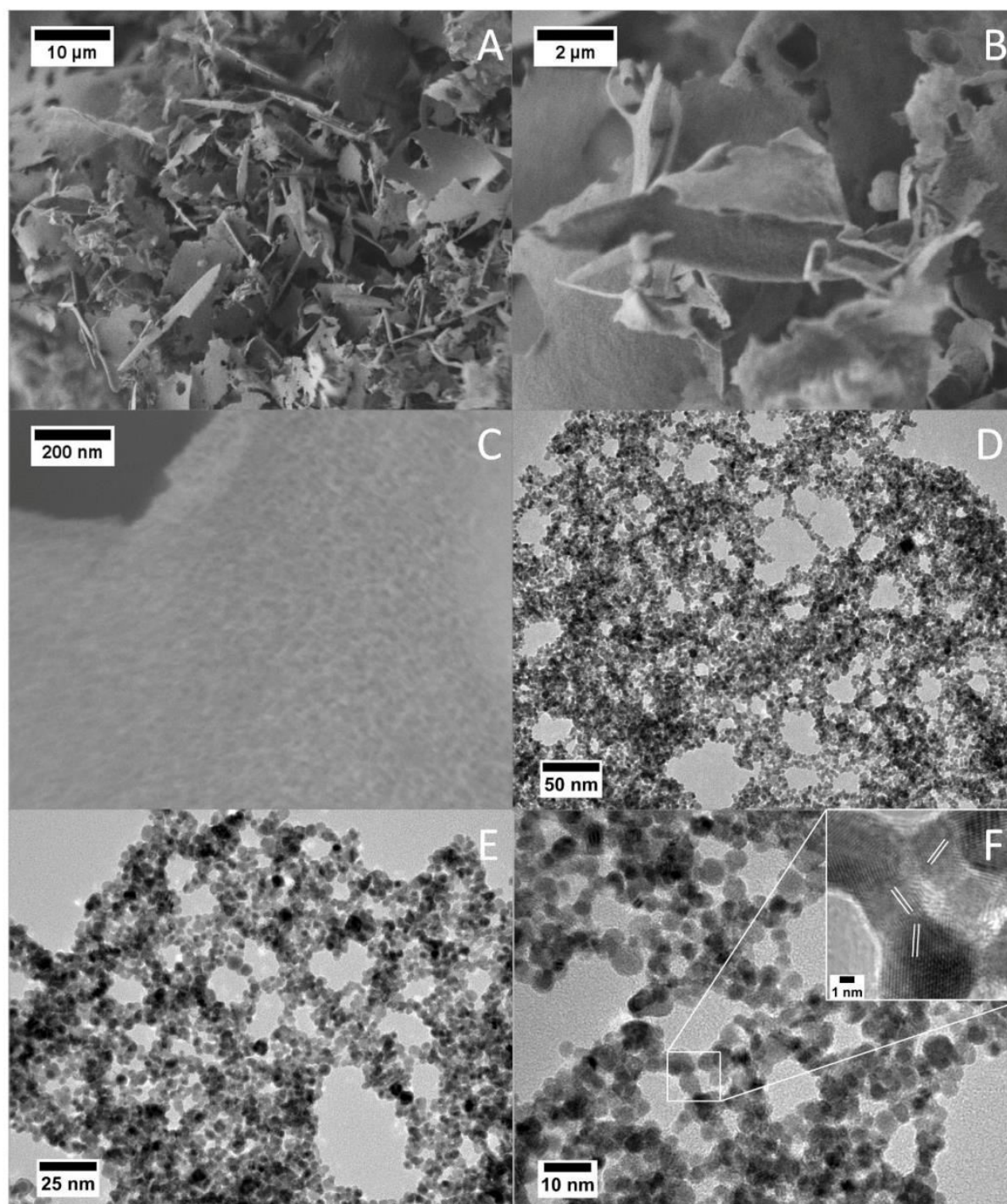


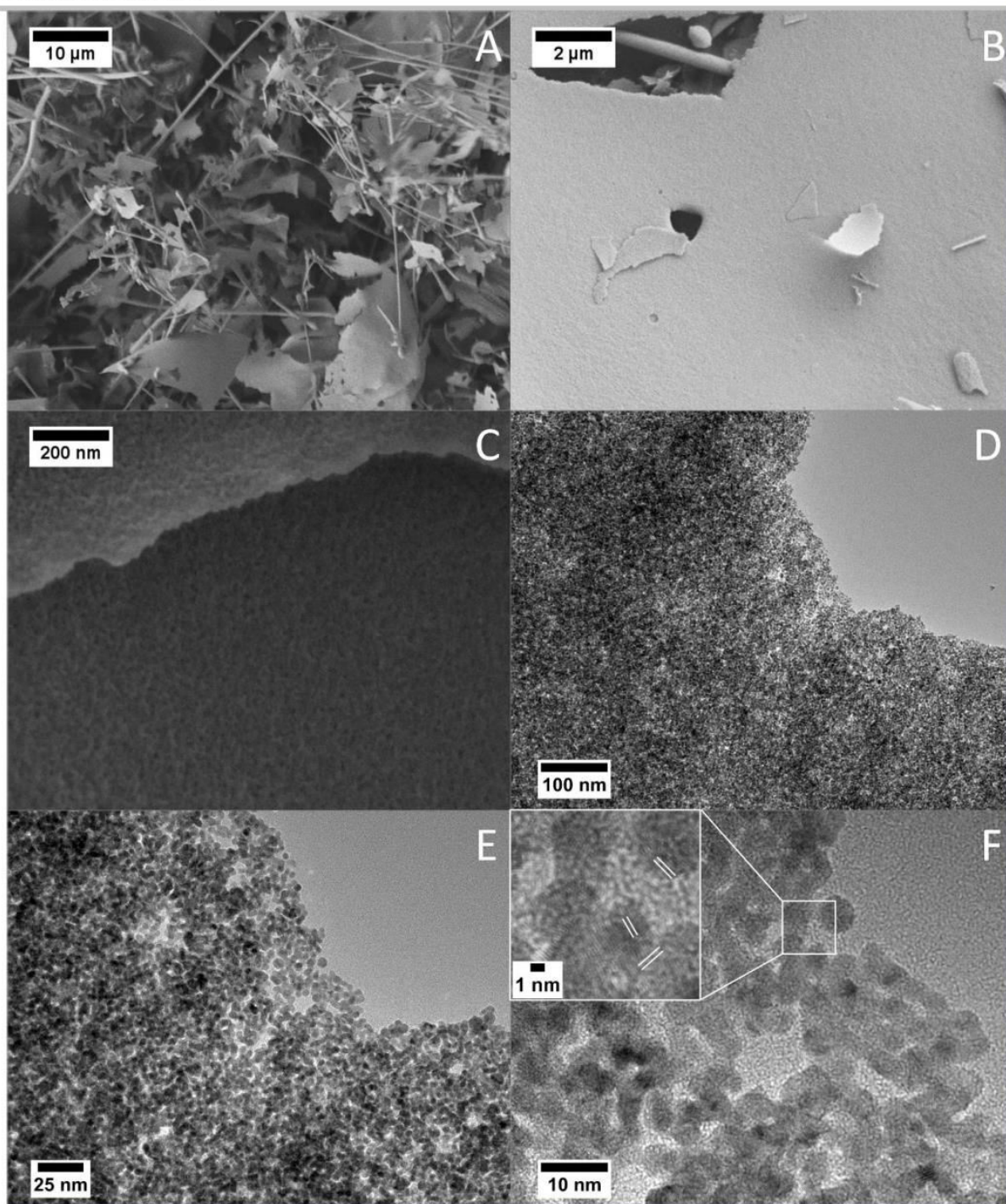
Figure SI-4.1. (A & B) SEM images of the macroscopic network of a gold aerogel. (C) SEM image of the assembly from gold nanoparticles into thin sheet-like structures. (D) TEM images of the sheet-like structure (E & F) TEM image of deformed gold nanoparticles in the sheets. The inset shows different lattice orientation of the (111) face from gold nanoparticles assembled in thin sheets.



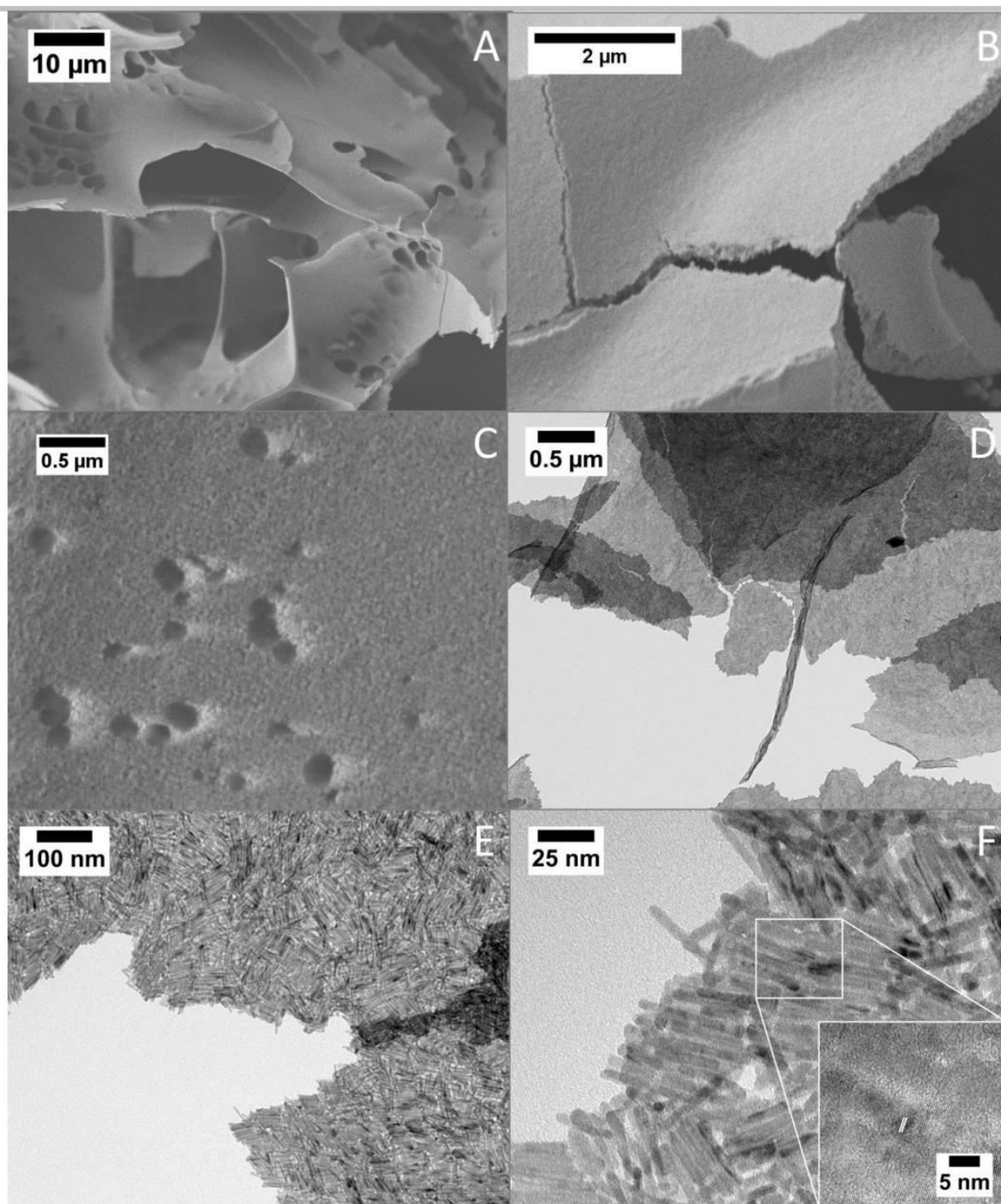
Supporting Information 4.2. A & B) SEM images of the macroscopic network of a silver aerogel. C) SEM image of the assembly from silver nanoparticles into thin sheet-like structures. D, E) TEM images of the sheet-like structure F) TEM image of deformed silver nanoparticles in the sheets. The inset shows different lattice orientation of the (111) face from silver nanoparticles assembled in thin sheets.



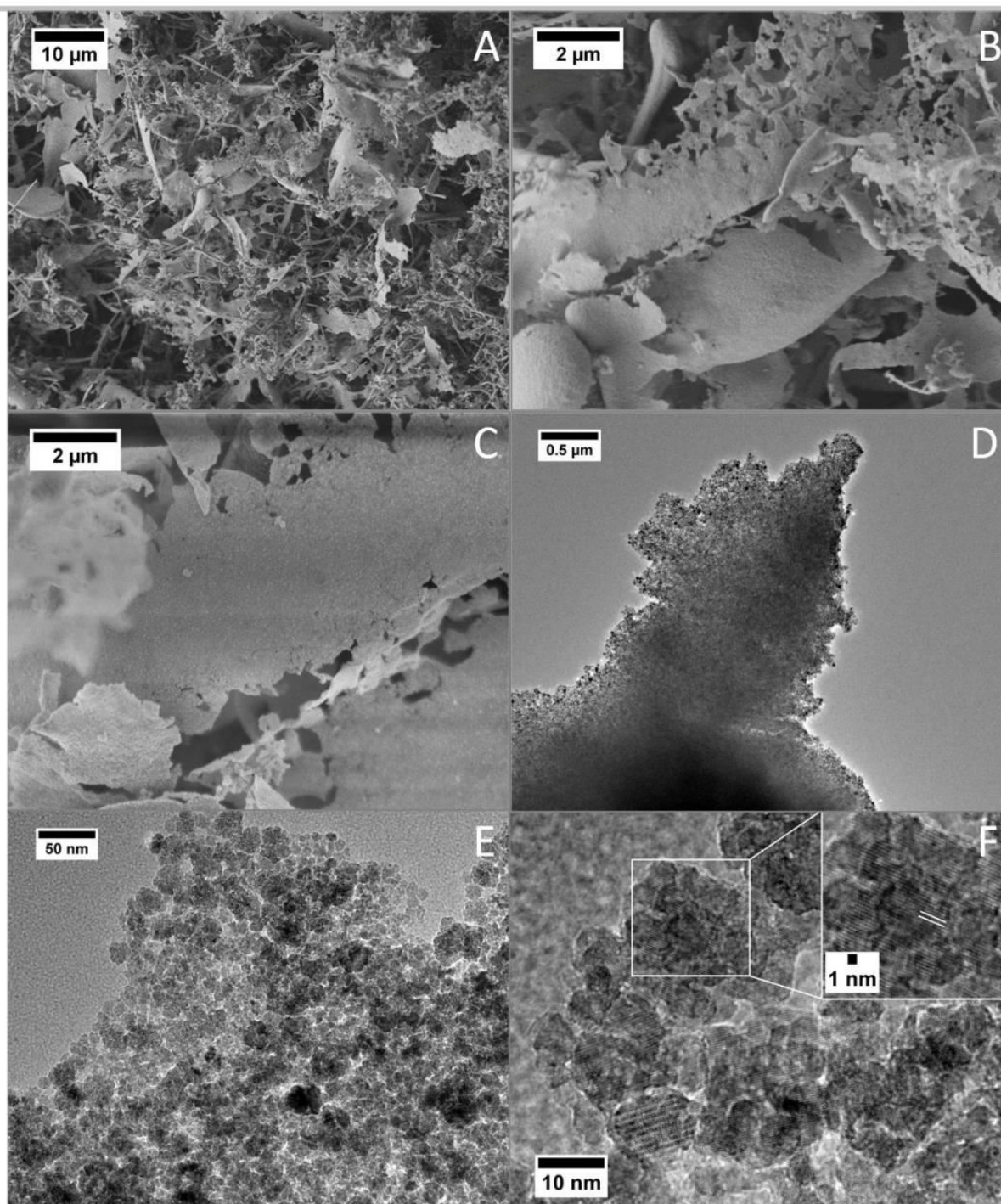
Supporting Information 4.3. (A & B) SEM images of the macroscopic network of a palladium aerogel. (C) SEM image of the assembly from palladium nanoparticles into thin sheet-like structures. (D) TEM images of the sheet-like structure (E & F) TEM image of assembled palladium nanoparticles in the sheets. The inset shows different lattice orientation of the (111) face from palladium nanoparticles assembled in thin sheets.



Supporting Information 4.4. (A & B) SEM images of the macroscopic network of a platinum aerogel. (C) SEM image of the assembly from platinum nanoparticles into thin sheet-like structures. (D) TEM images of the sheet-like structure (E & F) TEM image of assembled platinum nanoparticles in the sheets. The inset shows different lattice orientation of the (111) face from platinum nanoparticles assembled in thin sheets.



Supporting Information 4.5. (A,B) SEM images of the macroscopic network of a CdSe seeded CdS rod aerogel. (C) SEM image of the assembly from CdSe seeded CdS rod nanoparticles into thin sheet-like structures. (D) TEM images of the sheet-like structure (E,F) TEM image of assembled CdSe seeded CdS rod nanoparticles in the sheets. The inset shows direct contact of CdSe seeded CdS nanorods assembled in thin sheets.



Supporting Information 4.6. (A & B) SEM images of the macroscopic network of a hematite nanoparticle aerogel. (C) SEM image of the assembly from hematite nanoparticles into thin sheet-like structures. (D) TEM images of the sheet-like structure (E, F) TEM image of assembled hematite nanoparticles in the sheets. The inset shows direct contact from hematite nanoparticles assembled in thin sheets.

5. Shaping of the aerogels

If the volume fraction of nanoparticles increases over 0.1 vol% no shrinkage was observed for the resulting monoliths. This allows the possibility to shape the monolith into desired geometries. For example, thin films immobilized on glass slides can ease the handling for characterization and have in addition a less complex geometry compared to monolith. We prepared oriented thin films by doctor blading of the NC colloid, subsequent freezing and freeze drying. With this method we could produce oriented thin films with a thickness of around 20 μm (see SI-5.1 to 5.3). In addition trough using a mold, many more shapes can be acquired (see Scheme in SI-5.4 and 5.5). However due to the fragile nature of the aerogels it is possible that the shaped aerogels break during drying. To prevent such events the ligand concentration can be increased.

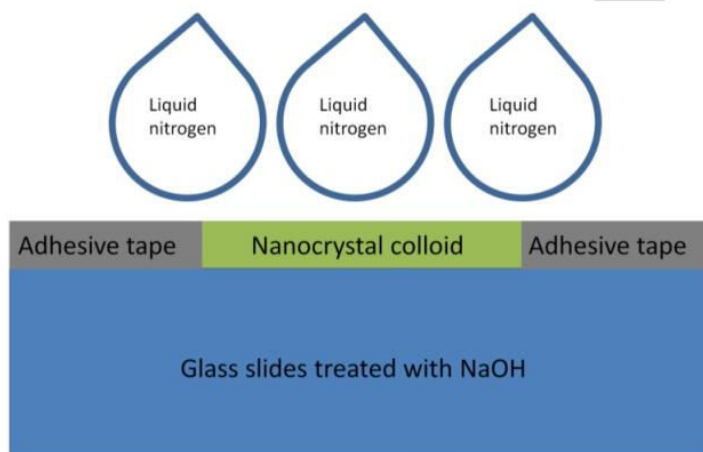


Figure SI-5.1. Scheme of the thin film fabrication

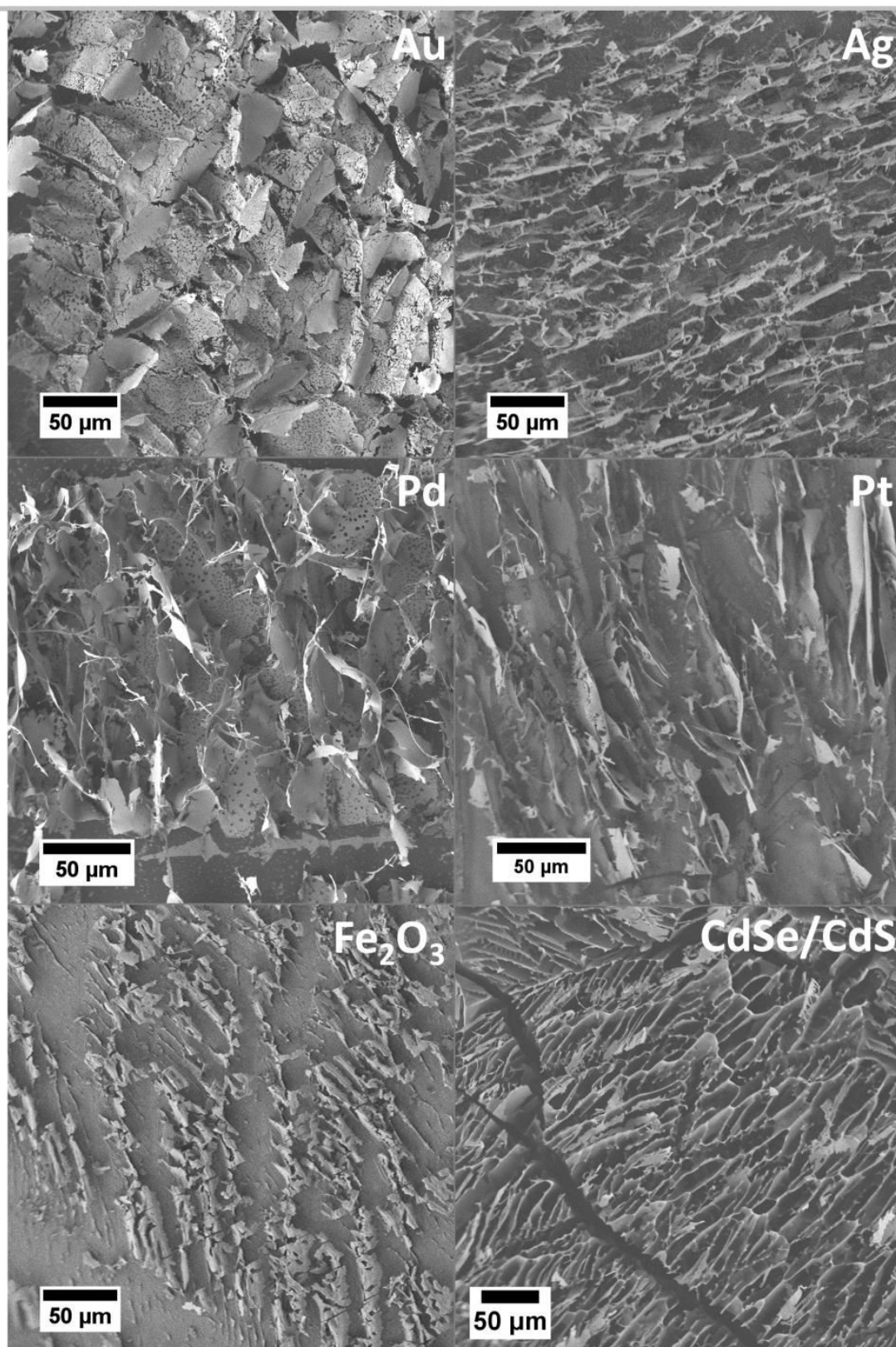


Figure SI-5.2 SEM images in top view of thin film aerogels of Au, Ag, Pd, Pt, hematite, and CdSe/CdS.

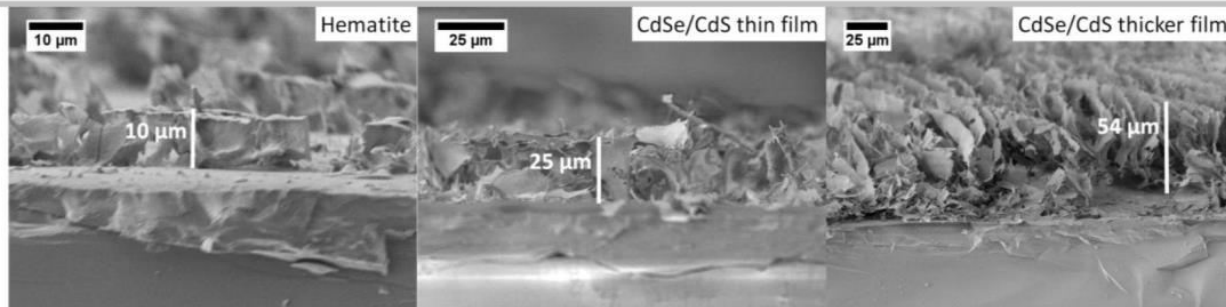


Figure SI-5.3 SEM images of thin film aerogels in the cross section of hematite (left) and CdSe/CdS with different intended film thicknesses.

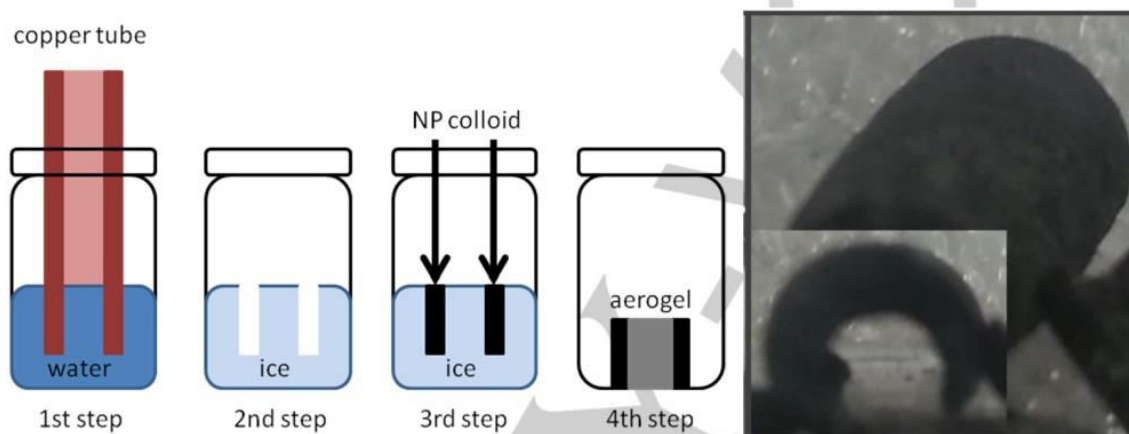


Figure SI-5.4. Scheme of the template approach for shaping aerogels and resulting aerogel structure



Figure SI-5.5 Shaping of the aerogels by the template approach to create a 3D smiley. (From left to right) The NP colloid is filled in a silicon mold and frozen in liquid nitrogen. While freezing due to the expansion of the water volume a “nose” is growing (note that this can happen all over the smiley). The mold is removed after freezing (where the smiley broke in the mouth area and had to be “fixed” with a “cigar”) and subsequent dried. A difficulty during the shaping is mainly the breaking apart of the shape due to the fragile nature of the aerogels.

6. Size/volume fraction dependency

We varied the concentration of the 3.5 nm Pt NCs (or the volume fraction of NC) in the colloid from the synthesis concentration (0.5 mM equalling a volume fraction of $2.5 \cdot 10^{-4}$ vol%) to a 1600 times concentrated solution (0.8 M equalling a volume fraction of 0.4 vol%). We can observe that the volume fraction has only little influence on a nanoscopic level. In general sheets made out of Pt NCs are formed. Sheets made from the original synthesis solution consist of about 2 NC layer (Figure SI-6.1 A), while the sheets from solutions with higher volume fractions show less porosity and more and more NC layer (Figure SI-6.1 from B to D). On a macroscopic level we see that aerogels with low volume fractions suffer a huge shrinkage, while increasing the volume fraction leads to lower shrinkage. Above a threshold of 0.1% volume fraction no shrinkage can be observed.

In addition we checked the influence of different sizes of NCs, ranging from 3.5 to 120 nm. As can be seen in Figure SI-6.2 the sheets still consist of assembled NCs. Since the particle size is bigger, the sheets also become thicker and the pores are wider. Apart from that effect they were pretty similar to the 3.5 nm Pt NCs. As long as the volume fraction is kept above 0.1% the aerogels suffer no shrinkage. When using a mixture of different particle sizes the biggest ones will form the sheets, while the smaller ones assemble in the pores in between (Figure SI-6.2 D). However the assembling in this case is not homogenous but will give areas where the number of a certain particle size is higher than in the rest of the sheet.

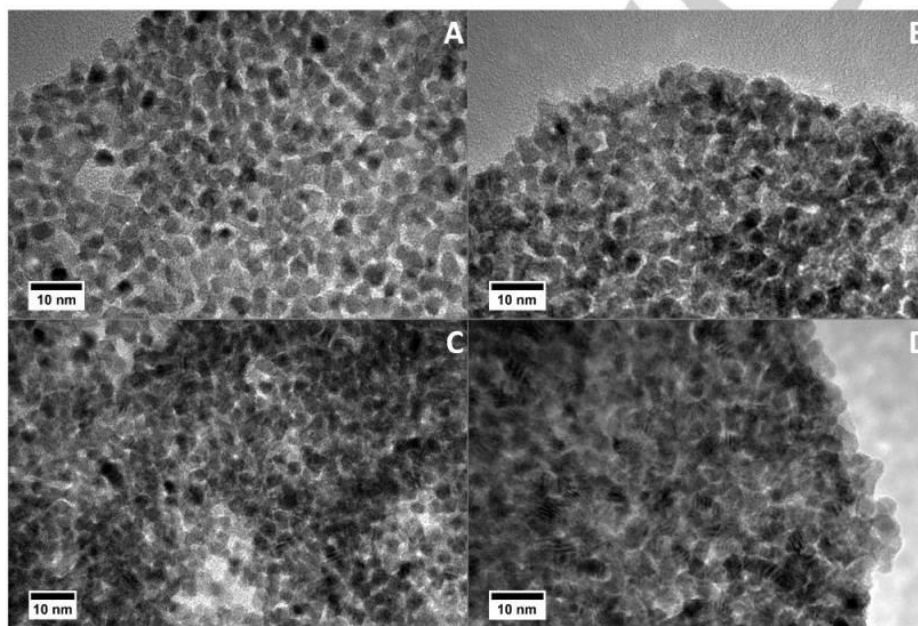


Figure SI-6.1. TEM images of platinum aerogels with a volume fraction of 0.00025 (A, corresponds to the synthesized particle colloid), 0.0025 (B), 0.025 (C) and 0.25 (D).

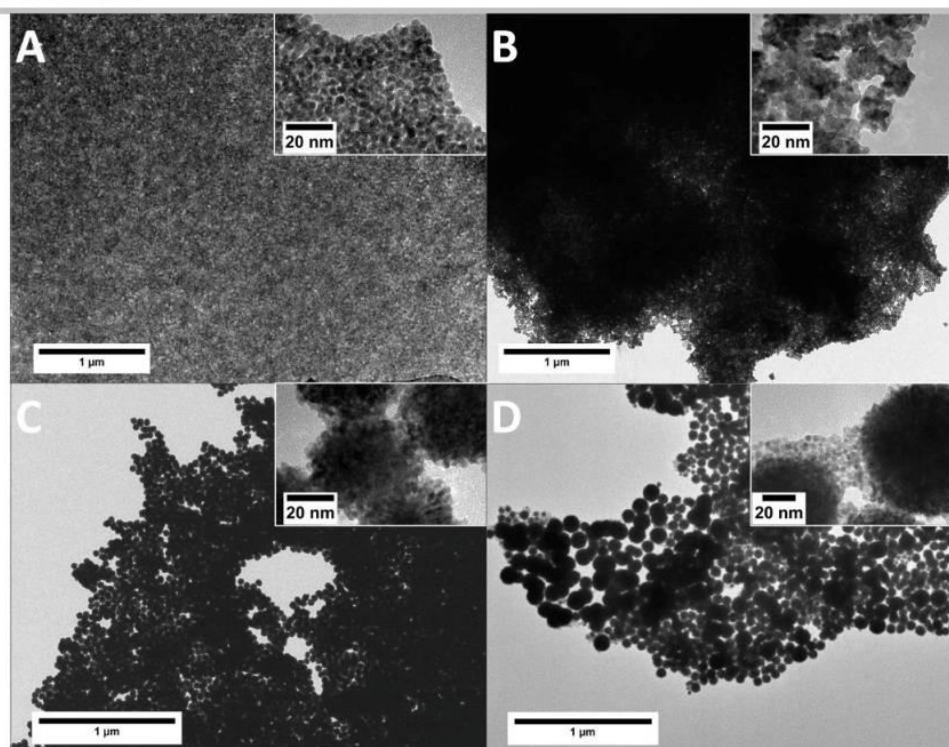


Figure SI-6.2. TEM images of platinum aerogels with a nanoparticle size of 3.5 nm (A), 15 nm (B), 40 nm (C) and mixed particle sizes ranging from 3.5 nm to 120 nm (D).

7. TGA & XRD measurements

Thermo gravimetric analysis (TGA) (see Figure SI-7.1) reveals that the residual water and organic compounds (especially citrate ligands from the nanoparticles synthesis), have a mass fraction smaller than 2 wt% for all aerogels except the one from palladium. The palladium aerogel, instead, exhibit a weight loss of around 10 wt% at around 120 °C. Summarizing the TGA measurements we can say that our noble metal superstructures are self-supporting and do not have a very high organic content. One should notice, that due to the lightweight nature of the samples (sample mass in the range of mg) the signal to noise ratio becomes pretty strong and effects like apparent increase of mass can occur (as can be seen for the Pd aerogel sample)

XRD measurements (see Figure SI-7.1) confirmed for all aerogels the face centered cubic crystal structure of the noble metals as expected. Calculations of the crystallite sizes via Debye-Scherrer equation^[9] showed average sizes of approximately 16 nm, 8 nm, 3 nm, and 3 nm for gold, silver, palladium, and platinum, respectively, which also confirms that only the size of the gold is altered during the aerogelation. This observation is in good agreement with the observations from TEM measurements. We attribute the growth of the NCs to the possibly enhanced pressure in the interstitial places between the ice crystallites where the particles are assembled during the freezing process.

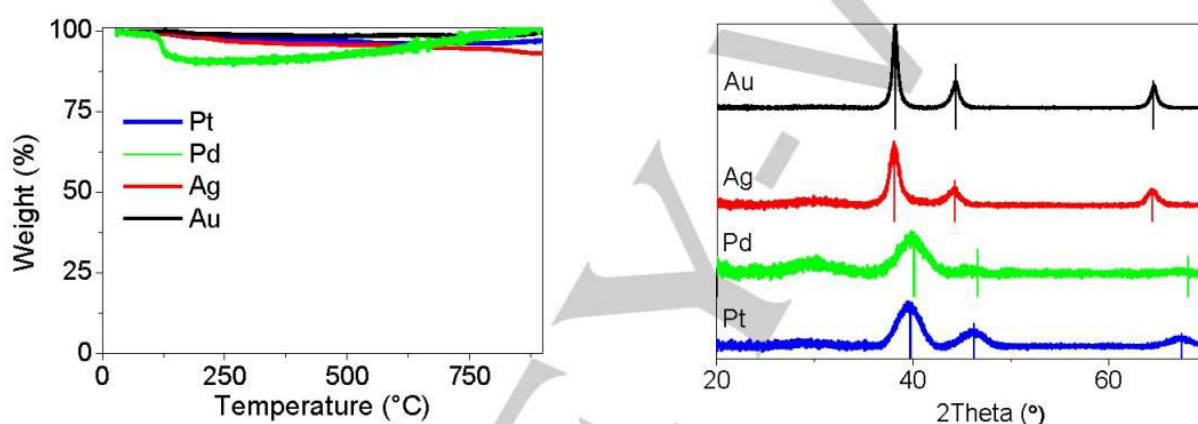


Figure SI-7.1. TGA measurements (left) of the Au, Ag, Pd and Pt aerogels. XRD measurements (right) of the gold, silver, palladium and platinum aerogels. Bars represent literature values for the (111), (200) and (220) reflexes respectively.^[9-12] The corresponding crystallite size for the (111) reflex via Debye-Scherrer equation were found to be 16 nm, 8 nm, 3 nm and 3 nm for gold, silver, palladium and platinum, respectively.

8. Specific surface area measurements

Physisorption

Due to their well interconnected structure the aerogel monoliths exhibit large specific surface areas in nitrogen adsorption measurements, as can be seen in Figure SI-8.1. All adsorption isotherms of the aerogels exhibit IUPAC type 3 behavior. Specific surface areas estimated via the Brunauer-Emmett-Teller equation (BET)^[13] were larger than 15 m² g⁻¹ for silver and palladium and amounted to 33 m² g⁻¹ for platinum. It was not possible to derive a specific surface area for gold samples since the adsorption isotherms could not be fitted with the BET approach. In comparison, the very same particles dried under ambient conditions showed specific surface areas far below the quantification limit. In agreement with the morphologies as derived from electron microscopy images, all isotherms exhibit sorption hystereses due to capillary condensation in the pores. The broad hysteresis without specific features is in agreement with a broad distribution of mesopores. Pore size distributions calculated from the desorption isotherm using density functional theory (DFT) show the presence of a majority of mesopores in the size range from 5 to 10 nm, which corresponds to the distances and small pores between the nanoparticles within the sheets as observed in SEM/TEM.

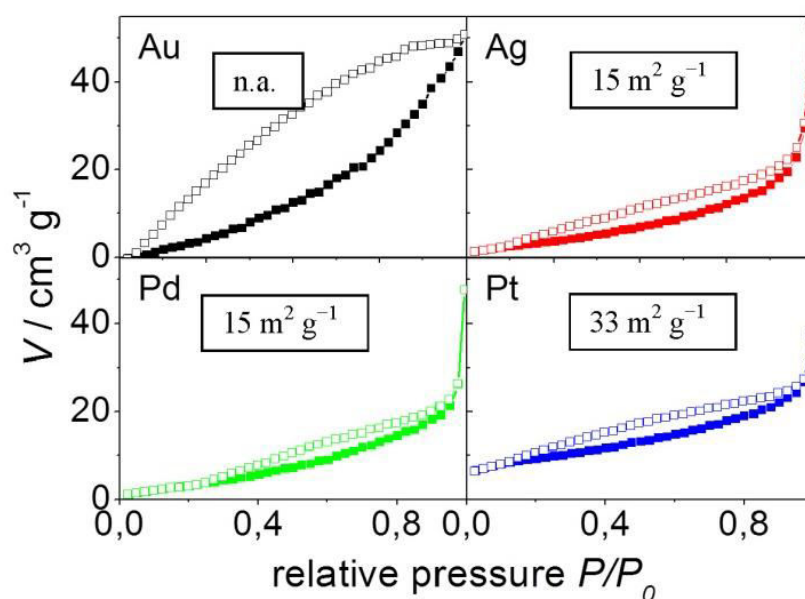


Figure SI-8.1. Nitrogen physisorption isotherms for the gold, silver, palladium and platinum aerogels. Filled squares denote adsorption, empty squares denote desorption.

Electrochemically active surface area

With cyclic voltammetric (CV) measurements the electrochemically active surface area (ECSA) for the platinum aerogels (Figure SI-7B) was determined. Here, the surface area is calculated from the signal of hydrogen adsorption on the Pt surface under consideration of the electric current. We observe within the first 10 scans a sharpening of the CV signal due to the decomposition of the organic ligand. We then cycled for several hundred runs and observed a weakening of the electric current, indicating a decreasing ECSA. In Figure SI-7C the ECSA is plotted against the CV cycles. After 4 cycles a maximum is reached at $16 \text{ m}^2 \text{ g}^{-1}$ that can be explained through the complete decomposition of the organic ligand. Afterwards the ECSA is steadily decreasing until after 500 cycles a plateau is reached. This decrease of surface is due to a transformation of the 3.5 nm spherical particles into flakes with a size of 10 to 20 nm (see Figure SI-7D).

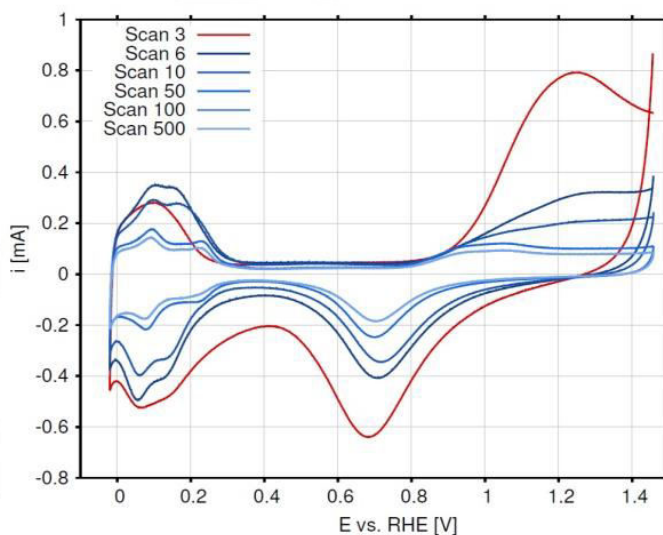


Figure SI-8.2. Cyclic voltammometric measurement of a Pt aerogel with TGA ligand out of a 1000 times concentrated solution (volume fraction 0.25%).

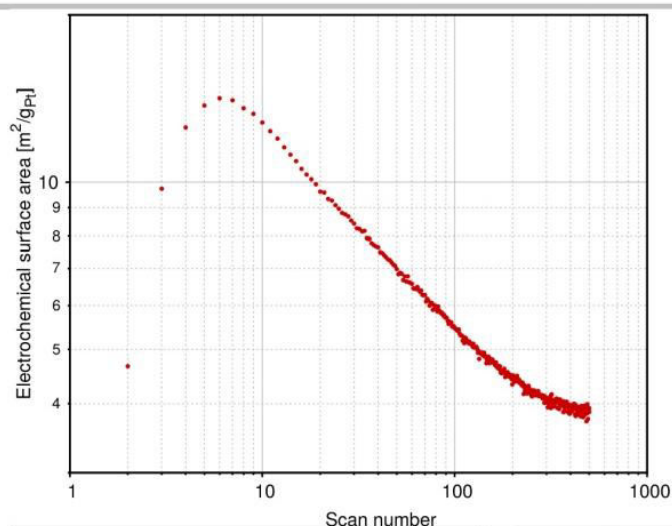


Figure SI-8.3. Electrochemically active surface area (ECSA) plotted against the CV cycles.

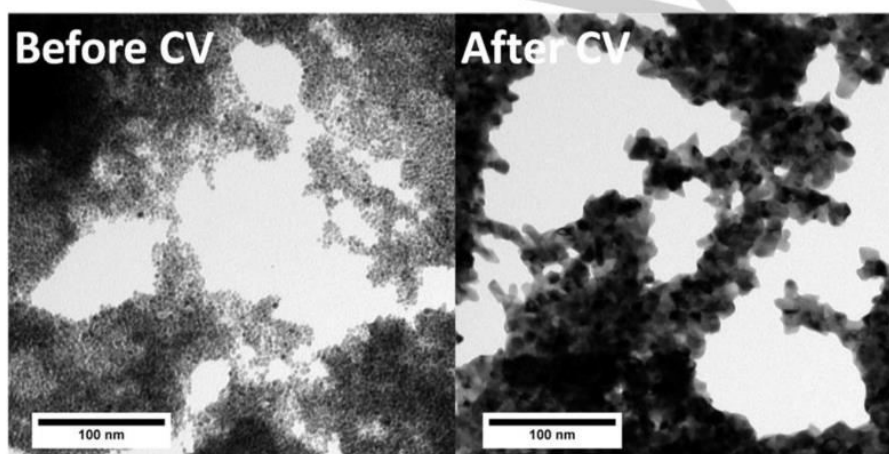


Figure SI-8.4. Influence of the CV measurements on the Pt aerogel with TGA ligand as determined by TEM.

9. Optical characterization

As already shown in Figure 1 the monoliths of Au and Ag have a coloured appearance which is greyish-green for silver and brownish-red for gold. This colour is most likely based on the presence of localized surface plasmon resonances (LSPRs). An appropriate optical characterisation of the aerogel monoliths is quite complex, since the light travels different light paths due to inhomogeneities in the thickness of the monoliths. Therefore, for the optical investigation, aerogel films were prepared on glass slides via doctor bladeing (see Figure SI-7.2) by employing colloids with a nanocrystal volume fraction of 0.25%. With this method we were able to synthesize mostly regular structures with a film thickness of $\sim 20 \mu\text{m}$. Scattering-free absorption (by means of an integrating sphere) and extinction measurements of the Ag films (Figure 4B in the manuscript) show absorption maxima near the LSPRs of the colloidal NPs, (at 390 nm and 510 nm for the Ag and Au aerogel, respectively), which is slightly shifted to smaller wavelengths, probably due to the different dielectric function of the surrounding medium (air) in comparison to that of the previous one (water). The absorption peak itself is broadened, which can be explained with the deformed, partly grown and connected particles (observable by TEM). For silver aerogels, an additional absorption band at 440 nm can be observed, which we attribute to the presence of larger particles, which was also observed by TEM measurements.

Due to the difference between extinction spectra and absorption spectra (the first mentioned also containing contributions due to scattering), an interesting behavior can be noted for both gold and silver nanoparticles: first of all, the absence of a Rayleigh scattering background which would be of higher intensity towards smaller wavelengths should be mentioned. Instead, an increase of the extinction due to scattering is observed for both samples towards larger wavelengths (for Ag, even a maximum is present at approximately 750 nm). It is likely that this behavior is caused by LSPRs of the plain-like nanoparticle assemblies (or by interplasmon coupling). This assumption is supported by the absorption spectra, which are weaker in intensities at this region of the spectrum (and in the case of silver also exhibit a maximum at larger wavelengths), since the plasmon scattering intensity being higher for

resonances corresponding to larger objects is a typical LSPR behavior. Therefore, we conclude that for both Au and Ag aerogels, plasmonic behavior is still observed, a pronounced optical behavior which is differing from that of the pristine colloidal solutions.

The CdSe/CdS aerogel monoliths and films were also characterized by means of an integrating sphere. Both monoliths and films exhibit similar absorption behavior with respect to the colloidal solution. The monolith exhibits a sharp absorption onset at the core position (603 nm). The absorption of the monolith furthermore is saturated at short wavelengths, which is an effect of the morphology and size of the sample: the excitation beam is larger and partially passes beside the monolith. The first CdS absorption onset is found at 463 nm for all three samples (solution, film and monolith). The core peak in the case of the film is not visible due to the low intensity of this signal and the type of measurement based on optical fiber. However, the presence of the core is confirmed by the emission spectra. The emission spectra of the film and the monolith aerogels excited at 454 nm show narrow band edge emission peaks (FWHM = 31 nm and 36 nm, respectively), which means that the size distribution of the nanoparticles in solution is kept in the solid structures. Compared to the rods in solution, the maximum in the emission peak is shifted to larger wavelengths for the gel in the film and the monolith, which can be explained by an increased rod-to-rod coupling in the dense in-plane assemblies (see Figure SI-4.5F), as previously reported in works on nanocrystal superstructures^[14]. The slight broadening of the emission spectra in comparison to those of the nanocrystal solution further confirms this assumption.

The photoluminescence quantum yield (PLQY) for the aerogel film was determined in absolute mode to be 14 %, with a measured luminescence decay time of 10 ns (excitation wavelength: 454 nm). Both PLQY and lifetime decrease slightly when assembling the rods on the film by cryogelation compared to the values of the aqueous solution. On the other hand, the monolith shows 4.8% PLQY (in absolute mode), and 7.5 ns measured lifetime. In this case, PLQY and lifetime decrease strongly with respect to the aqueous solution. This is the typical behavior of homogeneous quenching, in which the decrease in the measured quantum efficiency is typically followed by a decreased in fluorescence lifetime. And this can be explained by an increment in non-radiative processes. Homogeneous quenching is also confirmed by fluorescence decay measurement, showing typical monoexponential decay curves for the nanorods assemblies.

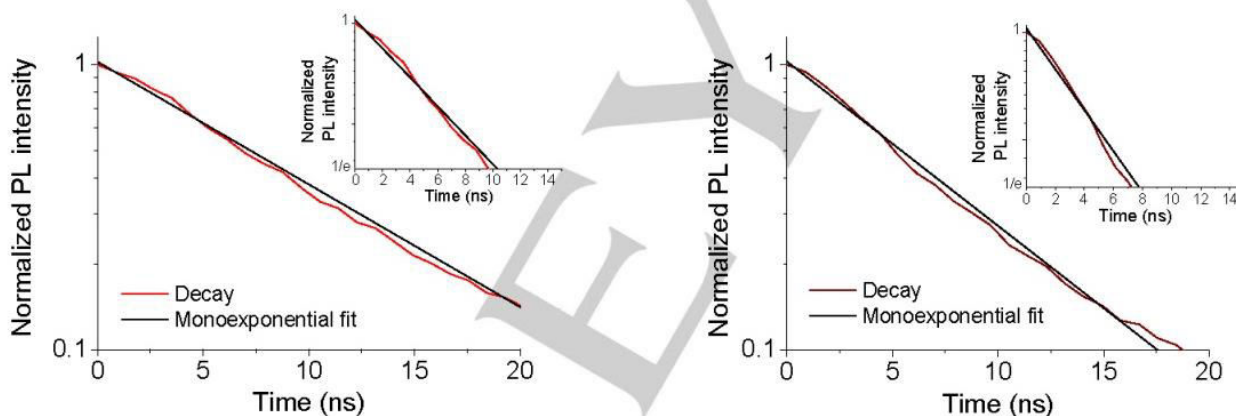


Figure SI-9.2. Normalized emission decay of the monolith (left) and film (right). The color lines are the measured data. The solid black lines correspond to a monoexponential fit. Insets: normalized emission decay from 1 to $1/e$ for a clear reading of the lifetime.

The solution used in this experiment was washed once (as already mentioned previously in the experimental section). When using non-washed samples, the aerogel structure observed in the SEM was completely different from those aerogels fabricated with the other types of nanoparticles due to the excess ligand. When washing the solutions three times, we observed a complete quenching in the fluorescence of the aerogel due to the loss of a high amount of ligands. A single wash was chosen then for all the experiments carried out with the rods because it provides the proper ligand concentration to yield a morphology similar to those of other nanoparticles.

10. References

- [1] N. C. Bigall, A. Eychmueller, *Philos. Trans. R. Soc., A* **2010**, *368*, 1385-1404.
- [2] B. V. Enustun, J. Turkevich, *J. Am. Chem. Soc.* **1963**, *85*, 3317-3328.
- [3] T. Hendel, V. Lesnyak, L. Kuehn, A.-K. Herrmann, N. C. Bigall, L. Borchardt, S. Kaskel, N. Gaponik, A. Eychmueller, *Adv. Funct. Mater.* **2013**, *23*, 1903-1911.
- [4] L. Carbone, C. Nobile, M. De Giorgi, F. D. Sala, G. Morello, P. Pompa, M. Hytch, E. Snoeck, A. Fiore, I. R. Franchini, M. Nadasan, A. F. Silvestre, L. Chiodo, S. Kudera, R. Cingolani, R. Krahne, L. Manna, *Nano Letters* **2007**, *7*, 2942-2950.
- [5] H. G. Bagaria, E. T. Ada, M. Shamsuzzoha, D. E. Nikles, D. T. Johnson, *Langmuir* **2006**, *22*, 7732-7737.
- [6] B. C. Faust, M. R. Hoffmann, *Environ Sci Technol* **1986**, *20*, 943-948.

- [7] E. Wolska, U. Schwertmann, *Z. Kristallogr.* **1989**, *189*, 223.
- [8] P. Scherrer, *Nachrichten von der Gesellschaft der Wissenschaften zu Göttingen, Mathematisch-Physikalische Klasse* **1918**, *1918*, 98-10.
- [9] H. E. Swanson, E. Tatge, *Natl. Bur. Stand. (U.S.)* **1953**, *volume 1*, 23.
- [10] H. E. Swanson, E. Tatge, *Natl. Bur. Stand. (U.S.)* **1953**, *volume 1*, 33.
- [11] H. E. Swanson, E. Tatge, *Natl. Bur. Stand. (U.S.)* **1953**, *volume 1*, 31.
- [12] A. Kern, W. Eysel, *Mineralogisch-Petrograph. Inst., Univ. Heidelberg, Germany* **1993**.
- [13] S. Brunauer, P. H. Emmett, E. Teller, *J. Am. Chem. Soc.* **1938**, *60*, 309-319.
- [14] D. Baranov, A. Fiore, M. van Huis, C. Giannini, A. Falqui, U. Lafont, H. Zandbergen, M. Zanella, R. Cingolani, L. Manna, *Nano Letters* **2010**, *10*, 743-749.

WILEY-VCH

2.3 Tailoring Composition and Material Distribution in Multicomponent Cryoaerogels

Axel Freytag, Carsten Günnemann, Suraj Naskar, Saher Hamid,
Detlef W. Bahnemann, Nadja C. Bigall

submitted

Tailoring composition and material distribution in multicomponent cryoaerogels

*Axel Freytag^{a,b}, Carsten Günnemann^{a,b}, Suraj Naskar^{a,b}, Saher Hamid^c, Detlef Bahnemann^{c,d},
Nadja C. Bigall**

^a Institute of Physical Chemistry and Electrochemistry (PCI), Leibniz Universität Hannover,
Callinstraße 3A, D-30167 Hannover, Germany

^b Laboratory of Nano and Quantum Engineering (LNQE), Leibniz Universität Hannover,
Schneiderberg 39, D-30167 Hannover, Germany

^c Institute for Technical Chemistry, Leibniz Universität Hannover, Callinstraße 3, D-30167
Hannover, Germany

^d Laboratory “Photoactive Nanocomposite Materials”, Saint-Petersburg State University,
Ulyanovskaya str. 1, Peterhof, Saint-Petersburg, 198504 Russia.

KEYWORDS multi component, aerogel, photocatalytic hydrogen evolution, cryoaerogelation

ABSTRACT In this article we demonstrate the fabrication of tailored multi component cryoaerogels from colloidal nanoparticles via the cryogelation method. With this method it is possible to control the amount of components very precisely. Furthermore, the distribution of the different nanoparticle components in the resulting monolithic structure is shown to be adjustable by simply mixing calculated amounts of colloidal nanoparticle

*Corresponding author: nadja.bigall@pci.uni-hannover.de

solutions with a suitable surface charge. The optical properties of synthesized titania-noble metal cryoaerogels are investigated in dependency of the composition. In addition titania-platinum cryoaerogels were tested for photocatalytic applications such as hydrogen evolution and showed a significant increase in performance and stability compared to their respective colloidal solutions. While showing comparable results for hydrogen evolution with aerogels as reported in literature, the fabrication is much faster and less complex and therefore might enable future industrial application.

Aerogelation is one way to assemble nanoparticles into macroscopic structures. These materials show unique features such as low density, low thermal conductivity and high specific surface area, which cannot be obtained by conventional materials.^{1,2} Aerogels found already applications as filter material for stardust or transparent thermal insulation even though only a few materials such as silica have been employed so far.^{3,4} However, the potential of aerogels is still not fully exploited, since recently they can be fabricated of colloidal nanoparticles such as (noble) metal, semiconductors as well as metal oxides.^{2, 5-12} Hence, it is more and more possible to tune aerogels with desired properties by using specific nanoparticles such as photoactive or conductive components, as well as catalytic components which are highly selective.^{8, 13, 14} Combined with the advantages of large specific surface area and large interface area between the components, and therefore shorter path lengths (e.g. in diffusion processes), aerogels are expected to be excellent catalysts and sensors.¹⁵⁻¹⁸ Yet, there are barely reports on aerogels applied in areas like catalysis industry or electronics for two main reasons. One reason is, that the stability (mechanical and thermal) of aerogels has not met the requirements for the aimed applications so far or when the requirements were met, the complexity in fabrication makes them unsuitable for larger scale application.^{13, 14, 17} Second, composite materials (which can overcome

the lack of stability) have certain limitations in distribution of the materials and yields that can be used to obtain aerogels.^{1, 19, 20} Recently we reported on a new method of fabricating aerogels, the cryoaerogelation.²¹ This method allows the employment of different nanoparticles without complex adjustments on the surface chemistry, as long as it is in an aqueous solution. Hence, this method seems promising also for low-cost and large scale aerogel fabrication. However, it needs to be investigated in respect of its potential for multicomponent aerogelation.

In the present work we demonstrate, that by cryogelation we are able to fabricate mixed composite cryoaerogels. We show that this route has basically no restriction on the inserted components and enables a freely variable composition ratio. This supports catalyst design e.g. for photocatalytic hydrogen evolution or many further applications. In detail, this article shows the fabrication of TiO₂-noble metal, hematite-noble metal as well as metal oxide hydroxide-Pt aerogel systems. We can control the distribution of the components within the aerogel by adjusting the ζ -potential of the employed nanoparticles. Furthermore, we can adjust the interface area between the two components in the resulting monolith by freely varying the composition ratio of the employed nanoparticles. We investigate how the optical properties of noble-metal TiO₂ cryoaerogels vary with changing the component ratios. Finally, we show proof-of-principle measurements for hydrogen evolution reaction with TiO₂-Pt cryoaerogels exhibiting 5.1 mmol h⁻¹ g⁻¹ for 1 wt% Pt content, which are promising results comparable to recent literature values.

Results and Discussion

We synthesized multicomponent monoliths of metal oxide-metal cryoaerogels after the cryogelation method. The resulting monoliths are highly voluminous, porous and lightweight. The series of material combinations includes hematite-noble metal (Au, Ag,

Pt), TiO₂-noble metal as well as metal oxide hydroxides-Pt. (see figure 1). Although they have different macroscopic appearances in color due to varying material and component ratios, the microscopic morphology is for all synthesized cryoaerogels similar. The morphology can be described as interconnected thin sheets, which again are made of assembled nanoparticles. To simplify, the morphology is a 3D structure made of 2D assemblies.

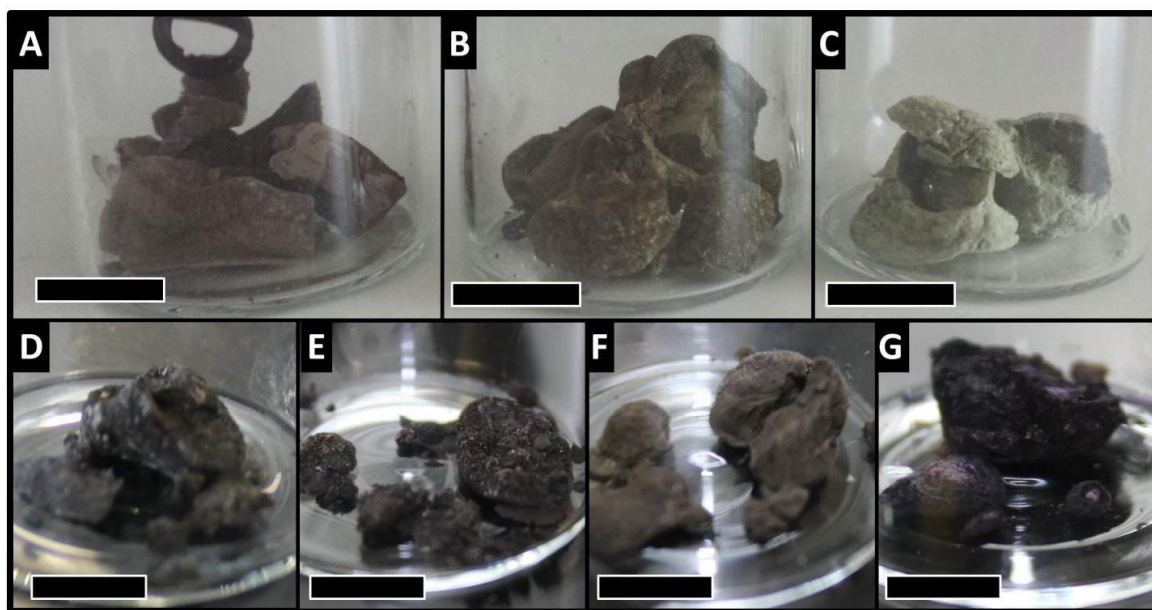


Figure 1 Various cryogelated aerogel monoliths from mixed systems. Cryoaerogel of (A) MnO(OH)_x-Pt (1 wt%), (B) CoO(OH)_x-Pt (1 wt%), (C) NiO(OH)_x-Pt (1 wt%), (D) hematite-Ag (50 wt%), (E) hematite-Au (50 wt%), (F) TiO₂-Ag (50 wt%) and (G) TiO₂-Au (50 wt%) were synthesized.

The structure is a result of freezing the aqueous colloidal solution, where the formed ice crystals act as template for the nanoparticles in order to yield the final cryoaerogel structure. The mechanism was described already in our earlier report.²¹ It has to be

mentioned, that for pure TiO₂ and hematite systems the monoliths easily disintegrate and are better described as voluminous powder. The fragile nature of the pure metal oxide system can be explained with low attractive interactions between the particles. While the intraparticle interactions (namely ionic bonding) are quite strong due to close proximity and high difference in electronegativity of the oxygen and metal ions, the interparticle interactions are relatively weak, which is mainly due to the fact that the average atom distances between the neighboring nanoparticles are higher than within the nanoparticles.²² Furthermore additional Coulomb forces may occur due to the application of ligands.

While being in a colloidal solution the ligands serve to stabilize the nanoparticle due the surface charge and prevent agglomeration. Out of the aqueous solution the ζ -potential is of no concern.^{23, 24} However, humidity at ambient conditions in a highly porous system may still effect the ligands on the particle surface. Therefore weak Coulomb interactions between the particle surfaces may occur and have to be taken into account. The presumptive reason for the monolithic structure to be self-supportive at all, is that cryogelation itself is presumably already a cold sintering technique for nanoparticles of a colloidal solution by applying pressure through ice crystals. Additionally the employment of ligands may lead to crosslinking effects and contribute to the cohesion of the monolith. Besides the stabilizing ligands for the noble metal nanocrystals (namely citrate and DMAT ligands remaining partially after excessive ultrafiltration) no further ligands were present to achieve the monolithic cryoaerogels, in order to warrant the accessibility of the nanoparticles in the superstructures. Yet, it would also be a possibility to add higher

amounts of ligands to create more crosslinking interactions like e.g. intercalation of steric ligands on purpose to obtain more stable monoliths.

Raising the metal content or applying heat treatment (for example 150°C) to these cryoaerogels leads to increased stability of the metal oxide monoliths which can be explained by two reasons. Firstly, sintering through pressure or heat can decrease interparticle distances and therefore enhance the mechanical and thermal stability.²² However care should be taken with the annealing parameters since e.g. sintering at higher temperatures such as 400°C resulted in strong shrinkage or collapse of our metal oxide hydroxide cryoaerogels. Secondly, by adding the significantly smaller noble metal nanoparticles, voids within the nanoparticle assembly sheets were filled with material decreasing the average interparticle distances within the monolithic structure.

We found that the ζ -potential of the nanoparticles influences the distribution within the colloid and therefore in the subsequent aerogel. It is a well-known method to stabilize nanoparticles in colloidal solution with a ζ -potential of the same charge, creating repulsion forces between the particles and preventing agglomeration. This repulsion also takes place when mixing two different colloids and prevents attachments of particles on each other.

When freezing this mixed colloidal solution and subsequently freeze drying it, we found a local segregation in the final assembly as can be seen for the TiO₂-Pt cryoaerogel (see figure 2A). We found local islands of Pt in the size of several hundred nanometer for 50 wt% and often TiO₂ nanoparticles with no attached Pt. The TiO₂ cryoaerogel with 1 wt% Pt shows minor inhomogeneous distributions, meaning regions of TiO₂ nanoparticles with no Pt nanoparticles in the surrounding area and local areas with a high concentration of Pt nanoparticles in the size of 50 nm. Since we can measure by DLS (see figure S2) that by simply mixing the two types of nanoparticles no agglomeration takes place, we attribute the compound segregation in case of the

cryoaerogels to the higher mobility of the smaller Pt nanoparticle being immobilized after the TiO₂ nanoparticles. However, if for example via ligand exchange, the ζ -potential of the employed nanoparticle is changed to opposite charges, we observed for the same TiO₂-Pt nanoparticle systems attraction of the nanoparticles to each other, giving a homogeneous material distribution in the resulting monolith (see figure 2B).

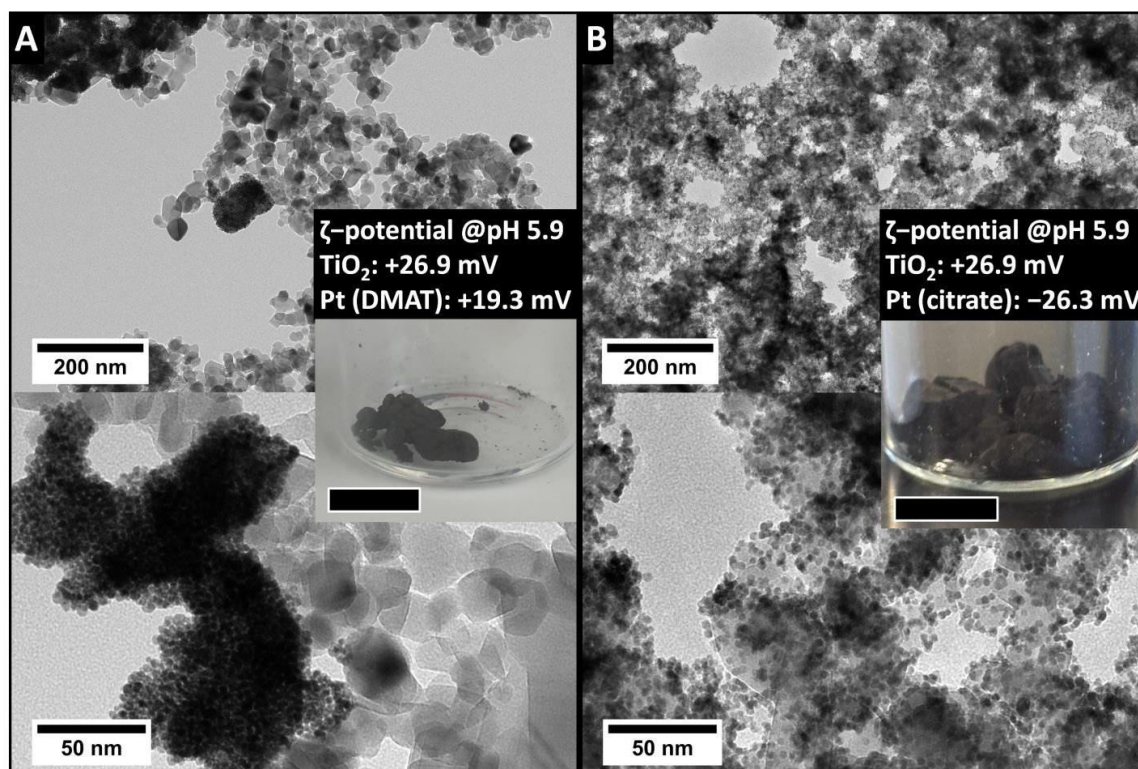


Figure 2 Component distribution of cryogelated aerogels in dependence of the surface potential of the employed nanoparticles. Left images (A) show a partly segregation of the nanoparticles due to same surface potential (Pt nanoparticles with 2-Dimethylaminoethanethiol (DMAT) ligands). The inset shows the TiO₂-Pt cryoaerogel (black bar represents 1 cm). Right images (B) demonstrate attraction of nanoparticle due

to different surface potential leading to a homogeneous component distribution. The inset shows the TiO₂-Pt cryoaerogel (black bar represents 1 cm).

We assume the attachment happens already in solution, shortly after mixing, due to the opposite surface charges. However, this assumption it is difficult to proof, since scattering-based techniques such as DLS are unsuitable upon colloid mixtures of such different sizes. We investigated the colloidal solution by TEM immediately after mixing the solutions, (see figure S1) as well as after cryogelation (figure 2). The distribution of the particles was found to be homogenous, meaning every TiO₂ or hematite nanoparticle has noble metal nanoparticle as direct neighbour in nearly all cases (exception: employment of already agglomerated Ag nanoparticles in the colloidal solution, see figure S6). However, the attachment of the noble metal to the metal oxide nanoparticles in this case could also be a consequence of the TEM grid preparation due to drying effects.

By adjusting the ζ -potential through ligand exchange we achieved always the intended homogeneous or heterogeneous component distribution for the TiO₂-noble metal and hematite-noble metal systems. The homogeneous compound distribution on a larger scale was proven by EDX mappings during SEM imaging (see SI Figure S3).

In a different set of experiments, we found that the composition of cryogelated aerogels can be freely varied by simply mixing the calculated amounts of colloidal nanoparticle solution. We prepared TiO₂ cryoaerogels with different loadings of Pt, Ag and Au. For the TiO₂-Pt system we selected, beside 0 and 100 wt% Pt nanoparticles, the optimal metal loading for water splitting applications (1 wt% after Kaise²⁵) as well as equivalent mass (50 wt%) and equivalent volume (84 wt%) of the employed nanoparticle fractions. The ζ -potential was negative for the Pt and

positive for TiO_2 , which is necessary in order to obtain a homogeneous distribution of the components (as discussed above). Characterization with transmission electron microscopy shows the distribution of the nanoparticles for all compositions (see figure 3). In these cryoaerogels, nearly all Pt nanoparticles were directly attached to the TiO_2 surface.

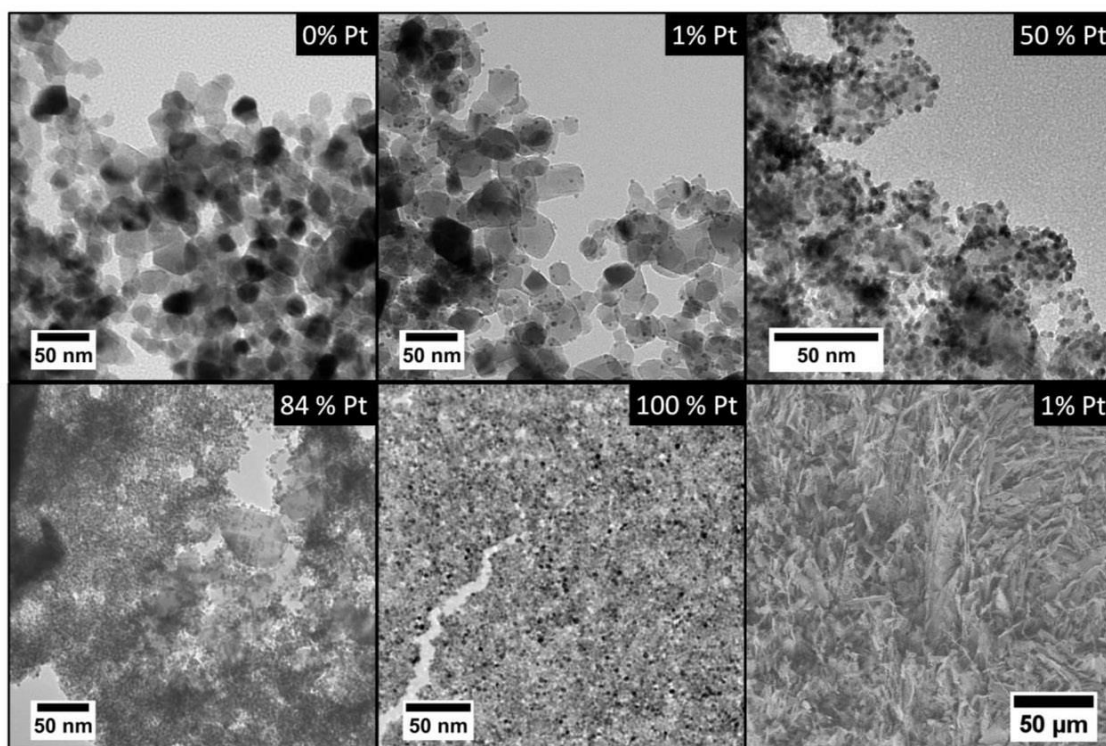


Figure 3 TEM characterization of TiO_2 cryoaerogels with increasing platinum loading ranging from 0 to 100 % Pt yield. Surface potential was positive for TiO_2 and negative for Pt nanoparticles ensuring homogenous distribution. The lower right image shows a SEM image to demonstrate the morphology in the micrometer size.

The optical characterization of cryoaerogel films from TiO_2 -Ag as well as TiO_2 -Au systems show that the properties of the employed single components (namely the occurrence of localized surface plasmon resonances LSPRs) could be transferred into multi component cryoaerogels (see

figure 4). The optical spectrum of the final mixed monolith is influenced by the optical properties of both components. Generally all spectra show absorption maxima at 350 nm, which corresponds to the band gap of TiO₂ of a nanoparticular size.

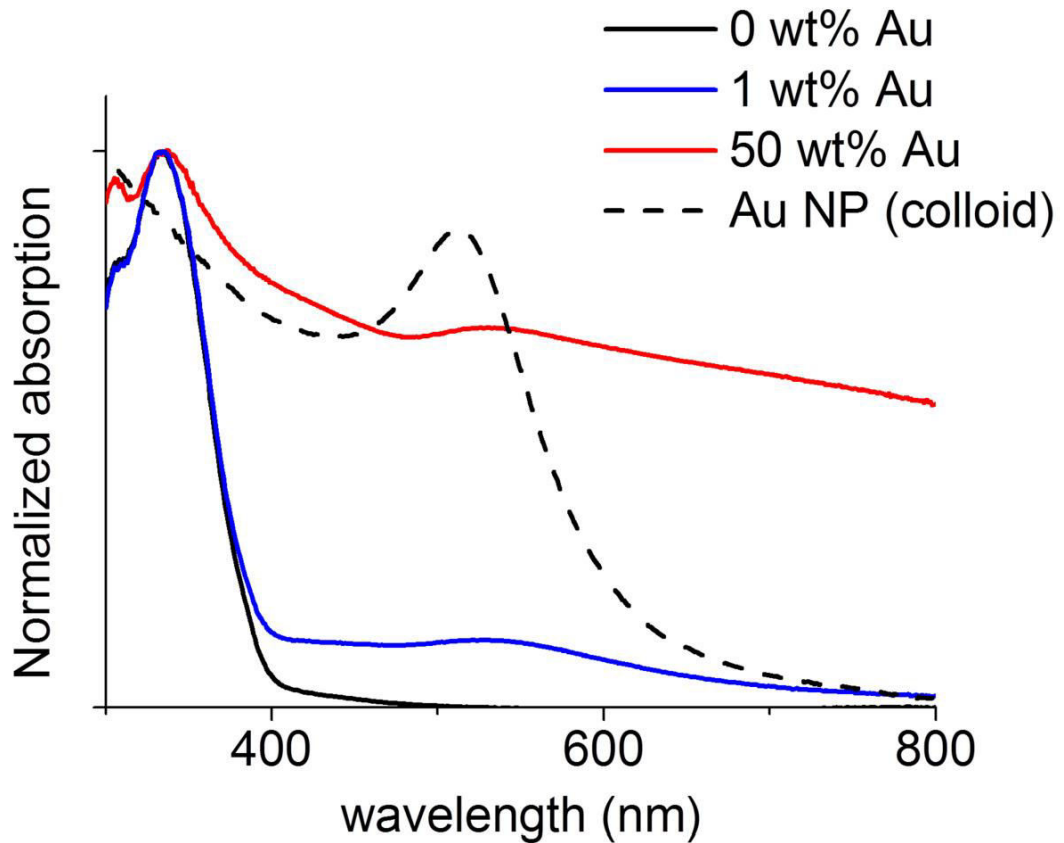


Figure 4 Normalized absorption spectra of mixed composite cryogelated aerogel films for the systems TiO₂-Au with composition ratios of 0 wt% (pure TiO₂ cryoaerogel), 1 wt% Au and 50 wt% Au. Black dotted lines show the spectra of the respective particle colloids.

The spectra of the systems of TiO₂-Au with 1 wt% and 50 wt% Au show an extinction maximum around 540 nm. The bathochromic shift of the LSPR of 15 nm compared to the colloidal solution can be explained by the change of the dielectric function caused by a changed

environment (see figure 4). The broadening of the maximum is presumably caused by interplasmon interactions caused by the various different interparticle distances in the assembled superstructure.^{26, 27} In conclusion, the optical spectra of the mixed cryoaerogel films differ significantly compared to that of the pure TiO₂ cryoaerogel. This means that the optical properties of the resulting monolith can be influenced to a certain degree by adjusting the ratio of both compounds.

Due to their good surface accessibility in combination with the ability of facile separation from the reaction mixture, gels are of interest for solution-based catalysis. In the present case, the fabricated cryoaerogel monoliths from mixed components are of potential interest for applications like e.g. in photocatalytic hydrogen evolution, due to their exact tunability of the compound ratios. For proof-of-principle, we therefore tested TiO₂-Pt systems with varying Pt amounts of 1, 50 and 84 wt% for their capability of hydrogen evolution from water under illumination with a 1000 W xenon lamp under assistance of methanol as hole scavenger. We choose this reaction since it is well investigated and enables comparison of the fabricated cryoaerogels with hydrogelated aerogels.¹³

First we varied the amount of Pt in the system TiO₂-Pt (see Figure 5). The highest hydrogen evolution could be observed for systems with 1 wt% Pt as already reported previously.²⁵ We measured the average specific hydrogen evolution to be 5.1 mmol h⁻¹ g⁻¹ for 1 wt% Pt, 3.0 mmol h⁻¹ g⁻¹ for 50 wt% Pt and 1.0 mmol h⁻¹ g⁻¹ for 84 wt% Pt and compared to the data of a non-gelated mixed TiO₂-Pt colloid (with 1 wt% Pt). Compared with literature (da Silva et al.¹³ achieved for a hydrogelated aerogel system with similar compositions 6.9 mmol h⁻¹ g⁻¹ but with an 400 W Hg lamp) we achieve comparable hydrogen evolution rates for aerogels, yet with a faster and less complex fabrication method.

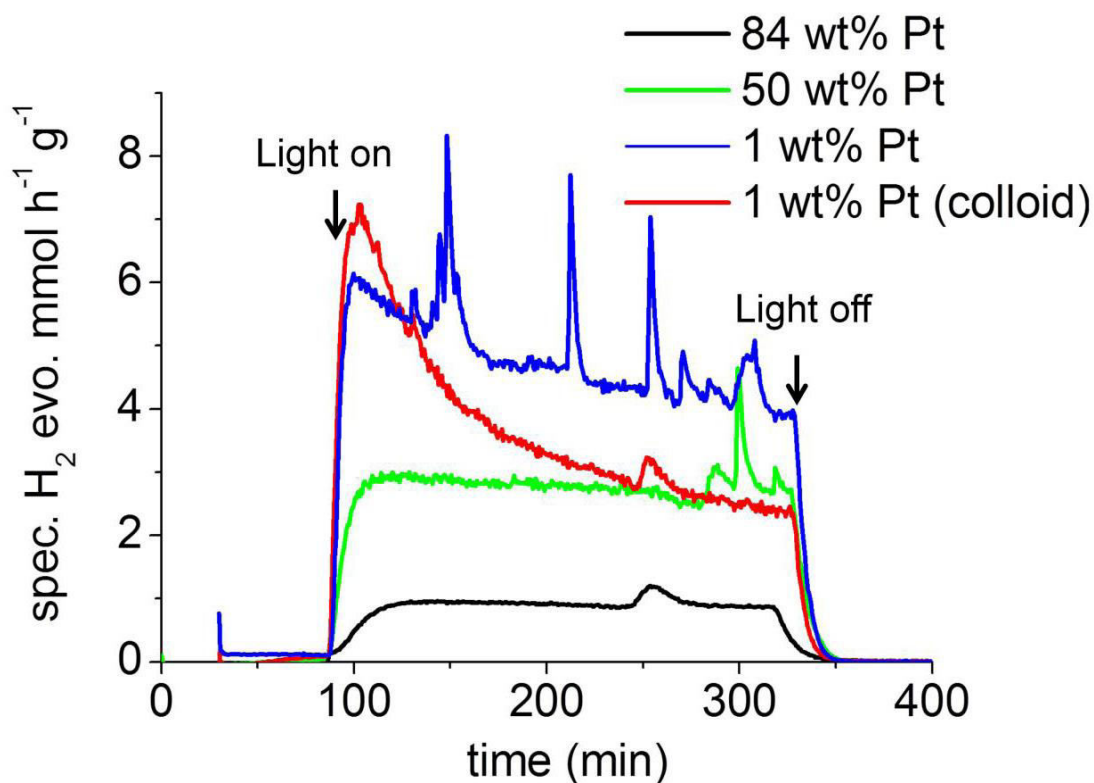


Figure 5 Specific hydrogen evolution for TiO₂-Pt cryoaerogels with varying Pt content of 1 wt%, 50 wt% and 84 wt% and the colloidal solution of TiO₂ with 1 wt% Pt to compare the effect of the cryoaerogelation with the colloidal solution.

The average specific hydrogen evolution was measured to be 3.1 mmol h⁻¹ g⁻¹ for the colloidal solution with 1 wt% Pt. We attribute the ability of producing hydrogen within the colloidal nanoparticle solution to the adsorption of the oppositely charged particles. It presumably takes place as soon as the two colloidal solutions are mixed because of the opposite zeta potential of the Pt (which we measured to be $-50.3 \text{ mV} \pm 1.5 \text{ mV}$ @ pH 7) and TiO₂ nanoparticles ($26.9 \text{ mV} \pm 0.3 \text{ mV}$ @ pH 7). The average performance for hydrogen evolution after cryogelation (integrated over the illumination time of 240 min) is raised by around 60% for cryoaerogels in comparison to the nanoparticle mixture. In addition the performance over time becomes more

stable compared to the colloidal system. This is probably due to the immobilization of the particles into fixed macroscopic structures (see discussion above – “cold sintering”), while the colloidal solution is only loosely bound through surface charges. The surface charge, especially from TiO₂, can locally change during the hydrogen formation reaction²⁵ leading to attaching and detaching of Pt nanoparticles onto and from TiO₂ nanoparticles, which leads to a decrease of the efficiency over time. For the cryogelated system we also observe spikes during the measurement. We attribute these spikes to the nanoporous structure of the cryogel. Produced hydrogen can be captured in these porous structures and is promptly released when reaching critical concentrations.

Conclusion

Fabricating composite aerogels via cryogelation of nanoparticle solutions offers a high degree of control over the resulting properties of the monoliths. Material compositions and particle distributions within the gels can be freely varied, and by this variation also the optical properties can be adjusted. We found in our experiments that the ζ -potential, material and the composition ratio of the employed nanoparticles are the crucial parameters for tuning the aerogel properties. This high degree of control can e.g. be exploited to fabricate tailored cryoaerogels for (photo)catalysis. Further applications such as optical or electronical sensing can be thought of. We could demonstrate with our cryoaerogel comparable hydrogen evolution rates compared to the best literature values for hydrogelated aerogels, and showed a significant increase of performance and stability compared to that of the respective colloidal solutions. Since the cryogelation synthesis is less complex as well as faster in comparison to previous gelation

methods, our results might make the cryoaerogelation interesting for creating a new generation of tailored photocatalysts, catalysts and sensors.

Methods

Materials

Dihydrogen tetrachloroaurate hexahydrate (99,99%), dihydrogen tetrachloroplatinate (IV) hexahydrate (ABCR, 99.95%), trisodium citrate (reagent grade) and sodium hydroxide (reagent grade) was purchased from ABCR. Sodium borohydrate (99,9%) was purchased from Fluka. Silver nitrate (>99.0%) and iron (III) chloride hexahydrate (99%) were purchased from Alfa Aesar. 2-Dimethylaminoethanethiol (DMAT, >99%), TiO₂ nanoparticles (P25), MnCl₂·4H₂O, (>99.0%), CoCl₂·6H₂O, (>99.0%), NiCl₂·6H₂O (>99.0%) and 37% hydrogen peroxide were purchased from Sigma Aldrich. All chemicals were used as received. Deionized water (DI) was used to dissolve the metal salts as described below.

Nanoparticle synthesis

Noble metal nanoparticles were prepared with the modified citrate reduction method from Enustun *et al.*²⁸ In detail, for Au nanoparticles we used 29 mL of a 0.2 weight percent (wt%) dihydrogen tetrachloroaurate hexahydrate aqueous solution stirring in a total volume of 500 mL deionized water. Then 11.6 mL of a 1 wt% trisodium citrate solution are added, and after 30 s a subsequent injection of 5.8 mL containing 0.07 wt% sodium borohydride and 1 wt% trisodium citrate. The solution turns immediately from yellow to red. For Pt nanocrystals a 1 L flask with 36.2 mL of an aqueous 0.2 wt% dihydrogen tetrachloroplatinate (IV) hexahydrate solution was added to a total volume of 500 mL of deionized (DI) water. The solution was stirred and heated

until boiling. 11.6 mL of a 1 wt% trisodium citrate solution were added and stirred for 30 s to reach the boiling point again. Subsequently, 5.5 mL of an ice cold sodium borohydride solution with 0.076 wt% were added. The solution immediately changed from yellow to brown colour. Ag nanocrystals were prepared similarly using 12 mL of an aqueous 0.2 wt% silver nitrate solution as noble metal precursor. When adding sodium borohydride the solution changed from colourless to yellow.

Hematite nanoparticles were synthesized following the method described by Faust *et al.*²⁹ 150 mL of a 0.1 M iron (III) chloride hexahydrate solution were added dropwise into 600 mL of boiling water under stirring. The solution turned to red immediately and was boiled under reflux for further 5 min. The solution was then dialyzed (dialyze tubes Medicell International, MWCO 12-14000 Dalton) for three days, with the tubes placed inside the distilled water, and was changed around 6 to 8 times.

Metal oxide hydroxide nanoparticles were synthesized following a modified synthesis route described by Deng *et al.*³⁰ by preparing a 1 wt% precursor solution of the corresponding metal (II) chlorides ($\text{MnCl}_2 \cdot 4\text{H}_2\text{O}$; $\text{CoCl}_2 \cdot 6\text{H}_2\text{O}$; $\text{NiCl}_2 \cdot 6\text{H}_2\text{O}$). To 10 mL of the precursor solution, 12 mL of a 1 wt% trisodium citrate solution (ABCR, 99%) were added and heated to 50 °C until the solution became coloured (formation of metal complexes). From this solution the metal oxide hydroxide nanoparticles were precipitated using a calculated volume (47 μL for the MnCl_2 solution and 167 μL for the CoCl_2 and NiCl_2 solution) of a mixture of 1 g sodium hydroxide carefully (!) dissolved in 5 mL 37% hydrogen peroxide.

Ligand exchanges were performed by adding 0.33 mmol DMAT per mL of a 0.011 M Pt NANOPARTICLE solution and letting the solution stir for 4 h at 40°C. The solution was washed

3 times with a tenfold volume of DI water over a centrifuge filter (Amicon Ultra-15, 10 kDa, Merck Millipore).

Cryoaerogel synthesis

The cryoaerogels were synthesized following a modified synthesis route from Freytag et al.²¹ To achieve volume fractions of nanoparticles of 0.1% or higher, we concentrated the colloidal solution of the single nanoparticles. Noble metal solutions were concentrated by a factor of 1000, hematite by a factor of 100, which equals a final volume fraction of 0.1 vol% of nanoparticles. Concentration of the colloidal solutions was achieved by an ultrafiltration cell (Solvent resistant filtration cell, Merck Millipore) with a pressure of 5.5 bar filtering over a regenerated cellulose membrane (10 kDa, Satorius Stedim) and subsequent filtration via ultrafiltration centrifuge filters (Amicon Ultra-15, 10 kDa, Merck Millipore) in a centrifuge at 3800 ref for 10 min. The concentrated colloidal solutions were mixed according to the intended and calculated compound composition (0 wt%, 1 wt%, 50 wt%, 84 wt%, 100 wt%) and subsequently added dropwise into liquid nitrogen to obtain monoliths, or knife bladed on washed FTO glass substrates and subsequently dipped in liquid nitrogen. After freezing for approximately five minutes, the monolith and film samples were brought into a freeze dryer (Christ, Alpha LD 1-2) and kept under vacuum (< 0.05 mbar) for 24 h (monoliths) or 6 h (films).

Characterization

UV/Vis absorption spectra of mixed TiO₂-noble metal cryoaerogels immobilized on the FTO glass substrate were recorded using slide holder and the spectrophotometer Cary 5000 (Agilent Technologies). Scattering free absorption measurements were carried out in the same spectrophotometer equipped with an integrating sphere (Agilent DRA 2500) measuring the films

in center mount position. Scanning electron microscopy (SEM) was performed using a JEOL JFM 6700F electron microscope operated at 2 kV. The samples were prepared by placing small aerogel pieces onto an adhesive carbon polymer pad. Energy dispersive x-ray spectroscopy (EDX) measurements were carried out in the same device operated at 10 kV using a EDX detector (Oxford Instruments INCA 300). Transmission electron microscopy (TEM) was performed by a FEI Tecnai G2 F20 electron microscope, operated at 200 kV. The samples were prepared by pressing a carbon film coated copper mesh (mesh width 300 μm , Quantifoil) gently onto the monolith or film. The particle size was (additionally to TEM imaging) determined using dynamic light scattering (DLS). For this measurement, a cuvette was filled with 3 mL colloid and directly measured (Zetasizer ZSP, Malvern Instruments). ζ -potentials were measured using a disposable folded capillary cell (DTS 1070, Malvern) within the Zetasizer ZSP.

Photocatalysis measurements

For photocatalysis measurements 25 mg of the respective cryoaerogel monolith with varying composition (0 wt%, 1 wt%, 50 wt%, 84 wt%, 100 wt%) were redispersed in 10 vol% aqueous methanol (Roth, 99%) solution (photocatalyst concentration 0.5 g L^{-1} , initial suspension volume 50 mL, irradiation time 4 h, irradiation intensity_{I₂₅₀₋₁₄₅₀} 30 mW cm^{-2}). A continuous double jacket quartz glass reactor attached to a quadruple mass spectrometer (QMS (Hiden HPR-20)) has been used in order to carry out the photocatalytic test reactions. Argon (Ar) was used as a carrier gas with a constant flow rate of 10 ml/min. In order to maintain the temperature of photocatalytic reaction a thermostat was used at 20 °C. For the removal of dissolved molecular oxygen Ar was purged into the suspension for 30 minutes. Later on the reactor was closed and flow of Ar gas was continued for 60 minutes until no traces of any other gas can be detected by QMS. Once the stabilization of the system achieved, the lamp was switched on and illumination was continued

for 4 hours. An Osram XBO 1000 Watt Xenon Arc Lamp in Müller LAX 1000 lamp housing was used as a light source. A sudden increase in the production rate for molecular hydrogen was detected immediately after the start of illumination. After 4 hours of illumination, as the lamp was switched off a decrease in the production rate for molecular hydrogen was observed. The advantage of using this system is that the time course for the reaction products can be monitored during the photocatalytic experiments. The details of QMS set-up are described by Kandiell *et al.*³¹

ASSOCIATED CONTENT

Supporting Information (SI): This material is available free of charge via the Internet at <http://pubs.acs.org>.

AUTHOR INFORMATION

Corresponding Author

*E-mail: Nadja C. Bigall: nadja.bigall@pci.uni-hannover.de

Acknowledgements

A.F. and N.C.B. are grateful for the financial support from the German Federal Ministry of Education and Research (BMBF) within the framework of NanoMatFutur, support code 03X5525.

Funding Sources

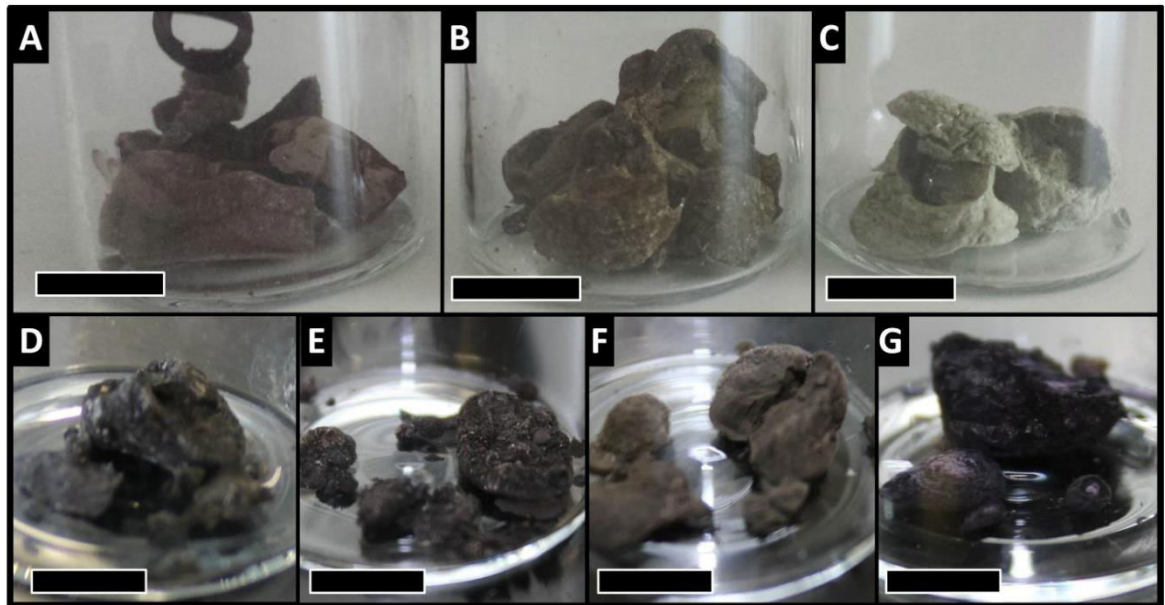
BMBF 03X5525

REFERENCES

1. Huesing, N.; Schubert, U., Aerogels - airy materials: chemistry, structure, and properties. *Angew. Chem., Int. Ed.* **1998**, *37* (1/2), 22-45.
2. Mohanan, J. L.; Arachchige, I. U.; Brock, S. L., Porous Semiconductor Chalcogenide Aerogels. *Science* **2005**, *307* (5708), 397-400.
3. Koebel, M.; Rigacci, A.; Achard, P., Aerogel-based thermal superinsulation: an overview. *Journal of Sol-Gel Science and Technology* **2012**, *63* (3), 315-339.
4. Elsila, J. E.; Glavin, D. P.; Dworkin, J. P., Cometary glycine detected in samples returned by Stardust. *Meteoritics & Planetary Science* **2009**, *44* (9), 1323-1330.
5. Bigall, N. C.; Herrmann, A.-K.; Vogel, M.; Rose, M.; Simon, P.; Carrillo-Cabrera, W.; Dorfs, D.; Kaskel, S.; Gaponik, N.; Eychmueller, A., Hydrogels and Aerogels from Noble Metal Nanoparticles. *Angew. Chem., Int. Ed.* **2009**, *48* (51), 9731-9734.
6. Heiligtag, F. J.; Rossell, M. D.; Sueess, M. J.; Niederberger, M., Template-free co-assembly of preformed Au and TiO₂ nanoparticles into multicomponent 3D aerogels. *J. Mater. Chem.* **2011**, *21* (42), 16893-16899.
7. Sánchez-Paradinas, S.; Dorfs, D.; Friebe, S.; Freytag, A.; Wolf, A.; Bigall, N. C., Aerogels from CdSe/CdS Nanorods with Ultra-long Exciton Lifetimes and High Fluorescence Quantum Yields. *Advanced Materials* **2015**, 6152-6156.
8. Naskar, S.; Schlosser, A.; Miethe, J. F.; Steinbach, F.; Feldhoff, A.; Bigall, N. C., Site-Selective Noble Metal Growth on CdSe Nanoplatelets. *Chemistry of Materials* **2015**, *27* (8), 3159-3166.
9. Bigall, N. C.; Haertling, T.; Klose, M.; Simon, P.; Eng, L. M.; Eychmueller, A., Monodisperse Platinum Nanospheres with Adjustable Diameters from 10 to 100 nm: Synthesis and Distinct Optical Properties. *Nano Lett.* **2008**, *8* (12), 4588-4592.
10. Dorfs, D.; Hartling, T.; Miszta, K.; Bigall, N. C.; Kim, M. R.; Genovese, A.; Falqui, A.; Povia, M.; Manna, L., Reversible Tunability of the Near-Infrared Valence Band Plasmon Resonance in Cu₂-xSe Nanocrystals. *J. Am. Chem. Soc.* **2011**, *133* (29), 11175-11180.
11. Hinrichs, D.; Galchenko, M.; Kodanek, T.; Naskar, S.; Bigall, N. C.; Dorfs, D., Chloride Ion Mediated Synthesis of Metal/Semiconductor Hybrid Nanocrystals. *Small* **2016**, *12* (19), 2588-2594.
12. Dorfs, D.; Salant, A.; Popov, I.; Banin, U., ZnSe quantum dots within CdS nanorods. A seeded-growth type-II system. *Small* **2008**, *4* (9), 1319-1323.
13. da Silva, R. O.; Heiligtag, F. J.; Karnahl, M.; Junge, H.; Niederberger, M.; Wohlrab, S., Design of multicomponent aerogels and their performance in photocatalytic hydrogen production. *Catalysis Today* **2015**, *246*, 101-107.
14. Freytag, A.; Colombo, M.; Bigall, N. C., Catalytic Properties of Cryogelated Noble Metal Aerogels. *Zeitschrift für Physikalische Chemie* **2016**, just accepted.
15. Munnik, P.; de Jongh, P. E.; de Jong, K. P., Recent Developments in the Synthesis of Supported Catalysts. *Chemical Reviews* **2015**, *115* (14), 6687-6718.
16. Wang, C.; Liu, R.; Zhang, W.; Wang, Y.; Xu, K.; Yue, Z.; Liu, G., Multichannel scan surface plasmon resonance biochip with stationary optics and baseline updating capability. *J. Biomed. Opt.* **2013**, *18* (11), 115002/115001-115002/115004.

17. Liu, W.; Rodriguez, P.; Borchardt, L.; Foelske, A.; Yuan, J.; Herrmann, A.-K.; Geiger, D.; Zheng, Z.; Kaskel, S.; Gaponik, N.; Koetz, R.; Schmidt, T. J.; Eychmueller, A., Bimetallic aerogels: high-performance electrocatalysts for the oxygen reduction reaction. *Angew. Chem., Int. Ed.* **2013**, *52* (37), 9849-9852.
18. Pajonk, G. M., Catalytic aerogels. *Catal. Today* **1997**, *35* (3), 319-337.
19. Heiligtag, F. J.; Kranzlin, N.; Suess, M. J.; Niederberger, M., Anatase-silica composite aerogels: a nanoparticle-based approach. *J. Sol-Gel Sci. Technol.* **2014**, *70* (2), 300-306.
20. Fricke, J.; Emmerling, A., Aerogels. *Journal of the American Ceramic Society* **1992**, *75* (8), 2027-2035.
21. Freytag, A.; Sanchez-Paradinas, S.; Naskar, S.; Wendt, N.; Colombo, M.; Pugliese, G.; Poppe, J.; Demirci, C.; Kretschmer, I.; Bahnemann, D. W.; Behrens, P.; Bigall, N. C., Versatile Aerogel Fabrication by Freezing and Subsequent Freeze-Drying of Colloidal Nanoparticle Solutions. *Angew. Chem., Int. Ed.* **2016**, *55* (3), 1200-1203.
22. Geguzin, J. E., *Physik des Sinterns*. VEB Deutscher Verlag für Grundstoffindustrie: Leipzig, 1973.
23. von Smoluchowski, M., Colloid statics and the mechanism of diffusion. *Kolloid-Z.* **1916**, *18*, 48-54.
24. von Smoluchowski, M., Mathematical theory of the kinetics of the coagulation of colloidal solutions. *Z. physik. Chem.* **1917**, *92*, 129-168.
25. Kaise, M.; Nagai, H.; Tokuhashi, K.; Kondo, S.; Nimura, S.; Kikuchi, O., Electron Spin Resonance Studies of Photocatalytic Interface Reactions of Suspended M/TiO₂ (M = Pt, Pd, Ir, Rh, Os, or Ru) with Alcohol and Acetic Acid in Aqueous Media. *Langmuir* **1994**, *10* (5), 1345-1347.
26. Haertling, T.; Alaverdyan, Y.; Hille, A.; Wenzel, M. T.; Kaell, M.; Eng, L. M., Optically controlled interparticle distance tuning and welding of single gold nanoparticle pairs by photochemical metal deposition. *Opt. Express* **2008**, *16* (16), 12362-12371.
27. Kodanek, T.; Freytag, A.; Naskar, S.; Härtling, T.; Dorfs, D.; Bigall, N. C., Macroscopic Aerogels with Controllable Nanoscopic Plasmonic Properties. *Chemistry of Materials* **2016**, submitted.
28. Enustun, B. V.; Turkevich, J., Coagulation of colloidal gold. *J. Am. Chem. Soc.* **1963**, *85* (21), 3317-3328.
29. Faust, B. C.; Hoffmann, M. R.; Bahnemann, D. W., Photocatalytic oxidation of sulfur dioxide in aqueous suspensions of .alpha.-iron oxide (Fe₂O₃). *The Journal of Physical Chemistry* **1989**, *93* (17), 6371-6381.
30. Deng, X.-y.; Xiang, L.; Jin, Y., Preparation of NiO nano-particles via liquid chemical precipitation. *Harbin Gongye Daxue Xuebao* **2002**, *34* (2), 214-216, 224.
31. Kandiel, T. A.; Ivanova, I.; Bahnemann, D. W., Long-term investigation of the photocatalytic hydrogen production on platinized TiO₂: an isotopic study. *Energy & Environmental Science* **2014**, *7* (4), 1420-1425.

Table of Content graphic



Supporting Information

Tailoring composition and material distribution in multicomponent cryoaerogels

*Axel Freytag^{a,b}, Carsten Günnemann^{a,b}, Suraj Naskar^{a,b}, Saher Hamid^c, Detlef Bahnemann^{c,d},
Nadja C. Bigall**

^a Institute of Physical Chemistry and Electrochemistry (PCI), Leibniz Universität Hannover,
Callinstraße 3A, D-30167 Hannover, Germany

^b Laboratory of Nano and Quantum Engineering (LNQE), Leibniz Universität Hannover,
Schneiderberg 39, D-30167 Hannover, Germany

^c Institute for Technical Chemistry, Leibniz Universität Hannover, Callinstraße 3, D-30167
Hannover, Germany

^d Laboratory “Photoactive Nanocomposite Materials”, Saint-Petersburg State University,
Ulyanovskaya str. 1, Peterhof, Saint-Petersburg, 198504 Russia.

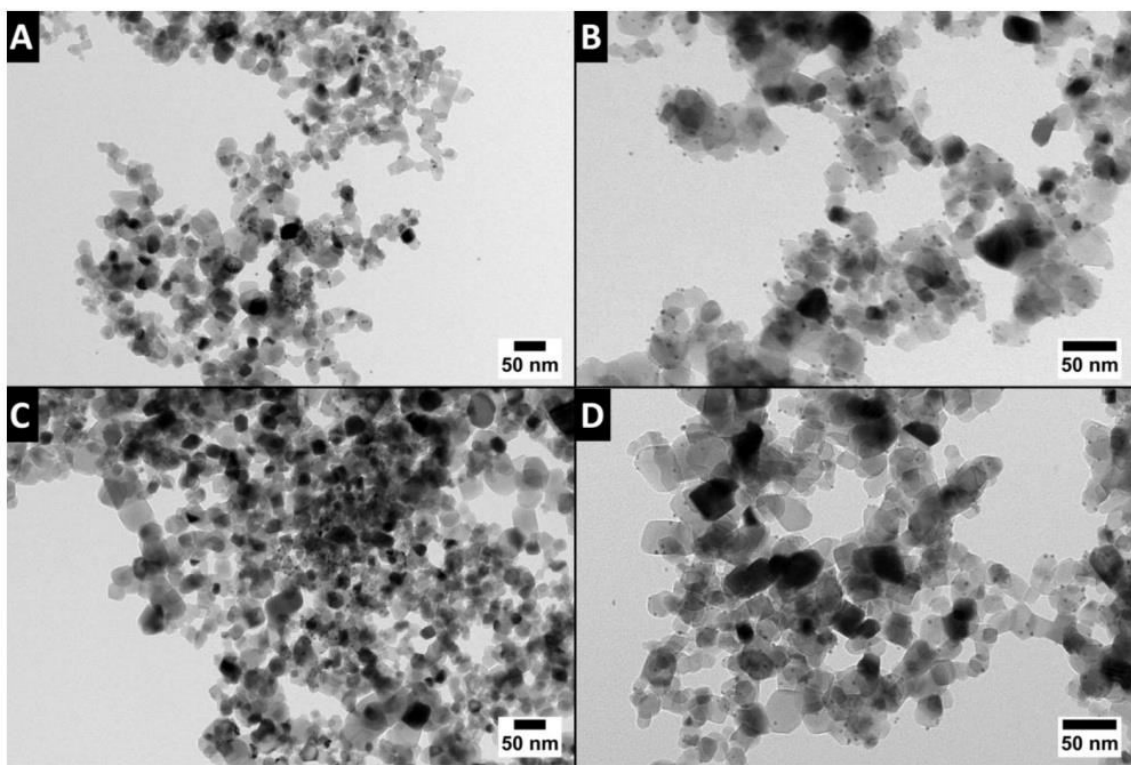


Figure S1. TEM imaging of the system TiO₂-Pt (1 wt%) showing (A) the colloidal solution with same ζ -potential for both components, (B) the colloidal solution with opposite ζ -potential for both components, (C) the cryoaerogel with same ζ -potential for both components, and (D) the cryoaerogel with opposite ζ -potential for both components. Note, that for the colloidal solution drying effects take place during the TEM preparation.

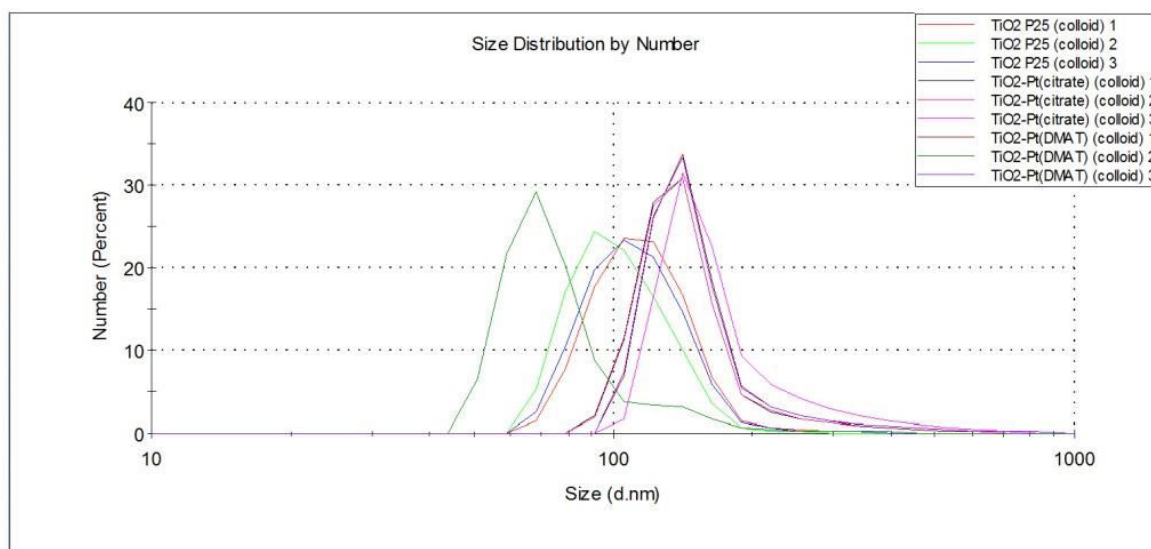


Figure S2 DLS measurements of the system $\text{TiO}_2\text{-Pt}$ (1 wt%) of the pure TiO_2 nanoparticle and the mixtures immediately after addition of Pt nanoparticle with the same ζ -potential (DMAT) and opposite ζ -potential (citrate).

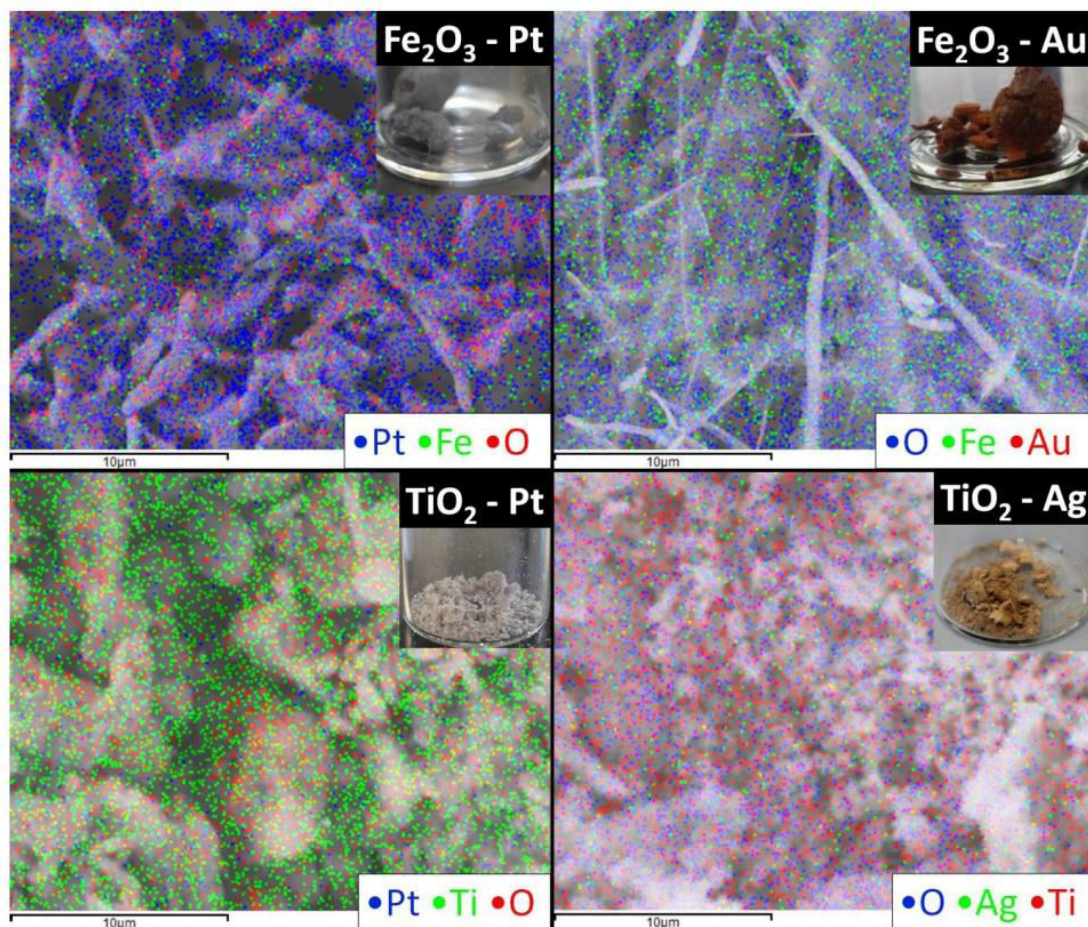


Figure S3 EDX mappings from SEM imaging of the cryoaerogel systems hematite-Pt, hematite-Au, TiO₂-Pt and TiO₂-Ag (always 1 wt% noble metal amount), revealing homogeneous distribution within the cryoaerogels.

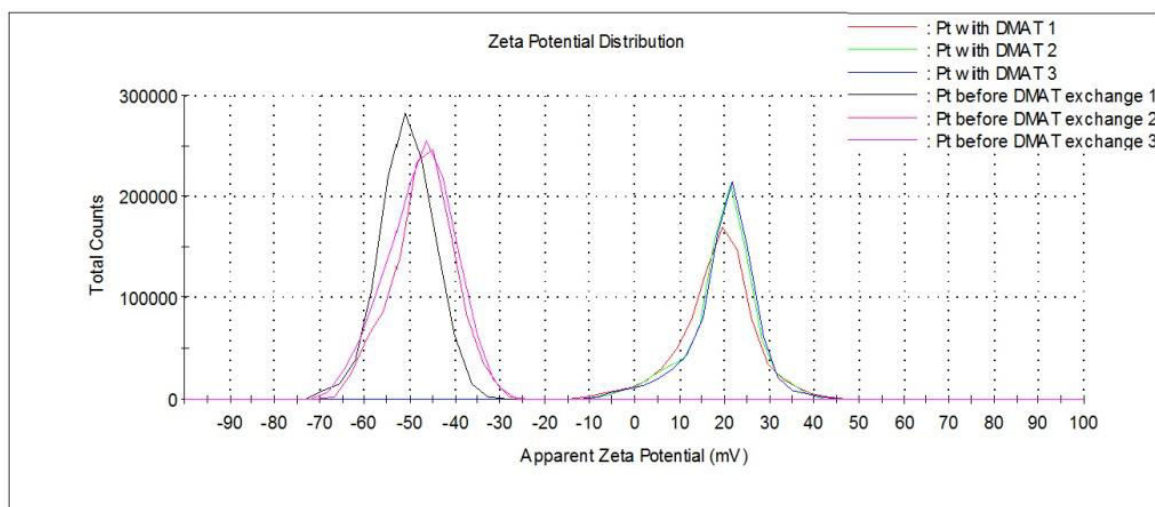


Figure S4 ζ -potential of the Pt nanoparticle before and after exchange of the surface ligands.

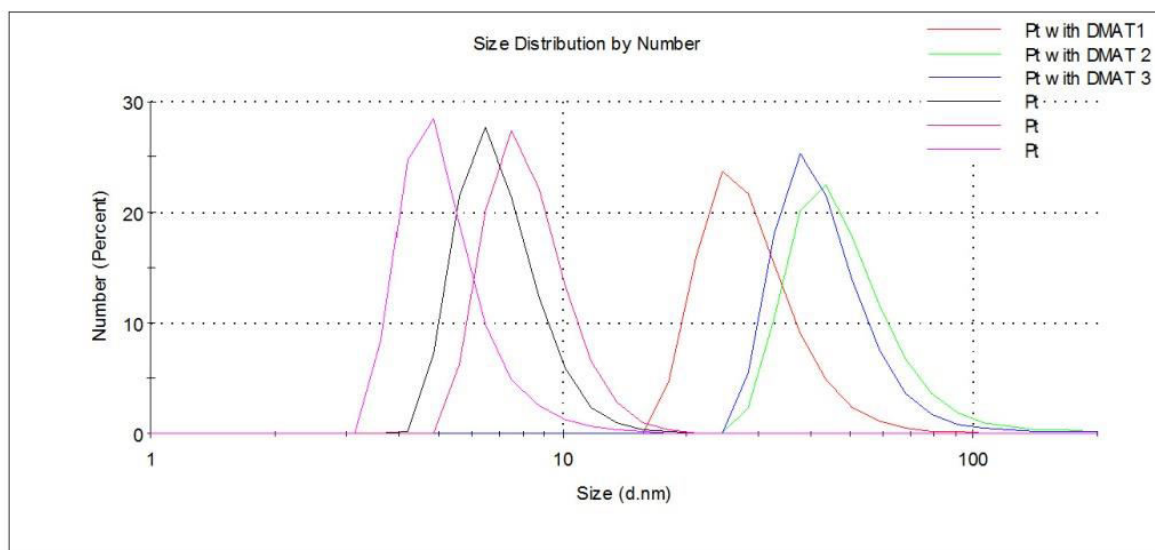


Figure S5 Size distribution measured by DLS for Pt nanoparticle before and after ligand exchange. The increase in size can be explained by the increased hydrodynamic radius of the particle and was not observed in TEM.

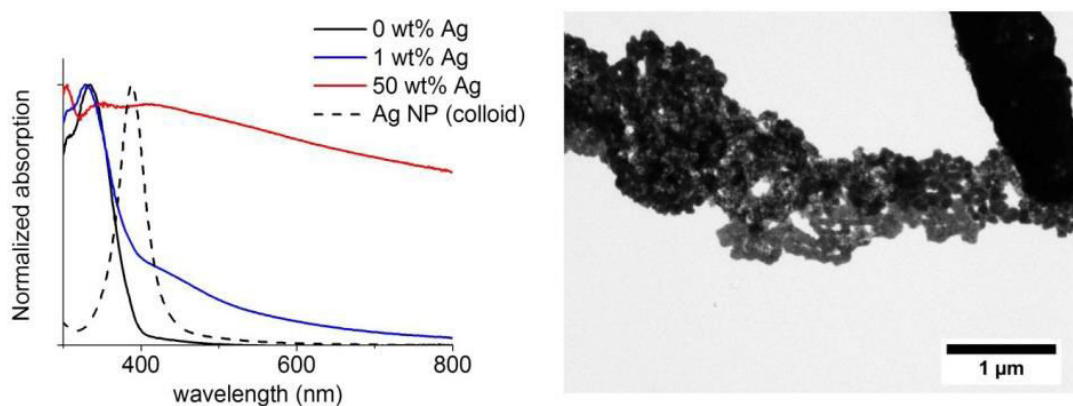


Figure S6 Normalized absorption spectra of TiO₂-Ag cryoaerogel films with varying composition ratios of 0 wt%, 1 wt%, 50 wt% Ag yield and TEM image of the cryoaerogel with TiO₂-Ag (50 wt %) showing local segregation due to agglomerated Ag NP already in the solution.

Figure S6 shows the normalized absorption spectra of TiO₂-Ag systems with 0, 1 and 50 wt% of silver NP within the cryoaerogel. The increase of the amount of the optically active component (Ag nanoparticles), results in a more pronounced absorption maximum at 400 nm, which is caused by the LSPR of silver. For the system with 1 wt% Ag, the absorption of the plasmon resonance is broadened compared to the colloidal NP. This effect may be caused by agglomerated silver particles or propagating plasmons.¹ In addition a bathochromic shift of the LSPR maxima can be observed, which is in part attributed to the change of the dielectric constant of the surrounding media (from water to titania), and in part to interplasmon interactions caused by aggregated Ag nanoparticles. For the 50 wt% Ag aerogel we additionally observe an extinction maximum at around 560 nm. This is probably related to the higher amount of silver and therefore the occurrence of interplasmon coupling.²

References

1. Haertling, T.; Alaverdyan, Y.; Hille, A.; Wenzel, M. T.; Kaell, M.; Eng, L. M. *Opt. Express* **2008**, *16*, (16), 12362.
2. Sonnichsen, C.; Reinhard, B. M.; Liphardt, J.; Alivisatos, A. P. *Nat Biotechnol* **2005**, *23*, (6), 741.

3. Controlling Nanoscopic Properties within Macroscopic Objects

3.1 Summary

In literature an often claimed aim is the transfer of NP out of their respective solution while keeping all the properties. LSPRs, for instance are possible for sputtered targets or could be shown for deposited single particle. However voluminous macroscopic structures were not achieved so far. In section 3.2 the cryoaerogelation method is employed to create plasmonic macroscopic monoliths and adjust the resulting properties. Ag NPs were chosen because of their characteristic LSPR in the visible region. The NP were coated with silica shells ranging from 0 to 13 nm and assembled into voluminous monoliths as well as thin aerogel film on glass substrates. It could be shown that depending on the distance of the Ag NP to each other, the position of the LSPR was shifted. In detail a bathochromatic shift can be observed of around 12 nm for increasing silica shell thicknesses. Furthermore new extinction maxima arise if the NPs are in contact with each other, while with shells of 13 nm or more the spectra of the resulting monolith resemble the spectrum of the colloidal solution. This observation is very complex. In an approach, it is explained as interplay of plasmon coupling, mie scattering and propagating plasmons. In summary, section 3.2 demonstrates the successful transfer of colloidal NP into macroscopic, voluminous cryoaerogels pointing out a possibility to bridge the gap from nanoscopic properties to macroscopic objects.

3.2 Macroscopic Aerogels with Controllable Nanoscopic Plasmonic Properties

Torben Kodanek‡, Axel Freytag‡, Suraj Naskar, Thomas Härtling, Dirk Dorfs* and Nadja C. Bigall*

submitted

DOI

Macroscopic Aerogels with Controllable Nanoscopic Plasmonic Properties

Torben Kodanek[†], Axel Freytag[†], Suraj Naskar, Thomas Härtling, Dirk Dorfs* and Nadja C. Bigall*

T. Kodanek, A. Freytag, S. Naskar, Dr. T. Härtling, Dr. D. Dorfs, Dr. N. C. Bigall

Institute of Physical Chemistry and Electrochemistry (PCI), Leibniz Universität Hannover, Callinstraße 3A, D-30167 Hannover, Germany

Laboratory of Nano and Quantum Engineering (LNQE), Leibniz Universität Hannover, Schneiderberg 39, D-30167 Hannover, Germany

Fraunhofer Institute for Ceramic Technologies and Systems IKTS, Maria-Reiche-Str. 2, 01109 Dresden, Germany

E-mail: dirk.dorfs@pci.uni-hannover.de, nadja.bigall@pci.uni-hannover.de

KEYWORDS plasmon coupling, aerogels, silver nanoparticles, core-shell heterostructures.

ABSTRACT: Aerogels can bridge the nanoscopic to the macroscopic world. One physical phenomenon typically limited to the nanoscopic world is the occurrence of localized surface plasmon resonances (LSPRs), which are observed in conductive nanoparticles. Once brought into close contact, assemblies or superstructures of these nanoparticles often lose their plasmonic properties in the transition stage towards the bulk material. Therefore, LSPRs are typically not observed in macroscopic objects. The present work aims at voluminous nanoparticle-based aerogels with optical properties close to that of the initial colloidal solution and the possibility to control the final plasmonic properties by bringing plasmonic particles into defined distances. In detail, Ag nanoparticles with silica shells ranging from 0 to 12 nm are employed as building blocks, which are assembled from their solution into macroscopic three-dimensional superstructures by freezing and subsequent lyophilization. These cryogelated aerogels are synthesized as monoliths or thin films in which the plasmonic Ag nanocrystals are arranged in defined distances due to their silica shell. The resulting aerogels exhibit controllable plasmonic properties ranging from a behavior similar to that of the building blocks for the thickest shell to a strongly particle-particle interaction dominated behavior for smaller shells or bare Ag particles.

1. Introduction

Optical properties of nanoparticles have raised a considerable amount of interest in the last years. While the effects of e.g. localized surface plasmon resonances (LSPRs) are known and researched for more than 100 years,^{1, 2} a fundamental understanding of the physics behind them was only obtained in the past two decades.^{3, 5} Nanochemistry utilized this knowledge for modifying the optical properties of materials by two complementary routes. The first route is to synthesize tailor-made nanoparticles by chemically controlling their composition, size and shape.⁶⁻⁹ Following this route allows to modify the optical properties to a large extent (e.g. the spectral position of the LSPR).^{10, 11} The second route is the assembly of nanoparticles into arrays or self-assembled ordered structures, and exploiting interparticle interactions like plasmon coupling.^{3, 5, 12-16} Typically, both methods need to be combined when it comes to utilization of nanomaterials in applications like sensing, spectroscopy or in (photo)catalysis.^{14, 15, 17, 18} However, the possibilities of assem-

bling colloidal nanoparticles are insufficient, especially in terms of controlling optical properties of the resulting macroscopic objects. Literature describes various methods for one- and two-dimensional assemblies.^{3, 12, 13, 19} Up to now there is no satisfying procedure to build voluminous macroscopic structures while retaining control on the plasmonic properties. Yet, one possible method to retain the nanoparticle properties and exploit interparticle interactions could be aerogel formation.^{20, 21} In principle there are two different methods to create these highly voluminous and porous systems, namely hydrogelation-based aerogelation or cryogelation-based aerogelation. Hydrogelated aerogelation is the supercritical drying of previously created jellies or hydrogels of metal oxides or polymers over sol-gel processes as developed by Kistler et al.^{22, 23} or of gelated nanocrystals of different materials via adjusting the surface chemistry as was developed recently.²⁴⁻²⁹ Cryogelation as a route to aerogels was recently published, and is based on freezing aqueous colloidal nanoparticle solutions in liquid nitro-

gen and freeze dry them.³⁰ The fabrication of hydrogelated aerogels is time consuming, has certain limitations in arranging the nanoparticles and could so far not show plasmonic properties in the resulting aerogel. Cryogelated aerogels are fabricated much faster and without the limitations from adjusting the surface chemistry.

In this work we investigate the impact of assembling nanoparticles into macroscopic monolithic aerogels using the cryogelation method. We concentrate on the optical properties of Ag nanoparticle aerogels without a silica shell and with two differently thick silica shells to fabricate voluminous macroscopic aerogels with optical properties close to that of the colloidal solution. These particles are assembled either as micrometer thin aerogel films on glass supports or as macroscopic monolithic aerogels. By assembling the particles with tuned silica shell thicknesses, the plasmonic cores are brought into defined distances to each other, which enables controlling the plasmonic coupling. The aerogels are investigated for their optical properties as well as their morphology via spectroscopic and electron microscopical characterizations, respectively. Finally we discuss the sophisticated nature of the aerogel extinction spectra which are affected by a complex interplay of plasmon coupling and further optical effects.

2. Experimental Section

Materials: Ethylene glycol (99 %) was purchased from ABCR. Polyvinylpyrrolidone (M_w 55000, PVP), sodium hydroxide (> 98 %, NaOH), acetone (99 %), (3-aminopropyl)trimethoxysilane (97 %, APTMS), sulfuric acid (95-97 wt%, H_2SO_4) and ammonium hydroxide solution (28-30 wt%, NH_4OH) were purchased from Sigma Aldrich. Silver nitrate (99.85 %, $AgNO_3$) was purchased from Acros. 2-propanol (99.5 %), hydrogen peroxide (35 wt%, H_2O_2) and ethanol (99.8 %) were purchased from Roth. Tetraethyl orthosilicate (> 99.8 %, TEOS) was purchased from Merck. All chemicals were used as received. Deionized water was used to disperse both the synthesized Ag nanocrystals and Ag-SiO₂ core-shell heterostructures.

Synthesis of colloidal Ag nanocrystals: The colloidal Ag nanoparticles were synthesized according to the procedure of Zhang et al.³ Initially, 2.5 g PVP was dissolved under vigorous stirring in 200 mL ethylene glycol. Then 0.5 g $AgNO_3$ was added to the same solution. After the dissolution of the Ag precursor, the reaction mixture was heated up to 130 °C with a heating rate of around 7.4 °C/min and the reaction was allowed to proceed for 90 min. When the solution has reached room temperature again, the nanocrystals were precipitated by adding 800 mL acetone. Finally, the sample was separated from the reaction mixture employing centrifugation at 3773 g for 15 min, followed by the redispersion in 40 mL deionized water.

Synthesis of colloidal Ag-SiO₂ core-shell heterostructures: In order to grow a silica shell around the colloidal Ag nanoparticles, a procedure described by Zhang et al. was performed.³ First of all, 7.52 mL of the in

water dispersed Ag nanocrystals was dissolved in 80 mL isopropanol using an ultrasonic bath. Subsequently, the solution was stirred at 40 °C for 30 min, followed by the addition of 4 mL NH_4OH . After the temperature has become stable again, a specific TEOS amount was injected into the reaction mixture initiating the shell growth. The thickness of the silica shell could be controlled by the added quantity of the silica precursor. In this regard, the TEOS amount was 20 μ L and 80 μ L respectively, in order to receive two different shell thicknesses. In total, the reaction was allowed to proceed under stirring for 2 h at 40 °C. The resultant heterostructures were washed successively several times with water and ethanol. Finally, the Ag-SiO₂ core-shell nanoparticles were redispersed in 4 mL deionized water.

Synthesis of cryoaerogels: As previously reported by us for the gelation of other nanoparticles,³⁰ the Ag-SiO₂ colloid were initially washed by means of a centrifuge filter (Merck Millipore, 10 kDa regenerated cellulose membrane) and concentrated up to a nanoparticle volume fraction of around 0.2 %. For preparing aerogel films the support (e.g. glass slides) has to be cleaned with piranha acid ($H_2O_2:H_2SO_4$ 1:5) and can be functionalized by storing the slides for several hours in 5 M NaOH or APTMS to provide a better wettability and binding of the aerogel to the substrate. Subsequently, the concentrated nanoparticle colloid was doctor bladed on the functionalized support and immediately dipped in liquid nitrogen. After 5 min in the liquid nitrogen bath the slide was brought into a freeze dryer (Christ, Alpha 1-2LD plus) for at least 4 h with a pressure of 0.025 mbar. The aerogel monoliths were prepared by drop-wise addition of the concentrated colloid direct into liquid nitrogen stored in a 20 mL vial. After storing it for around 10 min in liquid nitrogen, the complete sample vial was placed inside a freeze dryer for at least 24 h with a pressure of 0.025 mbar. For the fabrication of thin cryogelated aerogel films on a substrate, we first prepared the substrate by cleaning with piranha acid ($H_2SO_4:H_2O_2$) and eventually functionalizing with NaOH or (3-aminopropyl)trimethoxysilane (APTMS). Then the colloidal solution was brought on the substrate via doctor blading and immediate dipping into liquid nitrogen.

Optical characterization: The UV-VIS extinction spectra of the colloidal solutions were measured in a 3 mL quartz cuvette with a path length of 10 mm in transmission mode using a Cary 5000 spectrophotometer from Agilent Technologies. Absorption measurements were recorded with the same spectrophotometer equipped with an Agilent DRA-2500 integrating sphere and the cuvette always in center-mount position. For the measurements, the colloids were diluted with deionized water. Thin aerogel films and aerogel monoliths were measured in the same way using a film holder and a 1 mL quartz cuvette with a path length of 4 mm, respectively.

Scanning electron microscope analysis: The samples were measured with an electron microscope JEOL JFM 6700F operating at 2 kV. Samples were prepared by placing small pieces onto an adhesive polymer carbon pod on top of the sample holder.

Transmission electron microscope analysis: TEM analyses were performed by means of a FEI Tecnai G2 F20 microscope, equipped with a field emission gun operated at 200 kV. For this purpose, the colloidal solutions were initially diluted with deionized water and then dropped on a carbon coated copper grid (Quantifoil, 300 mesh). In the case of aerogels, the grid was carefully pressed several times against the sample.

3. Results and Discussion

First of all, a solution of spherical Ag nanocrystals was synthesized according to the method reported by Zhang et al. as described in the experimental section.³¹ Here, Ag⁺ ions were reduced by ethylene glycol in the presence of polyvinylpyrrolidone (PVP) at high temperatures producing nanoparticles with a mean diameter of 68 ± 12 nm (Figure S1, Supporting Information). The benefits of this synthesis are the simple scalability and the high quantity of nanoparticles, which are essential for the preparation of aerogels by lyophilization. As can be seen from the UV-VIS spectrum (Figure 1A, black curve), the sample exhibits an increased extinction in the wavelength regime from 350 nm to 500 nm with a maximum at 415 nm. This characteristic feature of nanoscaled silver is ascribed to the occurrence of the so-called LSPR and results from the resonant density oscillation of the conduction band electrons. In addition to the absorption, resonant scattering contributes increasingly to the LSPR as expected for this size regime (Figure S1, Supporting Information). In the case of small Ag nanoparticles with a radius less than 15 nm absorption entirely dominates their optical properties.³² However, the scattering rises drastically with increasing nanoparticle size and eventually becomes the prevailing component due to its r^6 dependency (r being the radius), while the absorption efficiency scales only with r^3 .³³

After synthesizing spherical Ag nanocrystals, these particles were coated with a defined silica shell which is supposed to act as spacer material.³⁴ Following the Stöber method, nanoparticles were dispersed in isopropanol and treated with tetraethyl orthosilicate (TEOS) under alkaline conditions to accelerate the shell growth. In contrast to the often used citrate ligand, PVP ensures the stabilization of nanoparticles without any aggregation in alcohols and additionally promotes the silica coating.³⁴ By changing the TEOS amount, the shell thickness can be adjusted precisely, whereby the distance d between the silver cores is finally determined in the three-dimensional aerogels. For the investigation two different shell thicknesses plus pure Ag nanoparticles without silica were employed. The corresponding transmission electron microscope (TEM) images of the colloidal Ag-SiO₂ core-shell nanoheterostructures are illustrated in Figure 1B and 1C. As can be seen, by means of the Stöber method a uniform coating around the Ag nanocrystals was realized, with a thickness of 4.6 ± 0.8 nm and 12.0 ± 1.5 nm, respectively. Moreover, it should be noted, that no multi-core nanoheterostructures were observed; indeed each

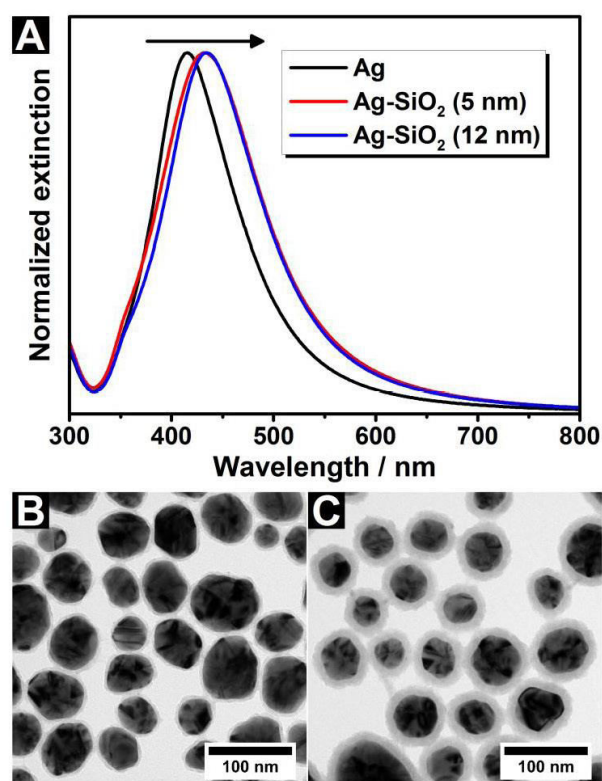


Figure 1. Normalized extinction spectra (A) of colloidal Ag nanocrystals (black curve) and colloidal Ag-SiO₂ core-shell heterostructures possessing a silica shell thickness of 5 nm (red curve) and 12 nm (blue curve), respectively. The measurements were performed in water for all samples. The arrow indicates the shift to longer wavelengths after the shell growth. The lower part shows the corresponding transmission electron microscope (TEM) images of the colloidal Ag-SiO₂ samples with a shell thickness of 5 nm (B) and 12 nm (C).

nanoparticle contains a single silver core. With regard to their optical properties, the extinction spectra do not reveal any significant changes after the encapsulation (Figure 1A). However, the LSPR of the colloidal Ag-SiO₂ heterostructures is slightly shifted to longer wavelengths (bathochromic shift) compared to the one of the starting material. This spectral displacement is expected for silica coatings due to the alteration of the refractive index of the surrounding medium. Generally, the LSPR wavelength and the refractive index of the medium exhibit a proportional relationship in the spectral range addressed here.³⁵ The change of the surrounding from water to silica leads to an increase of the refractive index at the particle surface from 1.33 to about 1.48.^{36, 37} Consequently, a bathochromic shift is both expected and observed.

To fabricate cryogelated aerogel monoliths the colloidal solutions were concentrated and the solutions were injected dropwise into a vial filled with liquid nitrogen. Afterwards, the frozen colloidal solutions were transferred into a lyophilizer and freeze dried for 24 h. As

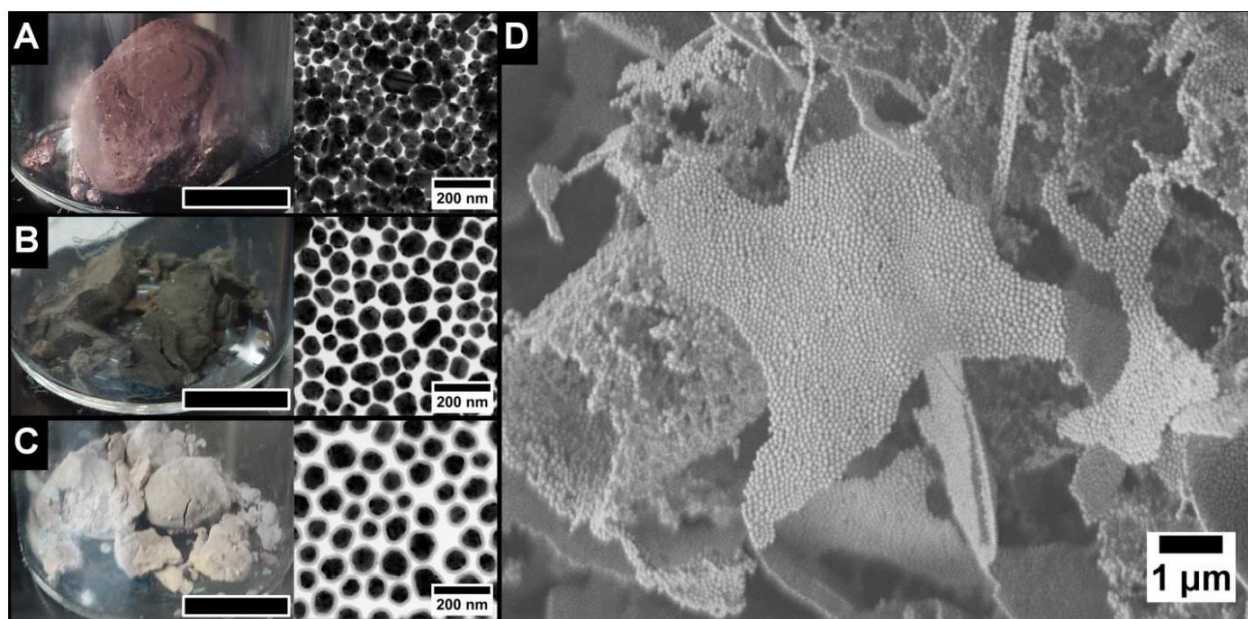


Figure 2. Photographs and TEM images of cryogelated Ag aerogels without silica shell (A), with a 5 nm silica shell (B) and a 12 nm silica shell (C). The black bar represents 1 cm. Scanning electron microscope image (D) reveals the microscopic morphology of interconnected, one layer thin sheets build from the Ag nanoparticles with a 12 nm silica shell.

already reported for other materials, during the freezing of the colloids, the Ag-SiO₂ nanoparticles are pushed into the voids between the ice crystals. Here, the building blocks assemble into sheet-like structures, consisting of approximately 1 to 4 layers of nanoparticles, which are interconnected with each other and randomly oriented (**Figure 2D**) hence building up the macroscopic monolith. Simplified, the resulting monoliths can be described as randomly oriented two-dimensional sheets building a three-dimensional structure.

The resulting aerogel monoliths are highly voluminous and have an estimated density of around 0.03 g cm⁻³, which corresponds to a relative density of around 0.3 % of the bulk silver. The porosity is calculated to 99.7 % with a pore size between the sheets in the micrometer range, while the pores within the sheets are nanometer sized. As can be seen from the photographs in **Figure 2**, the cryogelated monoliths can be distinguished already by means of their appearance. The monolith made out of Ag cores with a 12 nm silica shell shows a yellow brownish color (**Figure 2C**), which is similar to that of the starting colloidal solution. The aerogel composed of particles with a 5 nm shell has a green grayish appearance which is not similar to that of the solution (**Figure 2B**). In the case of the bare Ag, the monolith exhibits a reddish to violet color (**Figure 2A**). As will be discussed later, this change in appearance is attributed to an interplay of various optical effects whose contributions depend on the employed building blocks.

Subsequently, the frozen films were dried within a lyophilizer for about 1 h. We observed similar effects for

the thin aerogel films immobilized on glass substrates as for the monoliths (**Figure 3**). Again nanoparticles are assembled into thin sheets forming an interconnected network (**Figure 3E**). However, when immobilized on a substrate the sheets have a preferred orientation standing mostly perpendicular on the substrate (**Figure 3D**). This observation can be explained by the temperature gradient while dipping the glass in liquid nitrogen. The technique of aligning structures by an applied temperature gradient is known as directed freezing and was also exploited in our earlier work.^{30, 38} Similar as in the case of monoliths, the aerogel films have distinct optical appearances resulting from the same mechanisms occurring in the monoliths. Further SEM and TEM images of the fabricated aerogel monoliths and films can be found in **Figures S3 to S8** of the Supporting Information.

The last part of this work focuses on the optical properties of these three-dimensional nanoparticle aerogels. The monoliths could only be characterized in terms of their optical properties by means of reflectance measurements, since their volume is too big for transmission experiments. Therefore, we concentrate on the aerogel films as in contrast to the monoliths they were optically characterized by both extinction and absorption measurements. To ensure a better comparability, the UV-VIS spectra of the cryogelated aerogel films as well as of the related colloidal solutions are presented in **Figure 4**.

In the case of the pure Ag aerogel film, the extinction spectrum (**Figure 4A**, red solid curve) exhibits two bands whose maxima are located around 403 nm and 657 nm,

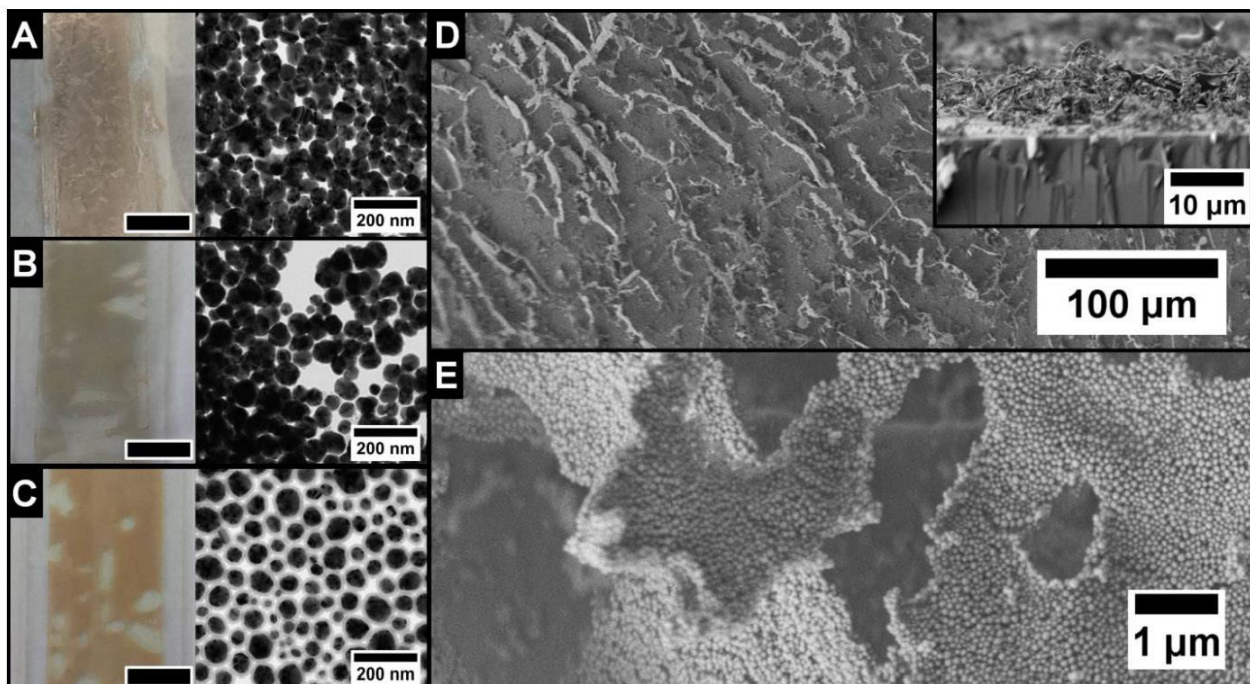


Figure 3. Photographs and TEM images of doctoral bladed cryogelated Ag aerogel films on a glass substrate without silica shell (A), with a 5 nm silica shell (B) and with a 12 nm silica shell (C). The black bar represents 1 cm. Scanning electron microscope image (D) reveals that the nanoparticle sheets preferably stand perpendicular on the substrate. As can be seen in the inset the thickness of the film is approximately 10 nm. The sheets itself are again build from Ag nanoparticles with a 12 nm silica shell (E) similar to the monolithic aerogels.

respectively. Due to its spectral position we attribute the short-wavelength peak to LSPR excitation in the nanoparticles. We conjecture that the reason for its rather pronounced appearance is the coverage of the Ag nanocrystals by insulating PVP ligands from the synthesis which hampers electronic interparticle transport. Hence, the short-wavelength peak represents optical features of single particles in the spectrum. However, their assembly to aerogel film induces a strong LSPR broadening and a spectral shift of 12 nm to shorter wavelengths (hypsochromic shift) compared to the one of the colloidal solution (Figure 4A, solid curves).

The corresponding absorption spectrum of the same sample (Figure 4A, red dashed curve) reveals a further interesting finding. In contrast to the extinction graph, the long-wave band has vanished and instead a small shoulder at around 590 nm can be noticed. The shape difference between the extinction and the absorption spectra in the long-wavelength range leads us to the conclusion that besides LSPR excitation further optical effects play a role which mainly contribute via scattering or reflection. Possible effects include the excitation of propagating surface plasmons in the aerogel sheets, scattering effects due to the surface roughness induced by depositing the material on the glass surface (see Figure 3D), and the formation of an effective medium formed from silver and air the effective refractive index of which may lead to spectrally inhomogeneous reflection. The shape differences between the extinction and absorption spectra are

also found for the aerogels consisting of Ag particles carrying a silica shell (Figure 4B and C). Both a precise understanding of the interplay of the abovementioned effects as well as a simulation of the optical properties of the complex surface structures is beyond the scope of this paper. However, we will discuss in detail the behavior of the short-wavelength peak as this can clearly be attributed to single-particle LSPR origin and its conservation during aerogel formation is the aim of this work. Generally, two tendencies become apparent by comparing the spectra of the three aerogel films (Figure 5A): While the extinction in the long-wavelength part of the spectrum decreases with increasing silica shell thickness, the LSPR peak exhibits a bathochromic shift. In other words, an increasing shell thickness leads to an increasing similarity between the optical properties of the colloidal particles and the aerogels.

The bathochromic shift of the short-wavelength peak can be explained as follows: In contrast to the colloidal solution, the individual nanocrystals in such assemblies are in direct contact with each other. As a result of this, the plasmon oscillations of the individual Ag nanocrystals can strongly interact with each other which is known as plasmon coupling. The efficiency of the coupling depends on the distance between the plasmonic cores defined in this case by the silica shell thickness. An established explanation of the mechanism is provided by the plasmon hybridization theory, which will be introduced via a dimer.³⁹⁻⁴¹ If two plasmonic nanocrystals form a pair with a

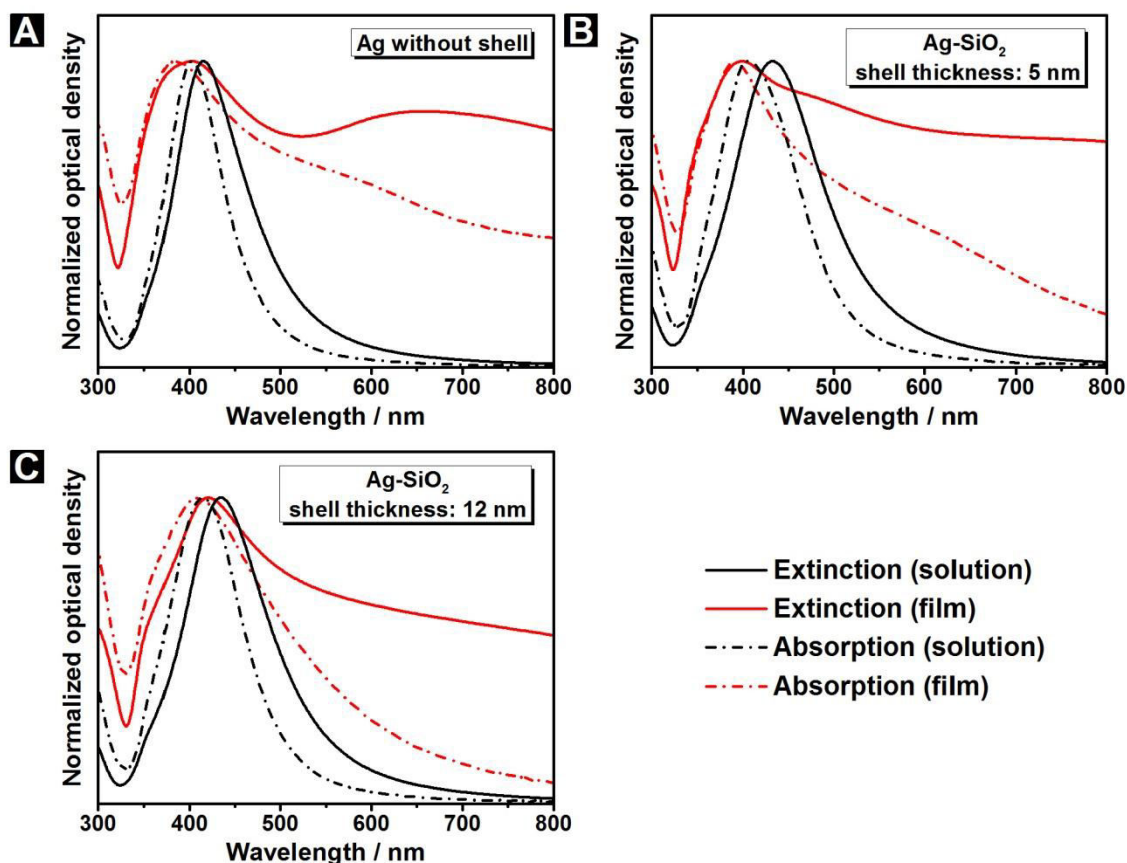


Figure 4. Normalized extinction (solid line) and normalized absorption (dashed line) spectra of the cryogelated aerogel films (red curve) as well as the corresponding colloidal solution (black curve): Ag (A) as well as Ag-SiO₂ with a shell thickness of 5 nm (B) and 12 nm (C).

defined distance to one another, also known as a dimer, the individual dipolar plasmon modes can be oriented in 4 different ways to each other, as illustrated in Figure 5B.^{39, 42} On the one hand, the oscillations are able to occur in a parallel or antiparallel fashion along the interparticle axis, which are labeled as longitudinal- or σ -modes. In contrast, the transversal-modes (π -modes) refer to orientations of the dipolar plasmon modes perpendicular to the interparticle axis. Considering the coupling ability to the incident light, both the longitudinal and transversal antiparallel configuration is not capable of inducing any surface plasmon, since the resulting net dipole moment becomes zero for identical spheres. Nonetheless, these so-called dark modes can turn into dipole-active as a consequence of symmetry breaking, for instance, through differing particle sizes. Here, the net dipole moment deviates from zero. As opposed to this, the parallel orientation always provokes a surface plasmon; therefore, these modes are classified as bright. From a mechanistic viewpoint, the parallel alignment influences the restoring forces within the nanocrystals determining the resonance wavelength of the plasmon. Looking at the σ -mode, the charge accumulations due to the induced polarization are arranged in a head-to-tail manner with alternating signs. Consequently, the restoring forces are supposed to be

reduced resulting in a bathochromic shift of the plasmon in relation to the one of an isolated nanocrystal. Accordingly, this effect continues to increase with decreasing interparticle distance. In contrast, an opposite behavior will be observed for the π -mode. Here, the restoring forces rise, leading to a hypsochromic shift, since the charge distribution exhibits a side-by-side orientation. In previous work we have shown that the distance dependence of the interparticle coupling in head-to-tail configuration at small particle separations is much stronger than the effect of the side-by-side coupling.^{43, 44} Hence, we attribute the bathochromic shift of the LSPR extinction maxima, which can be observed for increasing silica shell thicknesses to σ -mode coupling.

To summarize, the investigation of the Ag and Ag-SiO₂ aerogel films have revealed that the optical properties originate from different mechanisms. In this context, the degree of plasmon coupling as well as the occurrence of further optical effects greatly depends on the interparticle distance defined by the silica shell thickness. While a shell thickness of 12 nm leads to optical properties similar to the ones of the colloidal solution, the bare Ag aerogel film spectrum is heavily distorted in comparison to the colloidal case.

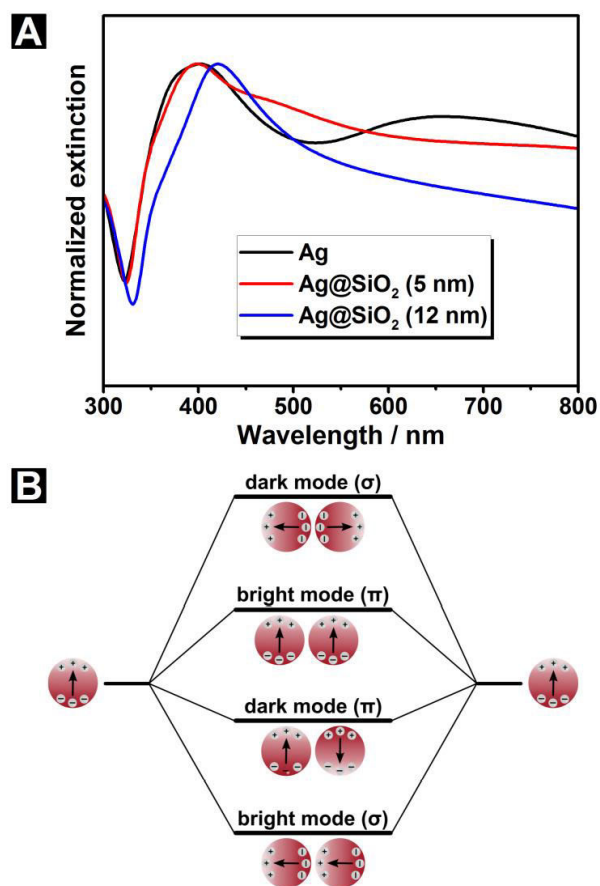


Figure 5. Normalized extinction (A) spectra of the cryogelated aerogel films: Ag (black curve) as well as Ag-SiO₂ with a shell thickness of 5 nm (red curve) and 12 nm (blue curve). Panel B shows a scheme of the plasmon coupling in a dimer.

Finally we turn to a discussion of the optical properties of the cryogelated monoliths. As can be seen from the reflectance spectra (Figure S9, Supporting Information), the spectral signature of all samples possesses a minimum at 324 nm, which becomes more defined with decreasing silica shell thickness.⁴⁵ This feature is ascribed to the so-called plasma edge and typically appears in the reflectance spectra of bulk materials. In comparison with the aerogel films, the processes affecting the optical properties in these structures are considerably more complex and not easy to explain due to the irregular arrangement of the sheet-like structural units. However, the same tendency becomes apparent like in the case of the aerogel films, by considering the development of the plasma edge. This means, that the optical properties of the monoliths more and more resemble the behavior of a bulk material with decreasing silica shell thickness.

4. Conclusion

In summary this work shows the fabrication of macroscopic, porous and voluminous silver nanoparticle structures with plasmonic single-particle characteristics conserved in the final object. While the assembly does not

modify the silver nanoparticle itself, predominantly plasmonic coupling occurs in dependence of the interparticle distance. These distances - and hence the optical properties of the aerogels - can be controlled and adjusted by employing silica shells of varying thickness. The observed plasmon coupling can be explained with the plasmon hybridization model. Concluding, we were able to demonstrate the fabrication of macroscopic aerogels with controllable nanoscopic plasmonic properties.

ASSOCIATED CONTENT

Supporting Information (SI): TEM images of the Ag nanocrystals, size distribution of the Ag nanocrystals as well as the silica shell thickness, further UV-VIS spectra and further SEM images of the aerogels. This material is available free of charge via the Internet at <http://pubs.acs.org>.

AUTHOR INFORMATION

Corresponding Author

*E-mail: Dirk Dorfs: dirk.dorfs@pci.uni-hannover.de

*E-mail: Nadja C. Bigall: nadja.bigall@pci.uni-hannover.de

Author Contributions

‡These authors contributed equally.

Funding Sources

Dr. Dirk Dorfs: DFG, research grants DO1580/2-1 and DO1580/3-1

Dr. Nadja C. Bigall: BMBF, NanoMatFutur, support code 03X5525

Dr. Thomas Härtling: FhG Internal Programs, Attract grant 692271.

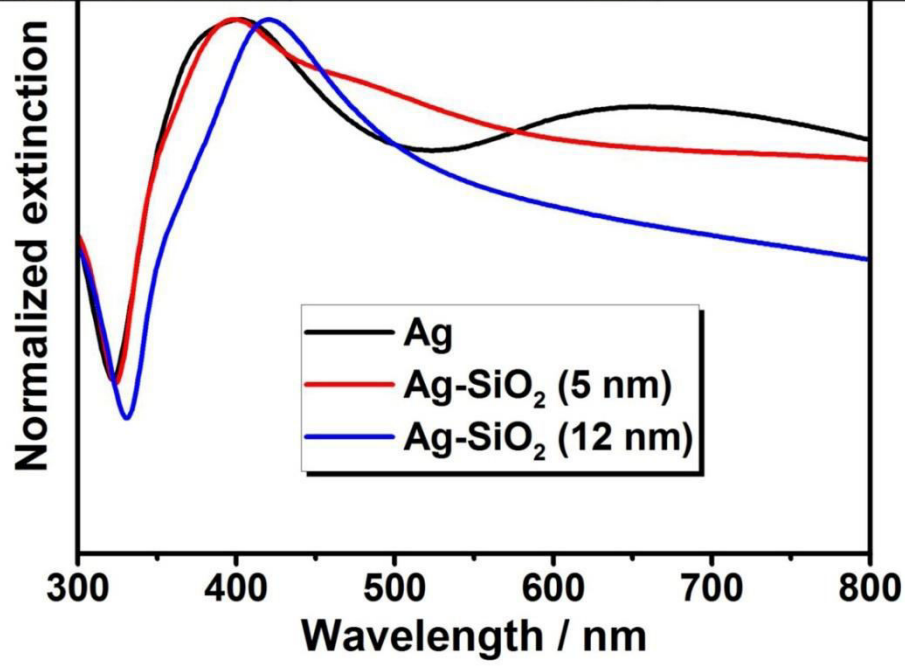
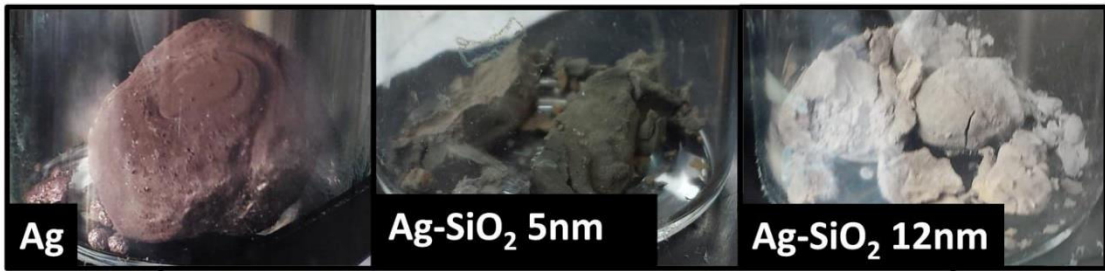
ACKNOWLEDGMENT

T. K. and D. D. want to thank the German research foundation (DFG, research grants DO1580/2-1 and DO1580/3-1) for funding. A. F., S. N. and N.B. are thankful for the financial support to German Ministry of Education and research (BMBF, NanoMatFutur, support code 03X5525). Moreover, T. K. is grateful to the Hannover School for Nanotechnology (hsn) for the financial support. T. K. and A. F. contributed equally to this work.

REFERENCES

- (1) Mie, G., Beiträge zur Optik trüber Medien speziell kolloidaler Metallösungen. *Ann. Phys.* **1908**, *25*, 377-445.
- (2) Siedentopf, H.; Zsigmondy, R., Über die Sichtbarmachung und Größenbestimmung ultramikroskopischer Teilchen mit besonderer Anwendung auf Goldrubingläser. *Ann. Phys.* **1903**, *10*, 1-39.
- (3) Sonnichsen, C.; Reinhard, B. M.; Liphardt, J.; Alivisatos, A. P., A molecular ruler based on plasmon coupling of single gold and silver nanoparticles. *Nat Biotechnol* **2005**, *23*, (6), 741-5.
- (4) Holland, W. R.; Hall, D. G., Surface-Plasmon Dispersion-Relation - Shifts Induced by the Interaction with localized plasma resonances. *Physical Review B* **1983**, *27*, (12), 7765-7768.
- (5) Wu, L.; Reinhard, B. M., Probing subdiffraction limit separations with plasmon coupling microscopy: concepts and applications. *Chemical Society Reviews* **2014**, *43*, (11), 3884-3897.

- (6) Murphy, C. J.; Sau, T. K.; Gole, A. M.; Orendorff, C. J.; Gao, J.; Gou, L.; Hunyadi, S. E.; Li, T., Anisotropic metal nanoparticles: synthesis, assembly, and optical applications. *J. Phys. Chem. B* **2005**, *109*, (29), 13857-13870.
- (7) Liz-Marzán, L. M.; Giersig, M.; Mulvaney, P., Synthesis of nanosized gold-silica core-shell particles. *Langmuir* **1996**, *12*, (18), 4329-4335.
- (8) Bigall, N. C.; Haertling, T.; Klose, M.; Simon, P.; Eng, L. M.; Eychmueller, A., Monodisperse Platinum Nanospheres with Adjustable Diameters from 10 to 100 nm: Synthesis and Distinct Optical Properties. *Nano Lett.* **2008**, *8*, (12), 4588-4592.
- (9) Dorfs, D.; Eychmueller, A., A series of double well semiconductor quantum dots. *Nano Letters* **2001**, *1*, (11), 663-665.
- (10) Dorfs, D.; Hartling, T.; Miszta, K.; Bigall, N. C.; Kim, M. R.; Genovese, A.; Falqui, A.; Povia, M.; Manna, L., Reversible Tunability of the Near-Infrared Valence Band Plasmon Resonance in Cu₂-xSe Nanocrystals. *J. Am. Chem. Soc.* **2011**, *133*, (29), 1175-1180.
- (11) Smith, D. D.; Snow, L. A.; Sibille, L.; Ignont, E., Tunable optical properties of metal nanoparticle sol-gel composites. *J. Non-Cryst. Solids* **2001**, *285*, (1-3), 256-263.
- (12) Tao, A.; Sinsernsuksakul, P.; Yang, P., Tunable plasmonic lattices of silver nanocrystals. *Nat. Nanotechnol.* **2007**, *2*, (7), 435-440.
- (13) Jain, P. K.; El-Sayed, M. A., Plasmonic coupling in noble metal nanostructures. *Chem. Phys. Lett.* **2010**, *487*, (4-6), 153-164.
- (14) Halas, N. J.; Lal, S.; Chang, W.-S.; Link, S.; Nordlander, P., Plasmons in Strongly Coupled Metallic Nanostructures. *Chemical Reviews* **2011**, *111*, (6), 3913-3961.
- (15) Ghosh, S. K.; Pal, T., Interparticle Coupling Effect on the Surface Plasmon Resonance of Gold Nanoparticles: From Theory to Applications. *Chemical Reviews* **2007**, *107*, (11), 4797-4862.
- (16) Jenkins, J. A.; Zhou, Y.; Thota, S.; Tian, X.; Zhao, X.; Zou, S.; Zhao, J., Blue-Shifted Narrow Localized Surface Plasmon Resonance from Dipole Coupling in Gold Nanoparticle Random Arrays. *The Journal of Physical Chemistry C* **2014**, *118*, (45), 26276-26283.
- (17) Jain, P. K.; Huang, X.; El-Sayed, I. H.; El-Sayed, M. A., Noble Metals on the Nanoscale: Optical and Photothermal Properties and Some Applications in Imaging, Sensing, Biology, and Medicine. *Acc. Chem. Res.* **2008**, *41*, (12), 1578-1586.
- (18) Rycenga, M.; Cobley, C. M.; Zeng, J.; Li, W.; Moran, C. H.; Zhang, Q.; Qin, D.; Xia, Y., Controlling the synthesis and assembly of silver nanostructures for plasmonic applications. *Chem. Rev. (Washington, DC, U. S.)* **2011**, *111*, (6), 3669-3712.
- (19) Gong, J.; Li, G.; Tang, Z., Self-assembly of noble metal nanocrystals: Fabrication, optical property, and application. *Nano Today* **2012**, *7*, (6), 564-585.
- (20) Sanchez-Paradinas, S.; Dorfs, D.; Friebe, S.; Freytag, A.; Wolf, A.; Bigall, N. C., Aerogels from CdSe/CdS Nanorods with Ultra-long Exciton Lifetimes and High Fluorescence Quantum Yields. *Advanced Materials* **2015**, *27*, (40), 6152-6156.
- (21) Naskar, S.; Miethé, J. F.; Sanchez-Paradinas, S.; Schmidt, N.; Kanthasamy, K.; Behrens, P.; Pfnur, H.; Bigall, N. C., Photoluminescent Aerogels from Quantum Wells. *Chemistry of Materials* **2016**, *28*, (7), 2089-2099.
- (22) Kistler, S. S., Coherent expanded aerogels and jellies. *Nature (London, U. K.)* **1931**, *127*, 741.
- (23) Huesing, N.; Schubert, U., Aerogels - airy materials: chemistry, structure, and properties. *Angew. Chem., Int. Ed.* **1998**, *37*, (1/2), 22-45.
- (24) Mohanan, J. L.; Arachchige, I. U.; Brock, S. L., Porous Semiconductor Chalcogenide Aerogels. *Science (Washington, DC, U. S.)* **2005**, *307*, (5708), 397-400.
- (25) Eychmueller, A., Aerogels from semiconductor nanomaterials. *Angew. Chem., Int. Ed.* **2005**, *44*, (31), 4839-4841.
- (26) Bigall, N. C.; Herrmann, A.-K.; Vogel, M.; Rose, M.; Simon, P.; Carrillo-Cabrera, W.; Dorfs, D.; Kaskel, S.; Gaponik, N.; Eychmueller, A., Hydrogels and Aerogels from Noble Metal Nanoparticles. *Angew. Chem., Int. Ed.* **2009**, *48*, (51), 9731-9734, S9731/S9731/10.
- (27) Brock, S. L.; Arachchige, I. U.; Kalebaila, K. K., Metal chalcogenide gels, xerogels and aerogels. *Comments Inorg. Chem.* **2006**, *27*, (5-6), 103-126.
- (28) Herrmann, A.-K.; Bigall, N. C.; Lu, L.; Eychmueller, A. In *Ordered and nonordered porous superstructures from metal nanoparticles*, 2012; Wiley-VCH Verlag GmbH & Co. KGaA: 2012; pp 339-359.
- (29) Herrmann, A.-K.; Liu, W.; Gaponik, N.; Bigall, N.-C.; Eychmueller, A., Metal nanoparticle aerogels and their applications. *ECS Trans.* **2013**, *45*, (20), Fullerenes, Nanotubes, and Carbon Nanostructures--221st ECS Meeting, 2012), 149-154, 6 pp.
- (30) Freytag, A.; Sanchez-Paradinas, S.; Naskar, S.; Wendt, N.; Colombo, M.; Pugliese, G.; Poppe, J.; Demirci, C.; Kretschmer, I.; Bahnmann, D. W.; Behrens, P.; Bigall, N. C., Versatile Aerogel Fabrication by Freezing and Subsequent Freeze-Drying of Colloidal Nanoparticle Solutions. *Angew. Chem., Int. Ed.* **2016**, *55*, (3), 1200-1203.
- (31) Zhang, F.; Braun, G. B.; Shi, Y.; Zhang, Y.; Sun, X.; Reich, N. O.; Zhao, D.; Stucky, G., Fabrication of Ag@SiO₂@Y₂O₃:Er Nanostructures for Bioimaging: Tuning of the Upconversion Fluorescence with Silver Nanoparticles. *Journal of the American Chemical Society* **2010**, *132*, (9), 2850-2851.
- (32) Evanoff, D. D.; Chumanov, G., Size-Controlled Synthesis of Nanoparticles. 2. Measurement of Extinction, Scattering, and Absorption Cross Sections. *The Journal of Physical Chemistry B* **2004**, *108*, (37), 13957-13962.
- (33) Craig F. Bohren, D. R. H., *Absorption and scattering of light by small particles*. John Wiley & Sons: Canada, 1983.
- (34) Christina Graf, D. L. J. V., Arnout Imhof, Alfons van Blaaderen, A general method to coat colloidal particles with silica. *Langmuir* **2003**, *19*, 6693-6700.
- (35) Uwe Kreibitz, M. V., *Optical properties of metals clusters*. Springer-Verlag Berlin, Heidelberg: 1995.
- (36) Khlebtsov, B. N.; Khanadeev, V. A.; Khlebtsov, N. G., Determination of the Size, Concentration, and Refractive Index of Silica Nanoparticles from Turbidity Spectra. *Langmuir* **2008**, *24*, (16), 8964-8970.
- (37) George M. Hale, M. R. Q., Optical Constants of Water in the 200-nm to 200- μ m Wavelength Region *Applied Optics* **1973**, *12*, (3), 555-563.
- (38) Qian, L.; Zhang, H., Controlled freezing and freeze drying: a versatile route for porous and micro-/nano-structured materials. *J. Chem. Technol. Biotechnol.* **2011**, *86*, (2), 172-184.
- (39) Nordlander, P.; Oubre, C.; Prodan, E.; Li, K.; Stockman, M. I., Plasmon Hybridization in Nanoparticle Dimers. *Nano Letters* **2004**, *4*, (5), 899-903.
- (40) Brandl, D. W.; Mirin, N. A.; Nordlander, P., Plasmon Modes of Nanosphere Trimers and Tetramers. *The Journal of Physical Chemistry B* **2006**, *110*, (25), 12302-12310.
- (41) Prodan, E.; Radloff, C.; Halas, N. J.; P., N., A Hybridization Model for the Plasmon Response of Complex Nanostructures. *Science* **2003**, *302*, (5644), 419-422.
- (42) Cunningham, A.; Mühlig, S.; Rockstuhl, C.; Bürgi, T., Coupling of Plasmon Resonances in Tunable Layered Arrays of Gold Nanoparticles. *The Journal of Physical Chemistry C* **2011**, *115*, (18), 8955-8960.
- (43) Härtling, T.; Alaverdyan, Y.; Hille, A.; Wenzel, M. T.; Kaell, M.; Eng, L. M., Optically controlled interparticle distance tuning and welding of single gold nanoparticle pairs by photochemical metal deposition. *Opt. Express* **2008**, *16*, (16), 12362-12371.
- (44) Weber, D.; Katzmann, J.; Neubrech, F.; Härtling, T.; Pucci, A., Spectral tuning of IR-resonant nanoantennas by nanogap engineering. *Optical Materials Express* **2011**, *1*, (7), 1301-1306.
- (45) J. Springer, A. P., L. Müllerova, M. Vanecek, O. Kluth, B. Rech, Absorption loss at nanorough silver back reflector of thin-film silicon solar cells. *Journal of Applied Physics* **2004**, *95*, (3).



Insert Table of Contents artwork here

Supporting Information

Macroscopic Aerogels with Controllable Nanoscopic Plasmonic Properties

Torben Kodanek, Axel Freytag, Suraj Naskar, Thomas Härtling, Dirk Dorfs* and Nadja C. Bigall*

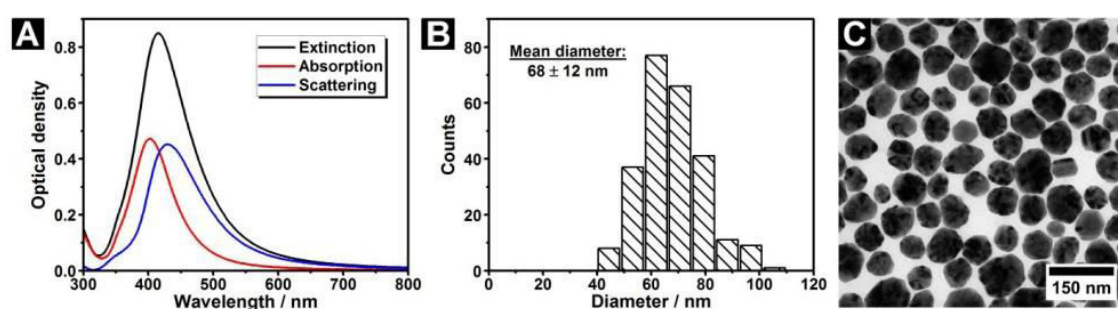


Figure S1. UV-vis spectra (A), particle size distribution (B) and TEM image (C) of the colloidal Ag nanocrystals. In the UV-vis spectra, the resonant scattering (blue curve) was calculated by the subtraction of the absorption (red curve) from the extinction (black curve).

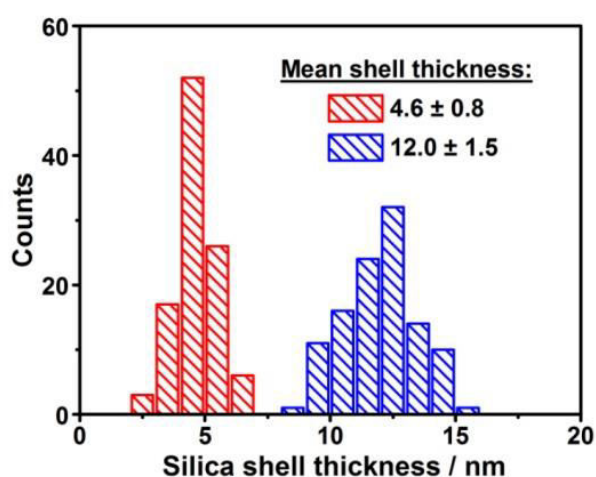


Figure S2. Shell thickness distribution of two different samples of colloidal Ag-SiO₂ core-shell heterostructures obtained by the addition of 20 μ L (red) and 80 μ L (blue) TEOS. The silica shell thickness was determined on the basis of TEM images.

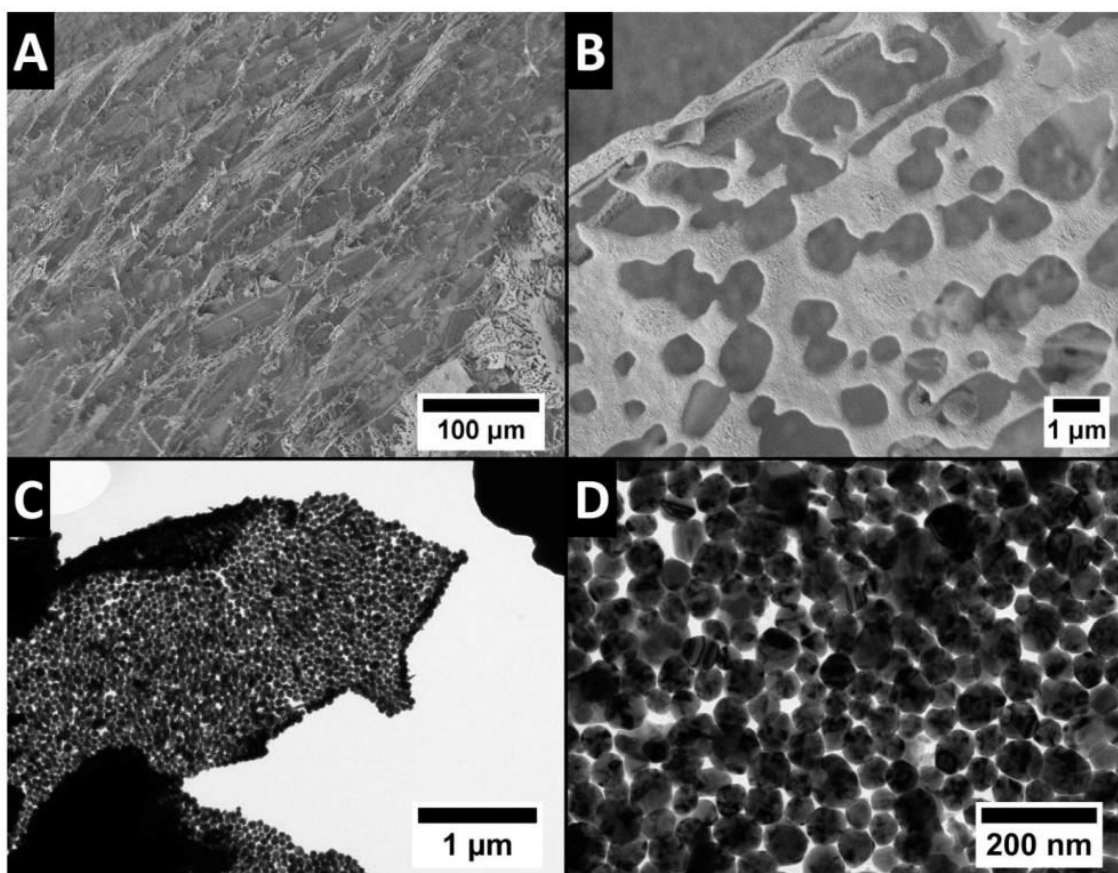


Figure S3. SEM (A+B) and TEM (C+D) characterizations of pure Ag nanoparticles assembled into micrometer thick aerogel films. It can be seen, that the sheets are oriented perpendicular to the substrate, while the nanoparticle are in close proximity.

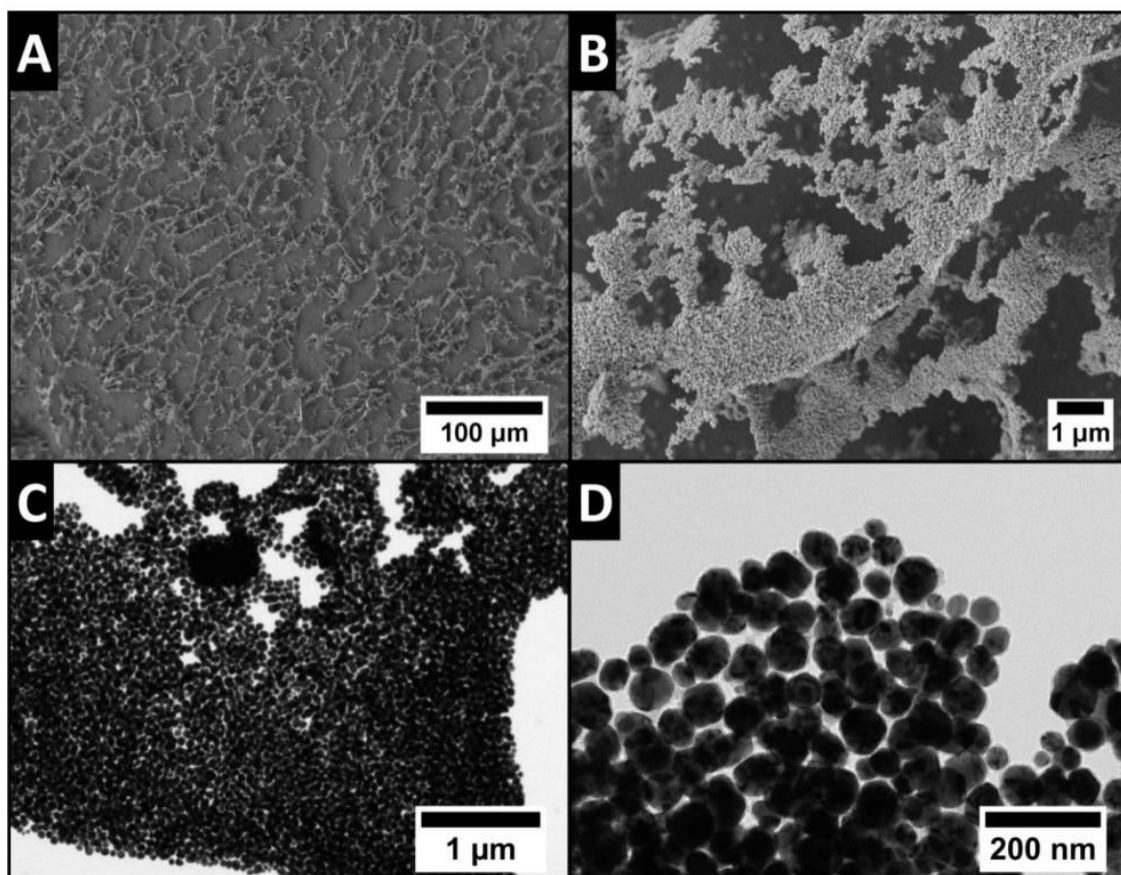


Figure S4. SEM (A+B) and TEM (C+D) characterizations of Ag nanoparticles with a 5 nm silica shell assembled into micrometer thick aerogel films. It can be seen that the sheets are preferably oriented perpendicular to the substrate, while the nanoparticles have a distance of around 10 nm.

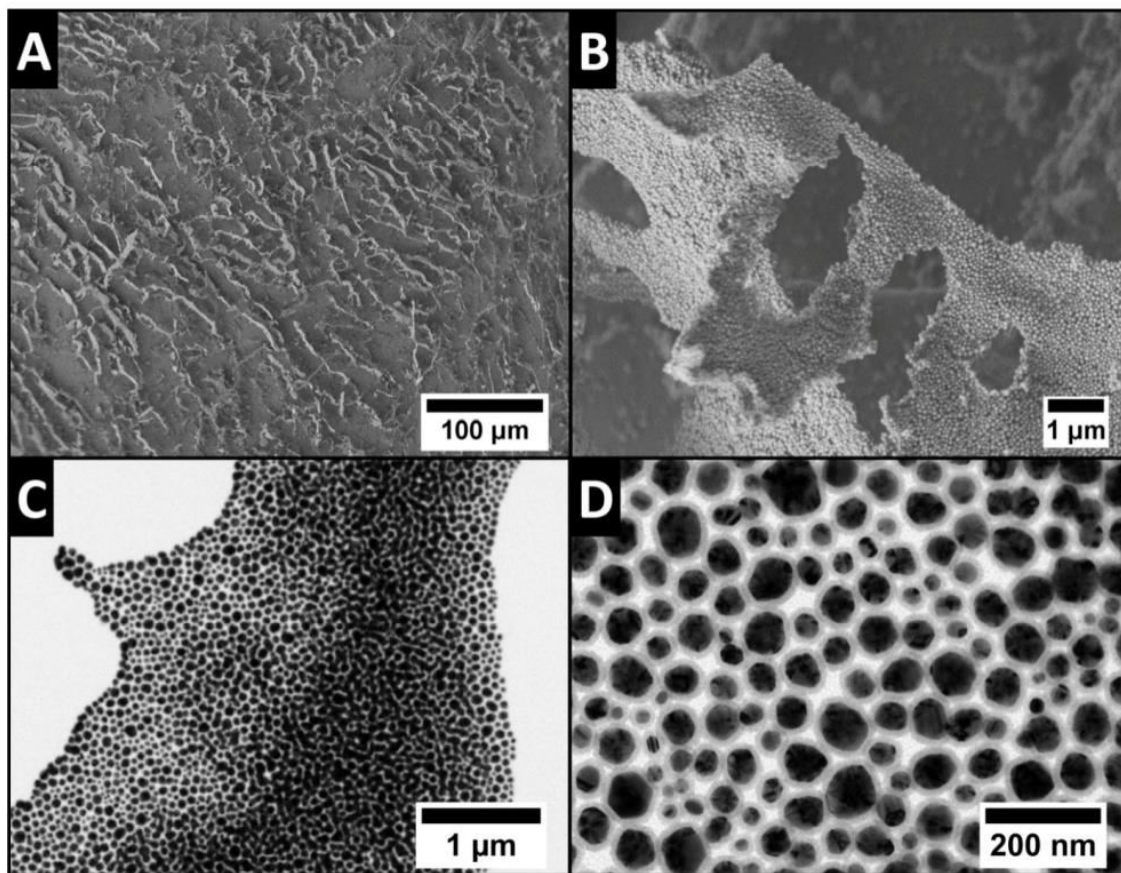


Figure S5. SEM (A+B) and TEM (C+D) characterizations of Ag nanoparticles with a 12 nm silica shell assembled into micrometer thick aerogel films. It can be seen that the sheets are preferably oriented perpendicularly to the substrate, while the nanoparticles have a distance of around 24 nm.

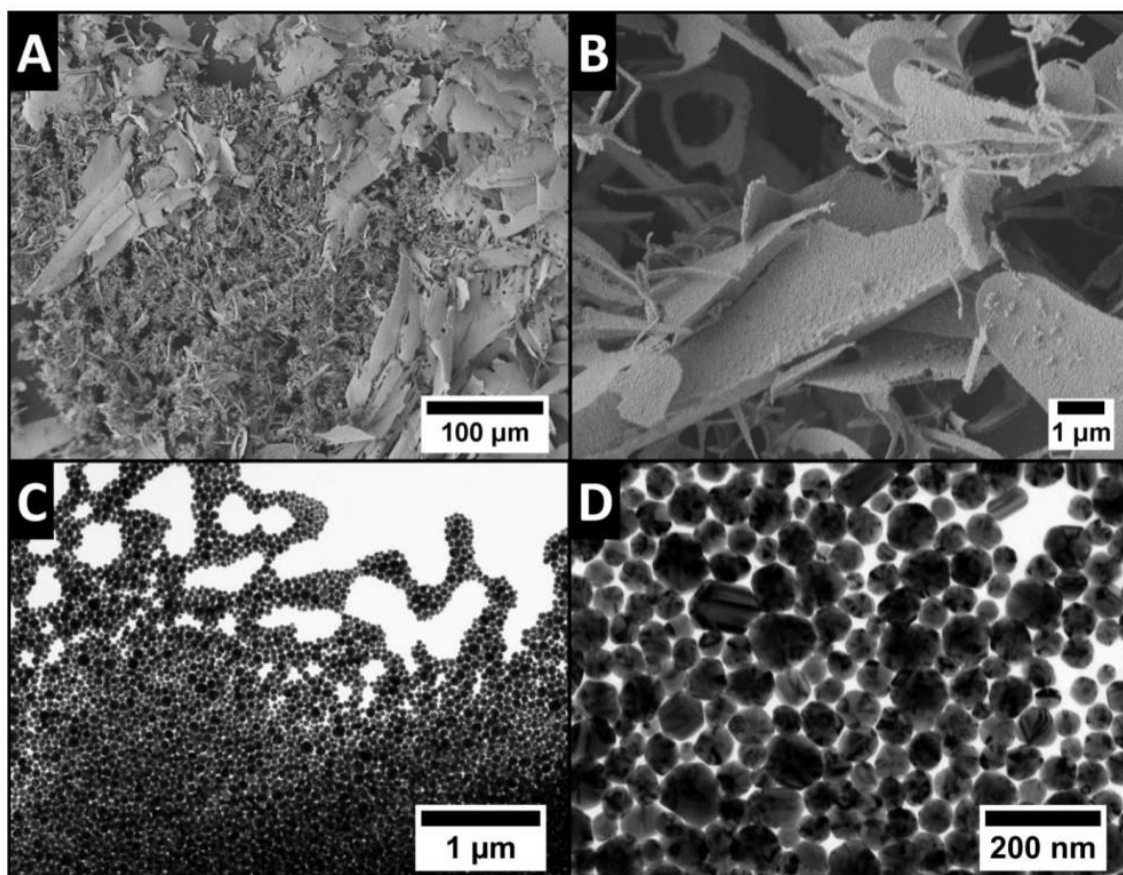


Figure S6. SEM (A+B) and TEM (C+D) characterizations of pure Ag nanoparticles assembled into macroscopic, porous monolithic aerogels. The nanoparticles are in close proximity.

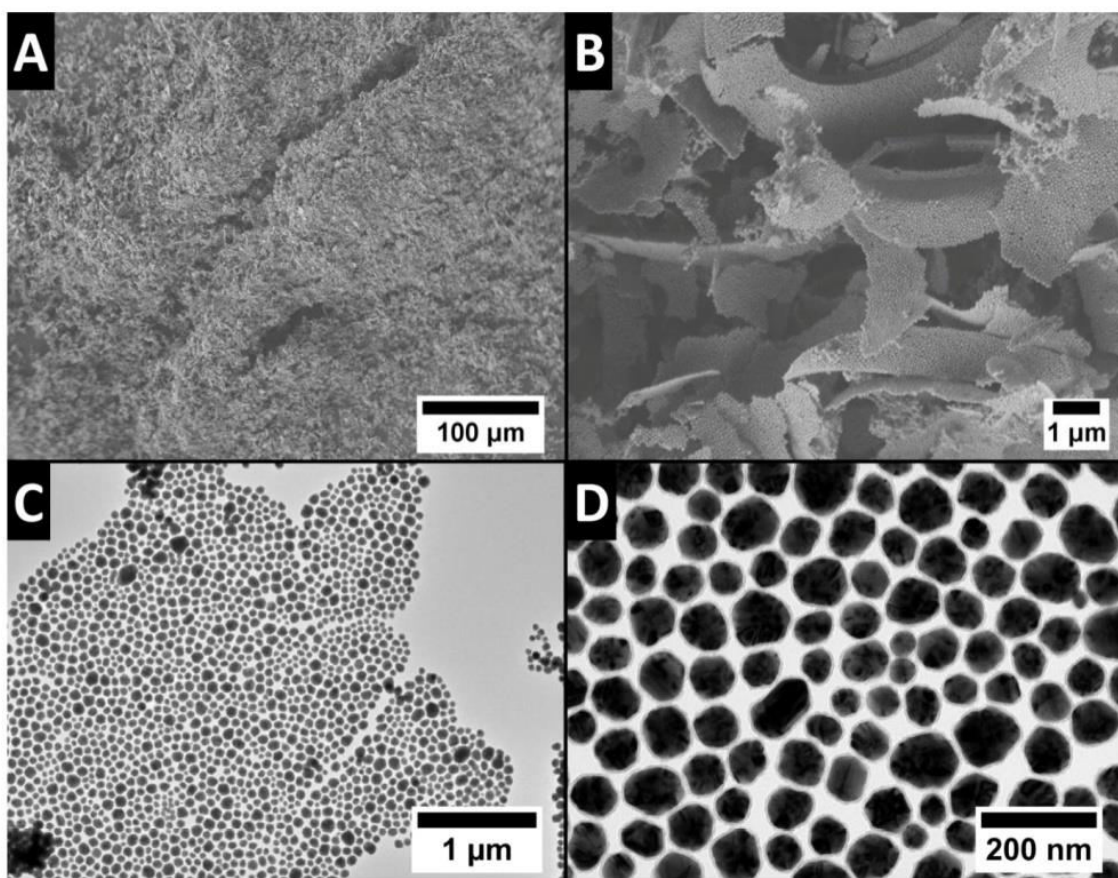


Figure S7. SEM (A+B) and TEM (C+D) characterizations of Ag nanoparticles with a 5 nm silica shell assembled into macroscopic, porous monolithic aerogels. The nanoparticles have interparticle distances of around 10 nm.

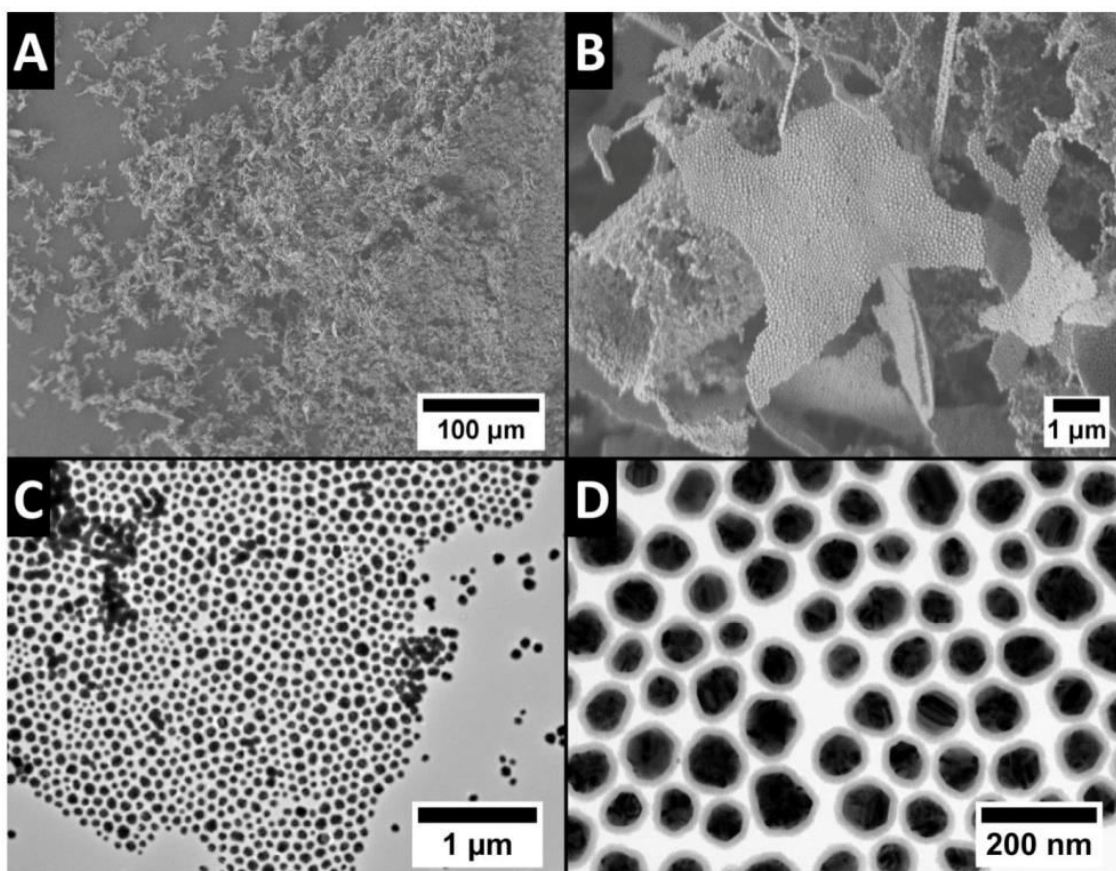


Figure S8. SEM (A+B) and TEM (C+D) characterizations of Ag nanoparticles with a 12 nm silica shell assembled into macroscopic, porous monolithic aerogels. The nanoparticles have interparticle distances of around 25 nm.

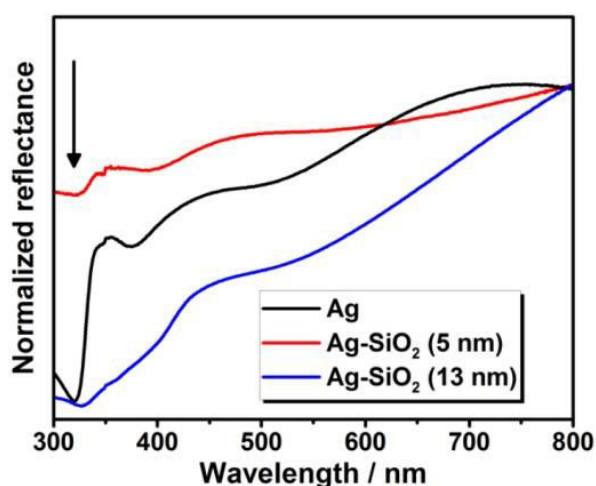


Figure S9. Normalized reflectance spectra of the cryogelated aerogel monoliths. These spectra show the bare Ag (black curve) as well as the Ag-SiO₂ core-shell heterostructures with a shell thickness of 5 nm (red curve) and 13 nm (blue curve). The arrow marks the plasma edge of silver located at around 324 nm.

4. From Knowledge to Application – Possibilities of Cryoaerogels in Catalysis

4.1 Summary

Since the cryogelation method enables the assembling of noble metal NPs i.e. platinum, while retaining their huge specific surface area, thus cryoaerogels are of high interest for catalytic applications. Additionally this procedure does not require surface chemistry which means the absence of oxidizing agents or complexing ligands. As a result the surfaces of the NP should be accessible, allowing catalytic reactions. Therefore the noble metal cryoaerogels presented in section 4.2 were throughout investigated for their catalytic activity and evaluated regarding their potential for actual application. Noble metal NPs from gold, silver, palladium and platinum were synthesized after a modified citrate reduction method, concentrated and assembled into monoliths by freezing the colloidal solution and subsequently freeze drying them. The monolith of platinum showed already high activity at room temperature by visibly catalyzing the oxidation of residual citrate ligands. The conversion of carbon monoxide to carbon dioxide was chosen as a model reaction for the catalytic activity and all fabricated monolith were measured. Furthermore the influence of particle concentration and size on the catalytic activity was determined. It was found that all noble metal aerogels showed catalytic activity at 200°C. While this could be expected for platinum and palladium it is surprising and not reported for gold and silver of this particle size so far. The platinum and palladium aerogels showed 100% conversion already at 175°C. Compared with literature the $T_{50,ignition}$ were similar. However the performance of the $T_{50,extinction}$ was much lower at around 160°C which could be attributed to the nature of the full material catalyst. Furthermore CO conversion could be observed already at room temperature for Pt and Pd but declined very fast through the saturation of active sites with CO_x species at this temperature. Experiments on the thermal stability of the monoliths showed sintering of the particle within the cryoaerogel to a size of around 10 to 20 nm which did not change afterwards. The performance of

platinum, silver and gold decreased while the palladium was stable over several runs. Concluding the section showed for the first time the direct testing of aerogel monoliths, without destroying them. It could be shown that these aerogels are capable of catalysis and that the material is much lighter than conventional catalysts.

Another interesting application in photocatalysis was already demonstrated in section 2.3. Multicomponent titania-platinum cryoaerogels possess promising hydrogen evolution rates and are significantly higher compared to their respective colloidal solution. Compared to literature values, the hydrogen evolution rates are similar to the best reported aerogels, yet with a much faster and less complex synthesis route.

4.2 Catalytic Properties of Cryogelated Noble Metal Aerogels

Axel Freytag, Massimo Colombo, Nadja C. Bigall

Zeitschrift für physikalische Chemie, ahead of print

DOI: [10.1515/zpch-2016-0856](https://doi.org/10.1515/zpch-2016-0856)

Reprinted with permission from *Zeitschrift für physikalische Chemie*. Copyright
(2016) DeGryuter

Axel Freytag, Massimo Colombo* and Nadja C. Bigall*
**Catalytic Properties of Cryogelated Noble
Metal Aerogels**

DOI 10.1515/zpch-2016-0856

Received July 15, 2016; accepted August 17, 2016

Abstract: The catalytic properties of cryogelated noble metal aerogel monoliths out of aqueous colloids are investigated using the oxidation of carbon monoxide (CO) as a model reaction, in order to evaluate their potential for catalytic applications. Aerogels built of self-supporting platinum (Pt) and palladium (Pd) nanocrystals (NCs) have a directly accessible catalyst surface and show catalytic performance similar to state of the art catalysts while being support-free and therefore ultralight materials. In addition, these materials provide properties like room temperature CO conversion and spontaneous catalytic reactions. However, full material aerogel catalysts come with the side effect of limited thermal stability, which will have to be overcome in future.

Keywords: aerogels; catalysis; cryogelation; freeze drying; noble metals.

1 Introduction

Colloidal nanocrystals (NCs) provide a set of unique physical properties. Having a huge surface-to-volume ratio is one of the most known properties and is true for all NCs regardless of their material. This peculiarity makes them interesting for many catalytic applications. Today NCs are employed as catalysts for a wide variety of reactions such as, e.g. alkylations, hydrogenations, selective oxidation reactions [1]. They are used as tunable catalysts in

*Corresponding authors: **Nadja C. Bigall**, Institute of Physical and Electrochemistry, Leibniz University Hannover, Callinstraße 3A, D-30167 Hannover, Germany, e-mail: nadja.bigall@pci.uni-hannover.de; and **Massimo Colombo**, Nanochemistry Department, Istituto Italiano di Tecnologia, Via Morego, 30, I-16163 Genova, Italy, e-mail: massimo.colombo@iit.it

Axel Freytag: Institute of Physical and Electrochemistry, Leibniz University Hannover, Callinstraße 3A, D-30167 Hannover, Germany

oxygen reduction reactions, as magnetically separable catalysts in oxidation and epoxidation and catalyze C–C coupling reactions like, e.g. the Suzuki reaction [1–5]. However, for the application as a colloidal catalyst system the particles have to be separated after the reaction [4, 6, 7]. Alternatively, they can be deposited onto a support and immobilized like, e.g. embedding them into metal organic frameworks, on metal oxides, on carbon supports or infiltrating them in aerogels [2, 8–10]. However, the interactions of NCs with the support can dramatically affect their properties [11, 12]. If, on the one hand, this interaction largely determine the catalytic activity, on the other hand, it prevents the exploitation of the catalytic function of the bare metallic NCs, which could exhibit peculiar features. As an example, self-supported nanoporous structures made of Au showed unique catalytic properties which are not achievable with supported Au NCs [13]. However, the fabrication methods for these kinds of structures are tedious and intrinsically limited, thus calling for novel preparation methods that could be applied to other metallic NCs. A way to overcome these problems could be hydro- or aerogelation of metals and metal oxides [14–18]. It is reported that high voluminous structures out of NCs, which also partly possess the properties of their respective colloidal solution, can be achieved [16, 19, 20]. Nonetheless aerogelation itself is a complicated multi-step process. It also takes time to gelate the NCs of the solution and fabricate a hydrogel prior to usually supercritical drying for yielding the aerogel. Just recently we reported on a different fabrication method of aerogels via fast freezing and subsequent freeze drying [21]. With this method it is possible to reduce the complicated multistep aerogelation procedure to become a fast two-step synthesis and therefore provides an applicable way for industrial nanostructured catalyst fabrication. In addition this method allows shaping and is therefore of great interest for actual shaped monoliths for catalytic reactions. In the future, combining this nanostructuring method with existing support technologies might overcome the lack of mechanical stability.

In the present work we test the catalytic properties and evaluate the suitability of cryogelated noble metal NCs aerogel monoliths as heterogeneous catalysts. We concentrate on aerogels made from noble metal NCs, especially platinum (Pt), as it is broadly used in heterogeneous catalytic reactions. We investigate the aerogels' morphology, their thermal behavior as well as their performance for CO conversion. In addition and to the best of our knowledge, this is the first report on catalysis measurements of aerogel monoliths made of NCs which could be directly measured as heterogeneous gas phase catalysts, without any previous milling or re-dispersion and deposition on substrates.

2 Experimental section

2.1 Nanocrystals synthesis

For the synthesis of the noble metal NCs, we use the modified citrate reduction of metal salts from Enustun and Turkevich [22]. In a 1 L flask 36.2 mL of an aqueous 0.2 wt% dihydrogen tetrachloroplatinate (IV) hexahydrate (ACS, 99.95%) solution was diluted with deionized (DI) water to a total volume of 500 mL. The solution was stirred and heated until boiling. Then 11.6 mL of a 1 wt% trisodium citrate solution (ABCR, 99%) were added and stirred for 30 s. Subsequently 5.5 mL of an ice cold sodium borohydride solution (Fluka $\geq 99\%$) with 0.076 wt% were added. The solution immediately changed the color from yellow to brown. Au NCs were prepared with the same method using 12 mL of an aqueous 0.2 wt% silver nitrate (AgNO_3) (Alfa Aesar, 99%) solution instead of dihydrogen tetrachloroplatinate (IV) hexahydrate. When sodium borohydride is added the solution changes from colorless to yellow.

For Pd NCs 0.051 g of Pd(II)chloride (0.288 mmol, Sigma Aldrich, 99.999%) were dissolved in 10 mL DI water and 37% hydrochloric acid (Sigma Aldrich, reagent grade) with a molar ratio of 1:2 and heated until the solution was clear. Afterwards it was diluted with distilled water to a total volume of 500 mL. The temperature of the solution before sodium borohydride addition was 80°C. The addition of trisodium citrate and sodium borohydride was the same as for Pt and Ag.

Gold nanocrystals (Au NCs) can be synthesized at room temperature using 29 mL of an aqueous 0.2 wt% hydrogen tetrachloroaurate (III) trihydrate solution (ABCR, 99.99%) diluted to 500 mL total volume with DI water. Thirty seconds after the addition of 11.6 mL of a 1 wt% trisodium citrate solution, 5.8 mL of an aqueous 0.07 wt% sodium borohydride solution were added. The solution immediately changed from yellow to red.

2.2 Aerogel fabrication

According to our previous results [21], beside employing an aqueous solution of the NCs, the requirement for aerogel fabrication via the cryogelation method is a volume fraction of NCs of at least 0.1%, in order to avoid shrinkage of the resulting monoliths. After the synthesis the particles were washed and concentrated by factor 100 over an ultrafiltration cell with a 30 kDa regenerated cellulose

membrane (Satorius Stedim) and a pressure of 5.5 bar. This solution can be stored for several weeks. To prepare them for aerogel fabrication the colloidal solution was concentrated again by factor 10 by means of centrifuge filters (Amicon Ultra 15, 10 kDa, Merck Milipore). These solutions were then injected into liquid nitrogen, cooled for 10 min to ensure complete freezing and subsequently freeze dried at a pressure lower than 0.05 mbar for at least 24 h (see Figure 1). If the structure is not completely dry, the remaining ice would melt and the structure would collapse.

2.3 Catalytic experimental setup

Catalytic activity measurements were carried out in a custom made flow-microreactor system (i.e. a quartz tube with internal diameter = 4 mm inserted in an electric furnace) where aerogel masses in the range of 15–40 mg were loaded between two quartz wool layers. For each experiment, the reactor was flushed for at least 30 min with a inert gas mixture of 6% O₂ balanced with He and afterwards heated from 25 to 200°C at 5°C/min while flowing 40–80 Ncc/min (norm cubic centimeters per minute: at standard pressure and room temperature) of reaction mixture (1.3% v/v CO, 10% v/v O₂, balance He), and then cooled back to room temperature. The CO and CO₂ outlet concentrations were continuously measured by means of a nondispersive infrared (NDIR) photometer (ABB Uras 26).

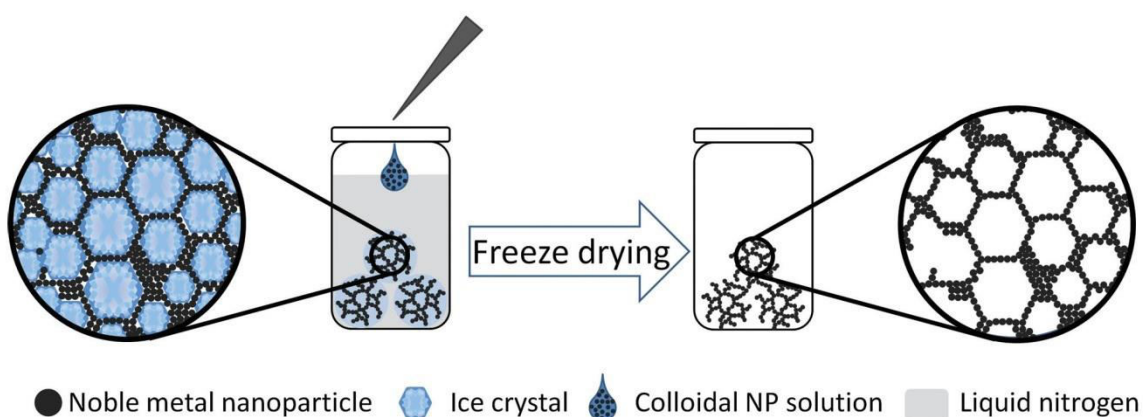


Fig. 1: Freezing mechanism of the aqueous NCs solution (left) in liquid nitrogen. Ice crystals form all over the liquid drop, pushing the NCs into a filigree network superstructure. After removing the ice crystals through freeze drying the self-supporting highly-porous NCs superstructure remains (right).

3 Results and discussion

3.1 Electron microscopy characterization

The macroscopic structure of the resulting aerogel monoliths can be described as highly porous, voluminous and therefore with low density. Weighing the monoliths gives masses ranging from 20 mg for Au and Pd NC aerogels to 60 mg for Au and Pt NC aerogels. With an applied starting solution volume of 1 cm³ and the visual confirmation of no shrinkage during cryogelation a density ranging from 20 to 60 mg cm⁻³ can be estimated. This corresponds to 0.2% of the respective bulk material density. Using electron microscopy the micro- and nanostructure of the monolith is characterized (see Figure 2).

On a microscopic scale the monoliths can be described as thin, interconnected sheets with random orientation forming the highly porous structure of the monoliths. The sheets show, in many cases, the tendency to bend or start to enroll. Within this structure wires can also be found which might be completely enrolled sheets. Higher magnifications and switching to transmission electron microscopy (TEM) reveals that the sheets are built up from the single NCs with random orientation. Through various scanning electron microscopy (SEM) and TEM images the thickness of the sheets can be estimated from perfectly perpendicular oriented sheets and is in the range of 5–50 nm corresponding to one to 10 particle layers for the given particle size. The shape and the size of the single NCs (see Supporting Information) do not change during the formation of the Pt aerogel. The structures shown are also representative for Pd aerogels. A more detailed characterization of the structure of the noble metal aerogels and their starting colloids can be found in our previous report [21]. However, softer (i.e. in terms of Young's modulus where Au and Ag have 79 and 83 GPa, respectively, while Pt has 168 GPa) noble metals show deformations of the NC. For example, in Au aerogels we observe ~10 nm platelets in lateral dimension instead of 4 nm spheres as already shown in our previous work [21].

3.2 Catalytic activity

For a full examination of the catalytic potential of the aerogels, the conversion of CO to CO₂ was chosen. This model reaction is frequently used to characterize new materials,¹ and the results obtained can be transferred to other

¹ 327 publications in 2014.

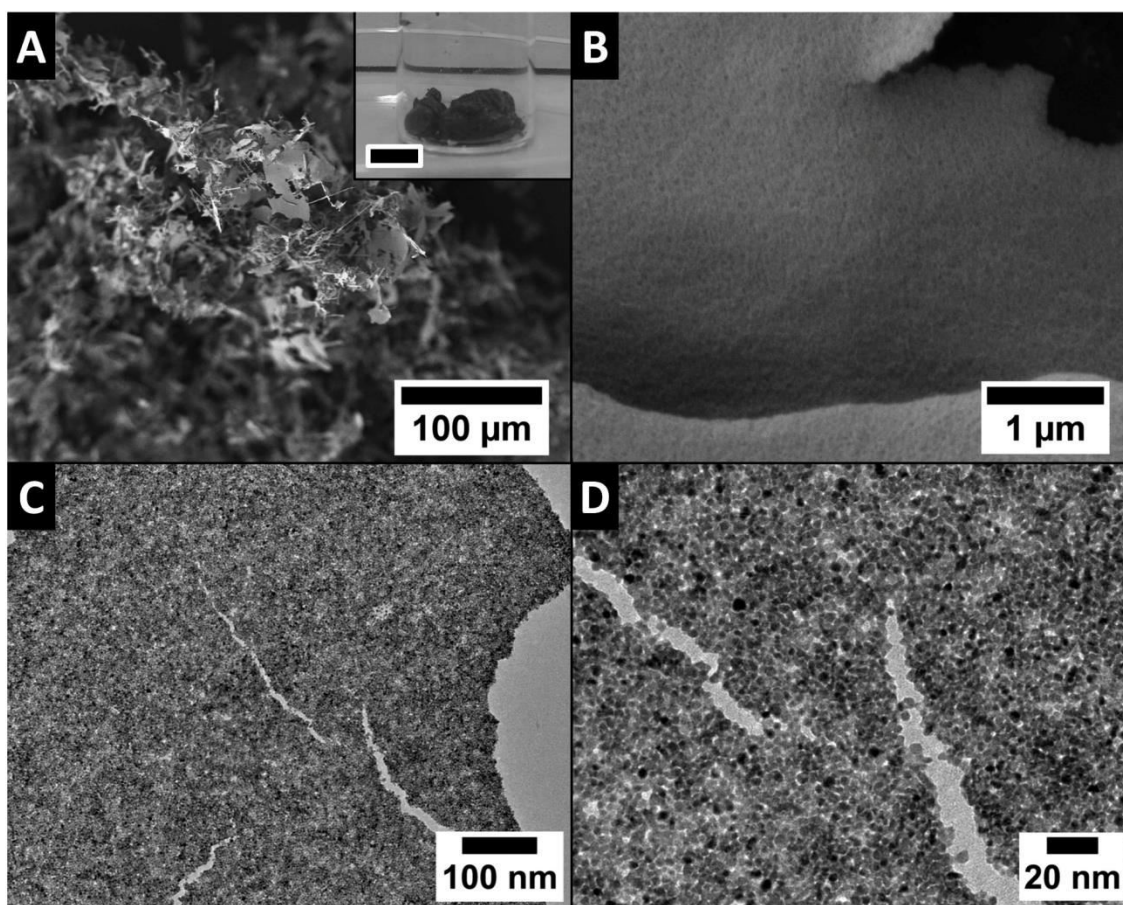


Fig. 2: Electron microscopic characterization of a Pt aerogel. SEM images showing the microscopic structure (A and B), which can be described as thin, interconnected sheets and wires. The inset in A shows the macroscopic Pt aerogel made from 1 mL of a 100 times concentrated NC solution (volume fraction of Pt NC $\sim 0.025\%$ /black bar is equal to 1 cm). Higher magnifications reveal the assembly of single NCs to form the just described sheets. Transmission electron microscope images (C and D) show that the NCs within the sheets are randomly oriented and retain the shape and size of the starting solution as already reported in our earlier work [21].

heterogeneous reactions, and they have also relevance from an industrial point of view (e.g. diesel oxidation catalysts, hydrogen production from fossil fuels) [23–25].

Figure 3A shows the first two test runs of a Pd aerogel with a total addition of 1.3% v/v CO. The results indicate clearly an excess of CO_x species around 3000 s elapsed time in the first run. We can observe this behavior for all aerogels (Au, Ag, Pt and Pd) and we attribute it to the removal of residual citrate ligands from the NCs surface. This is confirmed by the second reaction cycle, where the C balance is respected throughout the whole reaction cycle. In the case of the Pt aerogel, the removal of the ligands results in a violent reaction. By tilting the vial of the aerogel, the monolith starts a spontaneous oxidation as can be seen

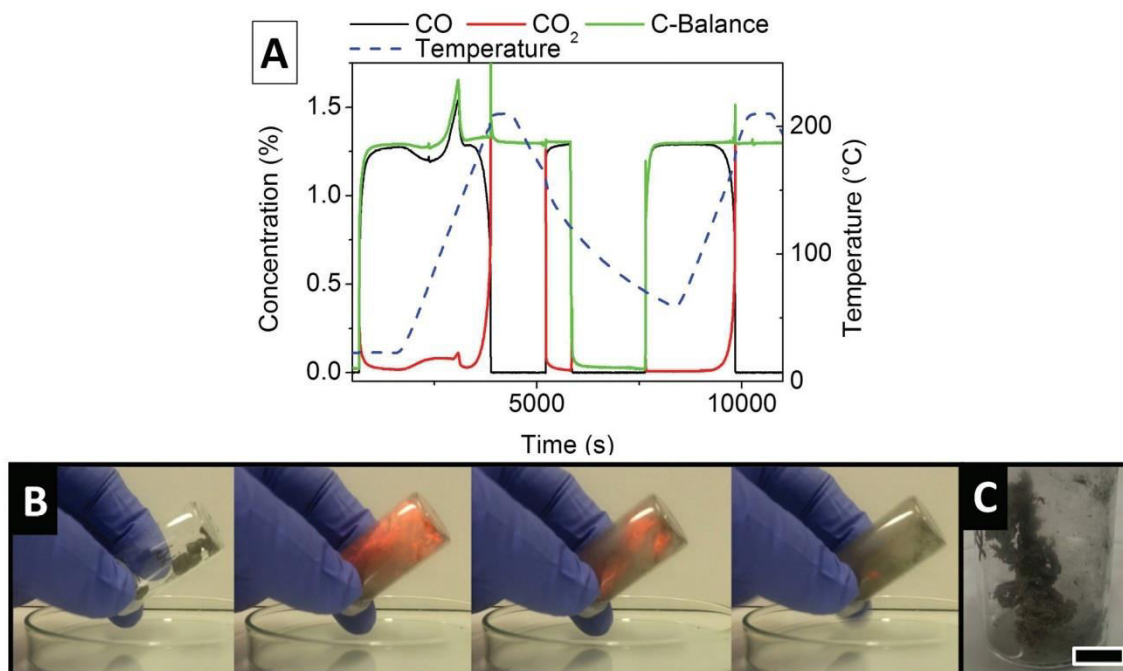


Fig. 3: (A) The CO_x species composition of a Pd aerogels over the first two test cycles showing additional C in the first run at around 3000 s due to ligand oxidation. (B) Image series of the “exploding” Pt aerogel. (C) Image of the Pt aerogel after the “explosion”.

in Figures 3B and C. This “explosion” is most likely related to the high specific surface and catalytic properties of Pt. The oxidation is also observed under inert atmosphere (while being in the freeze dryer flushed with nitrogen after drying) but with a pale colorless flame, which is attributed to the lack of oxygen. Additionally, this spontaneous oxidation can be inhibited, e.g. by changing the ligands of the Pt NCs from citrate ligands to thiol ligands (such as mercaptopropionic acid or mercaptosuccinic acid) before freezing. Alternatively, when lowering the NCs volume fraction below 0.025%, spontaneous oxidations was not observed.

The catalytic performances of the gels towards CO oxidation after this first “activation” cycle, can be seen in Table 1. Pt performs best and shows full conversion, as well as Pd, while Ag showed lower catalytic activity. Surprisingly, Au shows up to 40% conversion although the crystal size with ~ 10 nm is much bigger than 5 nm, which was reported as the minimum size before [26]. We also checked the influence of the NCs size and found that the catalytic performance decreased with increasing NCs size, which is most likely due to the decreasing specific surface area for bigger particles. To benchmark the aerogel activity, we prepared Pt NCs (5 wt%) on alumina by colloidal deposition with the very same particles. This technique is commonly employed to prepare state-of-the-art

Tab. 1: Catalytic activity in gas-phase CO oxidation with ignition and extinction temperatures (T_{50}) and weight hourly space velocity (WHSV).

| Metal | Nanocrystal size (nm) | Volume fraction of NC before freezing (%) | T_{50} ignition/ T_{50} extinction temperature (°C) | WHSV (Ncc h ⁻¹ g ⁻¹) |
|--|-----------------------|---|--|---|
| Pt | 4 | 0.25 | 160/113 | 170 k |
| | 4 | 0.025 | 182/142 | 170 k |
| | 10 | 0.25 | 196/160 | 140 k |
| | 15 | 0.25 | 174/129 | 140 k |
| Pt on Al ₂ O ₃ benchmark | 4 | 5 wt% | 165/144 | 240 k |
| Pd | 4 | 0.25 | 174/151 | 170 k |
| | 4 | 0.025 | 197/195 | 140 k |
| Au | ~10 | 0.25 | 300 ^a | 130 k |
| | ~10 | 0.025 | No activity | – |
| Ag | 10 | 0.025 | 198/197 | 130 k |

^a40% CO conversion.

model catalysts based on metallic NCs [27]. While the ignition temperature (temperature at which 50% conversion is reached during a heating transient) of the aerogel and of the supported NCs is similar in both cases, the extinction temperature (temperature at which 50% conversion is reached during a cooling transient) is lower in case of the aerogel (i.e. the gel outperforms the supported catalyst) as can be seen in Figure 4A. The hysteresis phenomena have been extensively studied over Pt/Al₂O₃ catalysts and has often been ascribed to the local overheating of the NCs due to the exothermicity of the

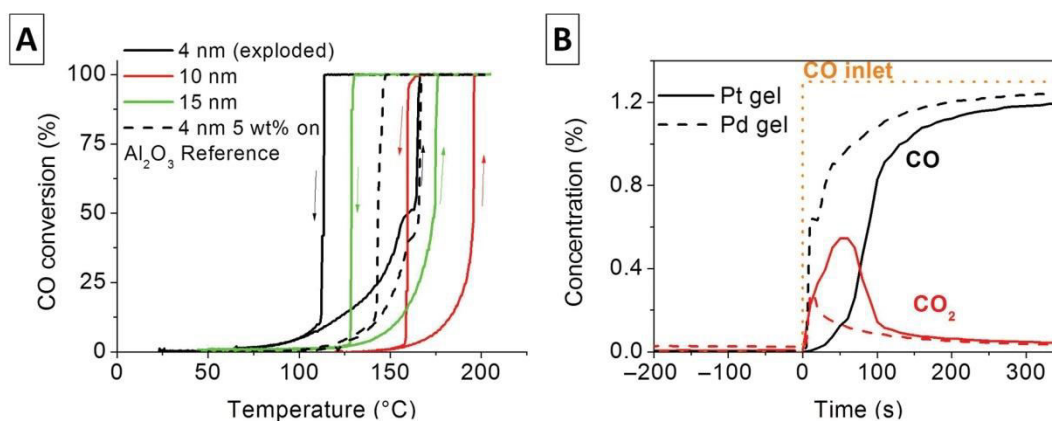


Fig. 4: (A) CO conversion in dependence on the temperature for different particle sizes. The best performance was achieved for gels built from 4 nm particles. The dotted line shows the benchmark experiment with the 4 nm particles deposited on alumina as it is state of the art for catalyst preparation. (B) Time evolution of the COx concentration at room temperature showing immediate conversion and self-poisoning for Pt and Pd aerogels.

CO oxidation reaction [28–32]. Our monolith is characterized by a fully active catalytic surface and by a better heat transfer in comparison with the Pt NCs deposited on alumina, where the support (i.e. Al_2O_3) acts as a heat sink. This property might justify the better performances of the aerogel in comparison with the supported catalyst.

The Pt and Pd monoliths show CO oxidation catalytic activity already at room temperature, proving the accessibility of the NCs surface. The activity drops then to zero within few 100 s of exposure to the CO/O₂ mixture (Figure 4B), in line with the well known poisoning effect of CO on the surface of Pt and Pd catalysts [33–35]: when carbon monoxide is fed at room temperature, the molecules adsorb onto the catalyst surface and convert to CO₂ (as can be seen in Figure 4B). So at first, all sites on the surface are available for reactions. However, at this temperature the reaction sites are blocked over time from the very same CO, which strongly binds to the metal surface hence leading to a decrease of activity. Thus, to enable fast kinetics for a full and continuous carbon monoxide conversion in our Pt or Pd aerogel samples, temperatures up to 200°C are necessary.

As shown in an earlier report [21], when varying the volume fraction of the NCs we observe a threshold at 0.25 vol% for yielding monoliths with the same volume as the employed NCs colloid. Below this value the aerogel monoliths shrink due to insufficient building blocks and therefore a partly or even complete collapse of the network structure. However, the particle layer of the sheets become also thinner up to a point where only sheets with a particle monolayer could be observed. While concentrations of 0.0025 vol% and below yielded no usable monolith, concentrations of around 0.025 vol% do (although they suffer strong shrinkage of around 70% during drying). Figure 5 shows the comparison of Pd and Pt, which was the most active material and therefore the best choice

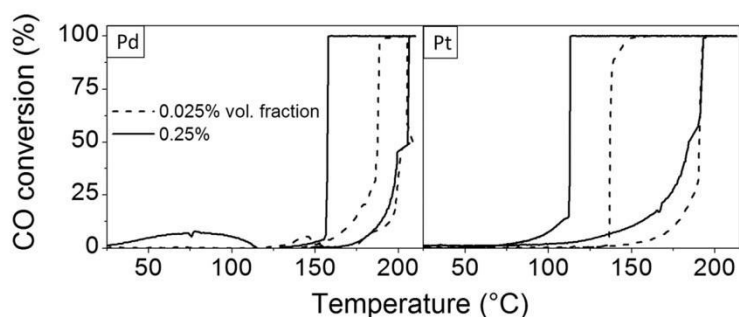


Fig. 5: Comparison of the CO conversion of aerogels made from Pd and Pt NCs. The solid lines show aerogels made from a start solution with 0.25% vol% NCs volume fraction while the dashed lines show those made from 0.025%.

to observe dependencies of morphology and catalytic performance. It turns out that lower volume fractions in the starting solutions have a negative impact on the catalytic performance of the aerogels. While the T_{50} ignition is similar, the T_{50} extinction temperature is around 20–30 K higher. The temperature decrease is related to the heat transfer within the aerogel and could be already observed in the system with Pt/Al₂O₃. Thinner sheets have a lower heat transfer and therefore a faster decrease in catalytic performances. The CO conversion, which can be seen for Pd below 125°C can be attributed to the oxidation of the surface ligands. Because of the low ligand amount, this can not be observed for Pt aerogels.

3.3 Thermal and catalytic stability

The thermal stability of the noble metal aerogels was investigated in the range within 25°C–200°C (as can be derived from Figure 6). All monoliths show shrinkage during the catalytic measurements. While Au and Ag aerogels show extremely low thermal stability and decreasing catalytic activity within the first runs, the catalytic activity of Pt is more stable but also decreases over five runs with an approximately 15 K higher T_{50} (see Figure 6A). Instead, Pd shows a completely stable performance in the entire temperature range (r.t. –200°C) for several runs (Figure 6B). TEM images of cycled Pt samples (Figure 7) were measured, showing that the NCs in the aerogel-building sheets are sintered together. However, the aerogel samples have still their porous and polycrystalline nature with an increased domain size of ≤ 20 nm.

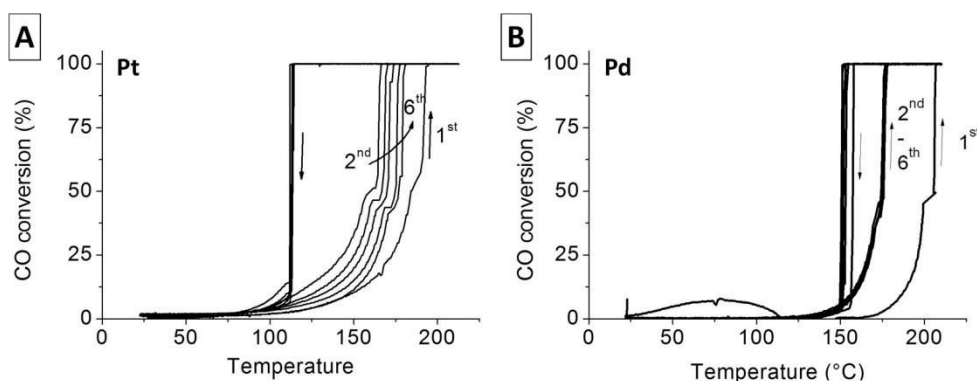


Fig. 6: (A) CO conversion of Pt aerogels over six cycles (each cycle takes 120 min). The T_{50} ignition temperature increases with each cycle showing a decreasing performance. (B) CO conversion of Pd aerogels over six cycles (each cycle takes 120 min). The T_{50} ignition temperature does not change at all.

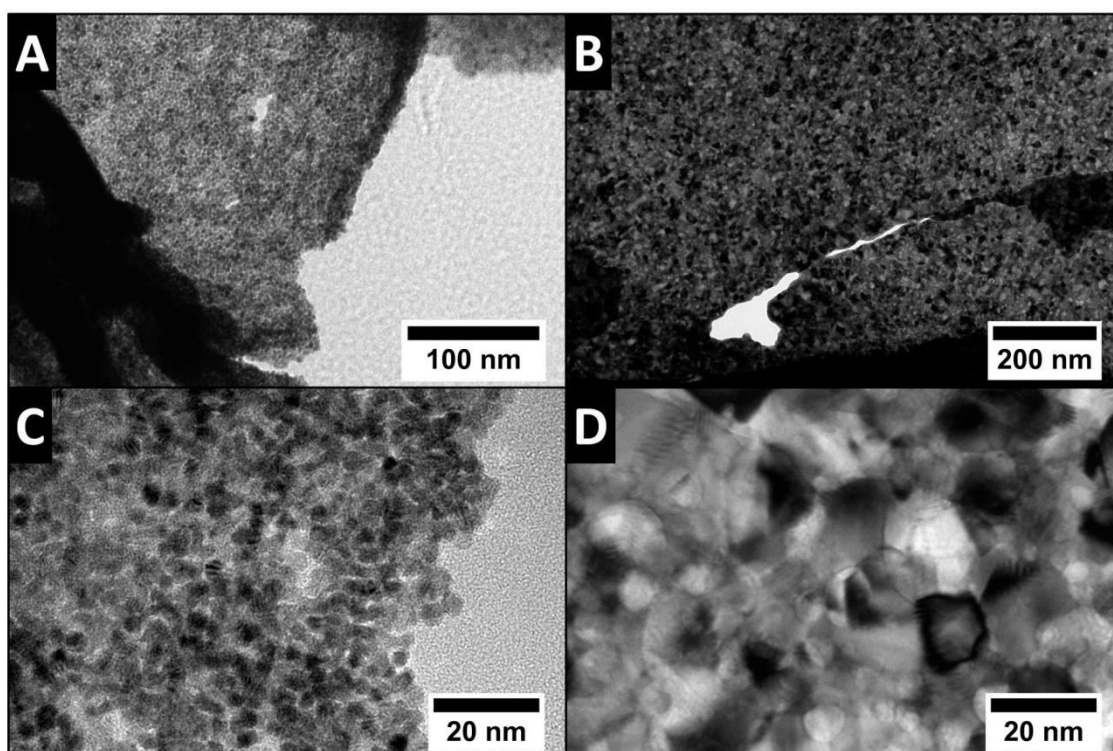


Fig. 7: TEM characterization of a Pt aerogel (volume fraction 0.025%) before (A and C) and after catalytic measurements (B and D) in two different magnifications.

4 Conclusion

Summarizing, it is possible to employ noble metal aerogel monoliths as heterogeneous catalysts. These aerogels synthesized by the cryogelation method have accessible NCs and exhibit good catalytic performance comparable to state of the art prepared catalysts. To the best of our knowledge, this is the first report on catalysis measurements of metal NCs based aerogel monoliths which could be directly employed as heterogeneous gas phase catalysts, without any previous milling or re-dispersion and deposition on substrates. Aerogel catalysts outperform supported catalysts in terms of heat transfer and active material per total weight including the support. As a drawback, pure noble metal aerogels displayed limited thermal stability and nearly all materials showed decreasing catalytic activity over several runs. An exemption thereof was Pd aerogels which exhibited a significantly higher stability. In future, further experiments will have to be conducted in order to overcome the above-mentioned problems so that the full potential of such full catalysts without additional support material can be exploited. The potential of pure noble metal gels themselves is unquestionable, although further work is needed to optimize their behavior as heterogeneous catalysts.

Acknowledgements: A.F. and N.C.B. are grateful for the financial support from the German Federal Ministry of Education and Research (BMBF) within the framework of NanoMatFutur, support code 03X5525. We also would like to thank the Laboratory of Nano and Quantum Engineering (LNQE) of Leibniz University Hannover for the support.

References

1. N. R. Shiju, V. V. Gulians, *Appl. Catal. A* **356** (2009) 1.
2. A. Roucoux, J. Schulz, H. Patin, *Chem. Rev.* **102** (2002) 3757.
3. S. Guo, S. Zhang, S. Sun, *Angew. Chem. Int. Ed.* **52** (2013) 8526.
4. S. Shylesh, V. Schuenemann, W. R. Thiel, *Angew. Chem. Int. Ed.* **49** (2010) 3428.
5. D. Astruc, F. Lu, J. R. Aranzaes, *Angew. Chem. Int. Ed.* **44** (2005) 7852.
6. R. Narayanan, M. A. El-Sayed, *J. Phys. Chem. B* **109** (2005) 12663.
7. P. Herves, M. Perez-Lorenzo, L. M. Liz-Marzan, J. Dzubielia, Y. Lu, M. Ballauff, *Chem. Soc. Rev.* **41** (2012) 5577.
8. A. Dhakshinamoorthy, H. Garcia, *Chem. Soc. Rev.* **41** (2012) 5262.
9. J. H. Kim, D. J. Suh, T. J. Park, K. L. Kim, *Appl. Catal. A* **197** (2000) 191.
10. H.-B. Ren, L. Zhang, *Colloids Surf. A* **372** (2010) 98.
11. M. Cargnello, V. V. T. Doan-Nguyen, T. R. Gordon, R. E. Diaz, E. A. Stach, R. J. Gorte, P. Fornasiero, C. B. Murray, *Science* **341** (2013) 771.
12. X. Liu, M.-H. Liu, Y.-C. Luo, C.-Y. Mou, S. D. Lin, H. Cheng, J.-M. Chen, J.-F. Lee, T.-S. Lin, *J. Am. Chem. Soc.* **134** (2012) 10251.
13. J. Biener, M. M. Biener, R. J. Madix, C. M. Friend, *ACS Catal.* **5** (2015) 6263.
14. S. S. Kistler, *Nature* **127** (1931) 741.
15. S. L. Brock, I. U. Arachchige, K. K. Kalebaila, *Comments Inorg. Chem.* **27** (2006) 103.
16. N. C. Bigall, A.-K. Herrmann, M. Vogel, M. Rose, P. Simon, W. Carrillo-Cabrera, D. Dorfs, S. Kaskel, N. Gaponik, A. Eychmueller, *Angew. Chem. Int. Ed.* **48** (2009) 9731.
17. N. C. Bigall, M. Reitzig, W. Naumann, P. Simon, K.-H. van Pee, A. Eychmueller, *Angew. Chem. Int. Ed.* **47** (2008) 7876.
18. W. Liu, A.-K. Herrmann, N. C. Bigall, P. Rodriguez, D. Wen, M. Oezaslan, T. J. Schmidt, N. Gaponik, A. Eychmueller, *Acc. Chem. Res.* **48** (2015) 154.
19. A.-K. Herrmann, P. Formanek, L. Borchardt, M. Klose, L. Giebeler, J. Eckert, S. Kaskel, N. Gaponik, A. Eychmueller, *Chem. Mater.* **26** (2014) 1074.
20. W. Liu, P. Rodriguez, L. Borchardt, A. Foelske, J. Yuan, A.-K. Herrmann, D. Geiger, Z. Zheng, S. Kaskel, N. Gaponik, R. Koetz, T. J. Schmidt, A. Eychmueller, *Angew. Chem. Int. Ed.* **52** (2013) 9849.
21. A. Freytag, S. Sanchez-Paradinas, S. Naskar, N. Wendt, M. Colombo, G. Pugliese, J. Poppe, C. Demirci, I. Kretschmer, D. W. Bahnemann, P. Behrens, N. C. Bigall, *Angew. Chem. Int. Ed.* **55** (2016) 1200.
22. B. V. Enustun, J. Turkevich, *J. Am. Chem. Soc.* **85** (1963) 3317.
23. A. Russell, W. S. Epling, *Catal. Rev. Sci. Eng.* **53** (2011) 337.
24. L. Gradisher, B. Dutcher, M. Fan, *Appl. Energy* **139** (2015) 335.
25. M. Steinberg, H. C. Cheng, *Int. J. Hydrogen Energy* **14** (1989) 797.

26. G. C. Bond, D. T. Thompson, *Catal. Rev. Sci. Eng.* **41** (1999) 319.
27. P. Munnik, P. E. de Jongh, K. P. de Jong, *Chem. Rev.* **115** (2015) 6687.
28. A. Abedi, R. Hayes, M. Votsmeier, W. S. Epling, *Catal. Lett.* **142** (2012) 930.
29. B. S. Gudkov, A. N. Subbotin, V. I. Yakerson, *React. Kinet. Catal. Lett.* **68** (1999) 125.
30. A. N. Subbotin, B. S. Gudkov, V. I. Yakerson, S. V. Chertkova, E. Z. Golosman, G. V. Kozyreva, *Russ. J. Appl. Chem.* **74** (2001) 1506.
31. A. N. Subbotin, M. P. Vorob'eva, B. S. Gudkov, V. I. Yakerson, L. M. Kustov, *Russ. J. of Appl. Chem.* **75** (2002) 582.
32. A. N. Subbotin, B. S. Gudkov, Z. L. Dykh, V. I. Yakerson, *React. Kinet. Catal. Lett.* **66** (1999) 97.
33. P.-A. Carlsson, L. Österlund, P. Thormählen, A. Palmqvist, E. Fridell, J. Jansson, M. Skoglundh, *J. Catal.* **226** (2004) 422.
34. P.-A. Carlsson, M. Skoglundh, *Appl. Catal. B* **101** (2011), 101, 669.
35. P.-A. Carlsson, M. Skoglundh, E. Fridell, E. Jobson, B. Andersson, *Catal. Today* **73** (2002) 307.

Supplemental Material: The online version of this article (DOI: 10.1515/zpch-2016-0856) offers supplementary material, available to authorized users.

Supporting Information

Axel Freytag, Massimo Colombo*, Nadja C. Bigall*

Catalytic Properties of Cryogelated Noble Metal Aerogels

Transmission electron microscopical characterization of the noble metal nanocrystals

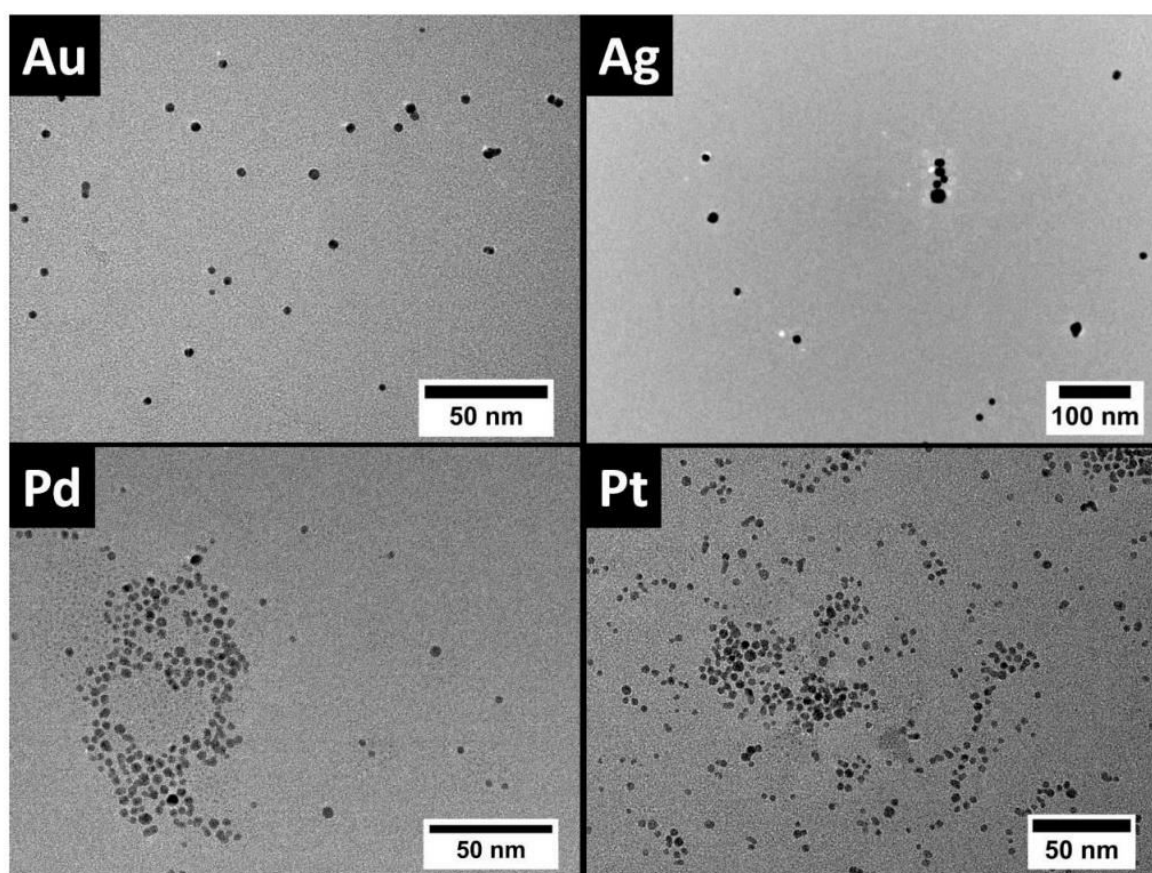


Fig. 1: Transmission electron microscopical characterization of Au, Ag, Pd and Pt nanocrystals from their aqueous solution

Particle size distribution of the noble metal nanocrystals

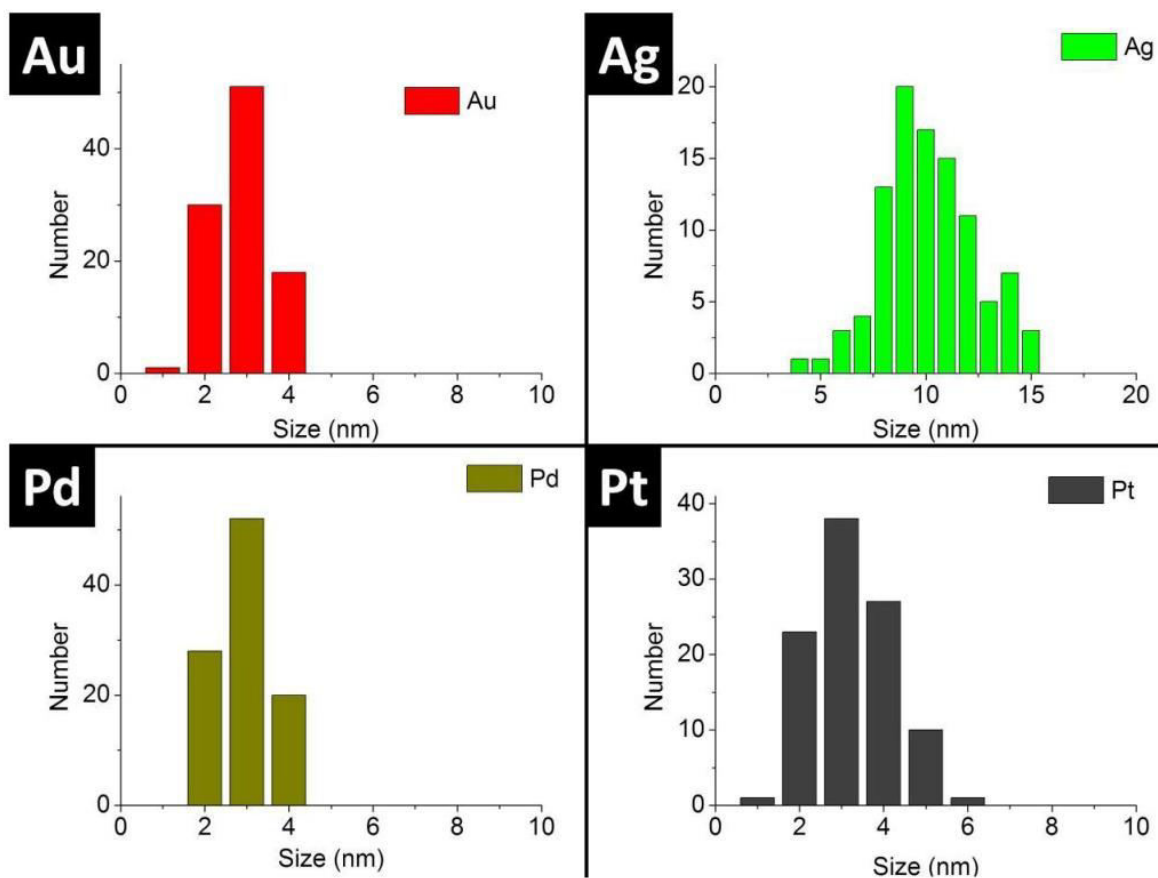


Fig. 2: Particle size distribution for the noble metals nanocrystals in their aqueous colloidal solution (100 NCs counted). The mean diameter of this particle was determined to be 3.4 ± 0.6 nm for Au, 10.7 ± 2.3 nm for Ag, 3.4 ± 0.6 nm for Pd and 3.8 ± 0.9 nm for Pt

5. Closing Remarks

Within this thesis a complete new procedure to synthesize aerogels, namely the cryoaerogelation, was developed. This method allows the prementioned control over particle interactions as well as the immobilization of aerogels on substrates. It outperforms current aerogel synthesis by enabling further techniques such as shaping of aerogels or being less complex (i.e. no surface chemistry or solvent exchange are needed) and faster than state of the art methods.

In detail, in section 2.2 it was discovered that aqueous colloidal NP solutions with volume fractions of NPs higher than 0.1vol% can be assembled into aerogel structures by freezing the colloidal solution with liquid nitrogen and subsequently freeze dry the materials. The resulting monoliths possess densities around a hundredth to a thousandth of the corresponding bulk material density and have a morphology which can be described as NP assembled into two dimensional sheets which again form a well interconnected three dimensional structure. Since this structure is caused by the ice crystals, which form at the freezing, it can be found every time even if the components are varied. The specific surfaces are within the magnitude of reported literature values and as components noble metals (Au, Ag, Pd, Pt), metal oxides (hematite) as well as metal chalcogenides (CdSe/CdS) were realized. Plasmonic properties could be demonstrated for noble metal aerogels of Au and Ag. Additionally shaping and immobilization of aerogels was demonstrated by synthesizing a smiley aerogel and doctoral blading.

Furthermore the thesis demonstrates in section 2.3 the synthesis of multicomponent cryoaerogels with mixed components of hematite, titania, metal oxid hydroxides of cobalt, manganese and nickel as well as noble metals (Au, Ag, Pt). The resulting monoliths can be synthesized in various desired composition ratios and the distribution of components within the aerogel can be controlled via surface charges of the NPs. The morphology and density is similar to earlier fabricated aerogels, while the optical spectra differ strongly due to varying composition.

The optical properties of resulting cryoaerogels can be adjusted very well according to section 3.2. The thesis demonstrates on the example of plasmonic silver NPs with and without silica shells

(which serves as spacer), how defined interparticle distances in three dimensional structures can be realised. This results in different optical behaviour of the monolith, which can be observed already by eye. The investigation showed that cryoaerogels from silver NPs without a shell showed a complex spectrum with interplay of mie scattering, propagating plasmons as well as interplasmon coupling. It strongly differs to the spectrum of the colloidal solution. However, when employing silver particles with silica shells of 12 nm the optical spectrum of the cryoaerogel resembles the spectrum of the colloidal solution and especially propagating plasmons and interplasmon coupling can be prevented.

Finally this thesis investigated in section 4.2 the ability of the newly synthesized cryoaerogels for actual application in catalysis and photocatalysis. The conversion of CO to CO₂ is chosen as model reaction for the catalytical measurements. The reaction is of importance in automotive application and the lightweight nature of cryoaerogels might further contribute in realising cryoaerogel catalysts. The measurements demonstrated that the surface of the noble metals is active and accessible. For Pt and Pd a significant conversion of CO can be observed already at room temperature. However the conversion decreases rapidly because of CO strongly binding to the metal surfaces at this temperature. Continuous full conversion was observed for Pt and Pd at around 180°C and 200°C respectively. While needing higher temperature for full conversion Pd did not show decreasing performance over several hours. Compared with state of the art prepared alumina/Pt catalyst the performance was similar. However, due to the nature of a full material catalyst and therefore having no heat sink through inert material, the extinction temperature $T_{50, \text{extinction}}$ is around 30 K lower compared to the benchmark material.

The hydrogen evolution reaction from water with methanol was chosen as model reaction for the photocatalytical measurements of the mixed composite cryoaerogels in section 2.3. For that a series of composition ratios was synthesized and measured. The titania cryoaerogel with 1wt% photodeposited Pt showed a specific H₂ evolution of around 6.0 mmol h⁻¹ g⁻¹. It performs similar compared to the best Pt/TiO₂ aerogel described in literature, despite being faster and much cheaper to synthesize.

This thesis expands the methods for synthesis of highly voluminous and porous superstructures of assembled NPs by the cryoaerogelation. It is faster and less complex compared to existing synthesis routes. In addition it enables aerogel processing such as shaping and direct immobilization and fabrication in one step. The tested optical and catalytical properties are promising and as a result of this high commercial potential, the method got already patented. However to fully exploit the potential of this method further work is necessary, which is beyond the scope of this thesis. The high degree of control for assembling NPs could be demonstrated for voluminous plasmonic superstructures but may be even more interesting for the metal-metal chalcogenide material combinations to achieve e.g. fluorescence enhancement, etc. Further research needs to be conducted on the mechanical and thermal stability to adjust to requirements of actual applications by e.g. mixing different components of metal, metal oxides and metal chalcogenides. The implementation in Additional immobilization techniques such as inkjet printing or 3D printing is interesting to transfer cryoaerogels from the lab into application e.g. printing high surface area electrodes for hydrogen evolution reactions. Cooperations showed also a high potential of noble metal aerogels to sense very specific heavy metals and might be applicable as heavy metal sensor. In general the next important step for this method would be to define a sensor or catalyst system, with or without an industry partner, to realize a final product. With the mentioned advantages such as fast production and simplicity, the cryoaerogelation should contribute to the transfer of recent research in the nanoscopic world into macroscopic objects and even might bridge the gap from laboratory experiment into industrial application.

Appendix

Publications included in this thesis

[1] A. Freytag, S. Sanchez-Paradinas, S. Naskar, N. Wendt, M. Colombo, G. Pugliese, J. Poppe, C. Demirci, I. Kretschmer, D. W. Bahnemann, P. Behrens, N. C. Bigall, Versatile Aerogel Fabrication by Freezing and Subsequent Freeze-Drying of Colloidal Nanoparticle Solutions, *Angewandte Chemie, International Edition* **2016**, 55, 1200-1203.

[2] A. Freytag, M. Colombo, N. C. Bigall, Catalytic properties of cryogelated noble metal Aerogels, *Zeitschrift für Physikalische Chemie* **2016**, accepted.

[3] Torben Kodanek‡, Axel Freytag‡, Suraj Naskar, Thomas Härtling, Dirk Dorfs* and Nadja C. Bigall*, Macroscopic Aerogels with tunable nanoscopic plasmonic properties, *Chemistry of Materials*, **2016**, submitted

[4] Axel Freytag, Carsten Günemann, Suraj Naskar, Saher Hamid, Detlef W. Bahnemann, Nadja C. Bigall, Tailoring composition and material distribution in multicomponent cryoerogels, *ACS Nano*, **2016**, submitted

Publications not included in this thesis

- [1] S. Sánchez-Paradinas, D. Dorfs, S. Friebe, A. Freytag, A. Wolf, N. C. Bigall, Aerogels from CdSe/CdS Nanorods with Ultra-long Exciton Lifetimes and High Fluorescence Quantum Yields, *Advanced Materials* **2015**, 6152-6156.
- [2] A. Freytag, N.C. Bigall, Versatile fabrication for aerogels by freezing and subsequent freeze-drying of nanoparticle solutions, *Atlas of Science*, 2016
- [3] P. Stolzenburg, A. Freytag, N. C. Bigall, G. Garnweitner, Fractal growth of ZrO₂ nanoparticles induced by synthesis conditions, *CrystEngComm*, 2016, **18**, 8396 – 8405
- [4] S. Naskar, F. Lübke, S. Hamid, A. Freytag, A. Wolf, I. Ivanova, D. Dorfs, D. W. Bahnemann, N. C. Bigall, Synthesis of Au and Pt Decorated CdSe/CdS Hybrid Nanoplatelets for Photocatalytic H₂ Generation, *Advanced Functional Materials*, submitted

Patents from this thesis

- [1] N.C. Bigall, A. Freytag, DE 10 2015 113 455, Verfahren zur Herstellung von nicht-geträgerten Nanopartikelanordnungen, nicht-geträgerte Nanopartikelanordnungen sowie deren Verwendung.

Contributions to conferences

oral

- [1] Axel Freytag, Versatile Fabrication of Highly Porous Cryogels from Noble Metal Nanoparticles, *Nanobiotechnology Lectures - Italian Institute of Technology Genova*, 04.03.2015
- [2] Axel Freytag, Nadja C. Bigall, Macroscopic Aerogels of Self-Supporting Nanocrystals, *European Materials Research Society Spring Meeting 2016*, 02.05.-06.05.2016

poster

- [1] Cansunur Demirci, Axel Freytag*, Imme Kretschmer, Nadja C. Bigall, Detlef W. Bahnemann, Hydrogels from alpha iron oxide nanoparticles, *113th General Assembly of the German Bunsen Society for Physical Chemistry*, 29.-31.05.2014
- [2] Axel Freytag, Natalia Wendt, Peter Behrens, Nadja C. Bigall, Voluminous superstructures of noble metal nanoparticles, *Nanoday 2014*, 01.10.2014
- [3] Axel Freytag, Sara Sánchez Paradinas, Massimo Colombo, Nadja C. Bigall, Versatile fabrication of voluminous nanocrystal superstructures, *Nanoscale Assemblies of Semiconductor Nanocrystals, Metal Nanoparticles and Single Molecules: Theory, Experiment and Application 2015*, 24.-28.08.2015
- [4] Axel Freytag, Sara Sánchez Paradinas, Massimo Colombo, Nadja C. Bigall, Versatile fabrication of voluminous nanocrystal superstructures, *Nanoday 2015*, 01.10.2015
- [5] Axel Freytag, Sara Sánchez Paradinas, Massimo Colombo, Nadja C. Bigall, Versatile fabrication of voluminous nanocrystal superstructures, *49. Jahrestreffen Deutscher Katalytiker*, 16.03.-18.03.2016
- [6] Axel Freytag, Franziska Lübke*, Sara Sánchez Paradinas, Massimo Colombo, Nadja C. Bigall, Versatile fabrication of voluminous nanocrystal superstructures, *115th General Assembly of the German Bunsen Society for Physical Chemistry*, 05.05.-07.05.2016
- [7] Axel Freytag, Nadja C. Bigall, Macroscopic Aerogels of Self-Supporting Nanocrystals, *Nanoday 2016*, 02.05.-06.05.2016 (**winner of the Nanoday poster price**)

Curriculum Vitae



Personal details

Date of birth: 09.09.1985
Place of birth: Dippoldiswalde, Germany

Awards

September 2016 Winner of the poster price of the Nanoday Conference 2016

Patents

Oktober 2016 Patent (DE 10 2015 113 455) for the cryoaerogelation process

Higher Education

Dec. 2013 – present **PhD student** and scientific coworker, Workgroup
Dr. Nadja Carola Bigall, Institute for physical Chemistry and
Electrochemistry, Gottfried Wilhelm Leibniz Universität,
Hannover

Oct. 2011 – Oct. 2013 **Master of Science**, Chemistry, Technische Universität Dresden

Oct. 2007 – Mar. 2011 **Bachelor of Science**, Chemical Engineering, Hochschule für
Technik und Wirtschaft, Dresden

Education

Aug. 1996 - Jul. 2004 **Abitur**, Glück-Auf Gymnasium (Intense course: German,
History), Dippoldiswalde